THESIS FOR THE DEGREE OF DOCTOR OF PHILOSOPHY

Characterising Resistance to Electrical Treeing in New XLPE-Based Materials for High-Voltage Cables

ANETTE B. JOHANSSON

High Voltage Engineering
Department of Materials and Manufacturing Technology

CHALMERS UNIVERSITY OF TECHNOLOGY

Gothenburg, Sweden 2015

Characterising Resistance to Electrical Treeing in New XLPE-Based Materials for High-Voltage Cables

ANETTE B. JOHANSSON
ISBN 978-91-7597-205-3

Doktorsavhandlingar vid Chalmers tekniska högskola
Ny serie nr 3886
ISSN 0346-718X

High Voltage Engineering
Department of Materials and Manufacturing Technology
Chalmers University of Technology
SE-412 96 Gothenburg
Sweden
Telephone + 46 (0)31-772 1000

Cover:
Several electrical trees experimentally initiated in XLPE around an ultrathin wire electrode.

Chalmers Bibliotek, Reproservice
Gothenburg, Sweden 2015

For there is hope for a tree,
If it is cut down, that it will sprout again,
And that its tender shoots will not cease.
Job 14:7

Abstract

This work looks into electrical treeing in cross-linked polyethylene-based materials (XLPE), where the ability to resist tree development is considered as an indicator of improved applicability for insulation in high voltage power cables. The thesis presents results of a twin PhD project involving joint work of two students. One of the students (author of this thesis with a background in electrical engineering) concentrated on developing new methodology for testing the resistance to electrical treeing in XLPE modified by addition of voltage stabilising agents, while the design and syntheses of these agents was the domain of the second student, Markus Jarvid (having his background in chemical engineering). The latter work has been published in a separate thesis.

In contrast to the traditionally used needle-electrode test objects, a wire-electrode geometry has been introduced for creating the highly divergent electric field distribution in the insulation, necessary for initiation of an electrical treeing process. The wire-electrode object has shown a benefit of producing several trees during each individual test, therefore providing more data for further analyses. These objects also allow for exposing a larger volume of the material and let trees incept in weak-spot locations. How to conveniently analyse the resulting treeing data from performed experiments is further analysed in the thesis. To increase the applicability of the elaborated methodology for testing materials characterised by different degree of transparency, optical observations of the treeing process were complimented by simultaneous detection of partial discharges (PDs). Analyses of the latter have allowed an interpretation scheme practical for measuring resistance to treeing in non-transparent materials.

To evaluate how voltage stabilisers influence the resistance to treeing in XLPE, a broad range of stabilisers have been identified and tested. A detailed analysis demonstrates a positive effect imposed by addition of 4,4'-didocyloxybenzil. This compound is thereafter compared with the effect of various other stabilisers, including benzil-, thiaxanthone- fullerene- and melamine-types. Finally the stabiliser efficiencies are correlated with molecular ionisation potential and electron affinity, where it has been found that the stabilising efficiency increases with electron affinity of the added molecules. The results from this twin PhD project opens up a possibility to design new types of practically useful voltage stabilisers and test their suitability for improving the insulation in future high voltage cables.

Acknowledgements

First of all, I wish to express my gratitude to Prof. Stanislaw Gubanski, who has been the main supervisor and examiner of this work. Secondly, I wish to thank Dr. Markus Jarvid, my twin Doctoral student at the division of Polymer Technology, for all the hours spent together, both in the high voltage lab as well as at the chemistry department, resulting in a several thousands of experimentally grown trees for us to analyse. Prof. Tord Bengtson, Dr. Thomas Hammarström and Dr. Xiangrong Chen have been helpful in discussions on PD measurement techniques. Valuable input on the subject of polymer physics and chemistry from Prof. Mats R. Andersson and Dr. Christian Müller, both at Polymer Technology, has been highly appreciated. I also want to thank all other fellow PhD students and colleagues at High Voltage Engineering as well as Mattias Andersson at Polymer Technology for the collaborations.

Chalmers Area of Advance in Materials Science are gratefully acknowledged for supporting this twin PhD project and the External Advisory Board are thanked for their input during discussions about our research, the Area of Advance in Energy are furthermore acknowledged for support of this work.

Finally my parents, Bo and Ruth Johansson, are cherished for always supporting me in the choices I have made during my life.

Gothenburg, Sweden
28th of May 2015

List of Abbreviations

CCD – Charge Coupled Device
DAQ – Data Acquisition Device
DSC – Differential Scanning Calorimetry
EA – Electron Affinity
EL – Electroluminescence
IP – Ionisation Potential
LDPE – Low Density Polyethylene
PD – Partial Discharge
PE – Polyethylene
PRPDA – Phase Resolved PD Amplitude
SAXS – Small-Angle X-ray Scattering
SEM – Scanning Electron Microscope
TGA – Thermal Gravimetric Analysis
TIF – Tree Initiation Field
TIT – Tree Initiation Time
TIV – Tree Initiation Voltage
XLPE – Cross-linked Polyethylene

Table of Contents

Chapter 1

Introduction

There is a rapid development world wide of the electric power networks which together with a wish for a more reliable power generation and distribution emphasizes the need for novel ideas. Today the public opinion is demanding a more environmentally sustainable choice of new solutions. Moreover local and national grids are gradually being connected to create a so called "supergrid", as it is for example planned that countries like the United Kingdom and Iceland are to be connected with the European continent. Progress is also made to further strengthen the grid by additional international links, both inland and across seas [1]. Many of these projects require installations of high voltage cables. In addition, the high voltage direct current (HVDC) technology is becoming attractive as it provides the most feasible technical and economical solution for many applications and especially new types of extruded polymeric cables are to be developed and used as a mean for electric energy transportation.

The increased use of high voltage cables for energy transmission is followed by a desire to further increase their operating voltage level for increasing transmission capacity and for reducing losses. This leads to a demand for better cable insulation materials that can withstand the resulting increase in electric stress. The choice of insulation material has over the past decades gradually changed from the traditional mass-impregnated paper in favour of cross-linked polyethylene. As the polyethylene-based insulation is improved, it also becomes more attractive for the higher voltage ratings.

So far the desired development has been achieved by producing insulation materials with fewer impurities, reducing the negative effects imposed by the presence of contaminants. Today it becomes more and more difficult to improve the insulation quality much further using this approach due to the high costs involved in making the materials even purer. There is a need for other paths for improving the resistance towards electrical failures. The most promising approaches considered nowadays rely on addition of either nano-sized particles or chemical additives known as "voltage stabilisers". In the work described in this thesis the effect of voltage stabilisers is in focus.

In parallel with the development of new materials, follows a need to elaborate suitable test methods that allows for evaluating and verifying which materials would prove reliable in the next generations of power cables. Several properties are necessary to consider, here the focus is on how to verify a material's resistance to electrical treeing and the proposed solution relies on optical observations along with detection and analyses of partial discharge (PD) activity during the treeing process.

This thesis describes part of a twin PhD student project performed in collaboration with the division of Applied Chemistry/Polymer Technology of the Department of Chemical and Biological Engineering at Chalmers University of Technology, financed by Chalmers Area of Advance in Materials Science. The other part of the project, performed by Markus Jarvid [2], focused on chemical aspects related to voltage stabiliser synthesis and performance. In a natural way the jointly performed activities overlap to some extent.

1.1 Outline of the Thesis

Chapter 2 presents background information that establishes a relation between the presented work and previously published results. Phenomena of degradation by electrical treeing as well as different testing methods used for tree detection are described. Approaches utilized for enhancing the electrical strength of XLPE as cable insulation material are also elucidated, as are means of data analyses.

Chapter 3 proposes a new methodology for testing and comparing material's resistance to high electrical stress. Four different test objects are compared and evaluated, two of wire type and two of needle type. It is further discussed how the multitude of trees appearing in the wire type objects can be statistically analysed and a verification that treeing is incepted on equal terms is provided.

Chapter 4 elucidates how optical detection of tree initiation can be complemented by analysing results of PD measurements during the tree formation. It shows how the PD activity reflects the tree growth and an approach on how this information can be used for estimating the electrical tree initiation is suggested. Additionally, some interesting results are shown that illustrate the influence of gas release from tree channels on the tree growth rate.

Chapter 5 uses the developed test methodology and analysis for evaluating how various voltage stabilising agents affect the tree initiation of modified XLPE-based materials. Several different voltage stabilisers are compared, some yielding in a considerable increased performance. The voltage stabilising efficiency is further correlated to values on electron affinity and ionisation potential of the added molecules.

Chapter 6 summarises the important results of this thesis and in Chapter 7 some suggestions for continuing future work are presented.

1.2 List of Publications

The thesis is based on the work contained in the following publications, referred to by their Roman numerals in the text:

I. A. Johansson, S. Gubanski, J. Blennow, M. Jarvid, M. Andersson, B. Sonerud, V. Englund and A. Farkas, *"A Versatile System for Electrical Treeing Tests under AC and DC Stress using Wire Electrodes"*, Proceedings of Jicable Conference, Versailles, France, 2011.

II. A. Johansson, A.-M. Sandberg, B. Sonerud, J. Blennow and S. Gubanski, *"Wire-Plane Electrode System for Electrical Tree Initiation Exposed to AC and DC Voltage Stress"*, Proceedings of the 17th International Symposium on High Voltage Engineering (ISH), Hannover, Germany, 2011.

III. M. Jarvid, A. Johansson, V. Englund, S. Gubanski and M. Andersson, *"Electrical Tree Inhibition by Voltage Stabilizers"*. Conference on Electrical Insulation and Dielectric Phenomena (CEIDP) Montreal, Canada, 2012.

IV. M. Jarvid, A. Johansson, J. Blennow, M. Andersson and S. Gubanski, *"Evaluation of the Performance of Several Object Types for Electrical Treeing Experiments"*, IEEE Transactions on Dielectrics and Electrical Insulation, vol. 20, issue 5, pp. 1712-1719, 2013.

V. A. Johansson, T. Hammarström, M. Jarvid and S. Gubanski, *"Analysis of Multiple Electrical Trees Incepted at Wire Electrode Test Object by Means of PD Detection"*, Jicable HVDC'13, Perpignan, France, 2013.

VI. M. Jarvid, A. Johansson, J. M. Bjuggren, H. Wutzel, V. Englund, S. Gubanski, C. Müller and M. R. Andersson, *"Tailored Side-Chain Architecture of Benzil Voltage Stabilizers for Enhanced Dielectric Strength of Cross-Linked Polyethylene",* Journal of Polymer Science Part B: Polymer Physics, vol. 52, issue 16, pp 1047-1054, 2014.

VII. M. Jarvid, A. Johansson, R. Kroon, J. M. Bjuggren, H. Wutzel, V. Englund, S. M. Gubanski, M. R. Andersson and C. Müller, *"A New Application Area for Fullerenes: Voltage Stabilizers for Power Cable Insulation"*, Advanced Materials, vol. 27, issue 5, pp 897-902, 2015.

VIII. H. Wutzel, M. Jarvid, J. M. Bjuggren, A. Johansson, V. Englund, S. Gubanski and M. R. Andersson, *"Thioxanthone Derivatives as Stabilizers against Electrical Breakdown in Cross-Linked Polyethylene for High Voltage Applications"*, Polymer Degradation and Stability, vol. 112, pp 63-69, 2015.

IX. M. Jarvid, A. Johansson, V. Englund, A Lundin, S. Gubanski, C. Müller and M. R. Andersson, *"High Electron Affinity: a Guiding Criterion for Voltage Stabilizer Design"*, Journal of Materials Chemistry A, vol.3, pp 7273-7286, 2015.

The following publications are out of the scope of this thesis:

X. E. Doedens, A. Johansson, M. Jarvid, S. Nilsson, M. Bengtsson, J. Kjellqvist, *"Effects of Inclusions of Oxidized Particles in XLPE on Treeing Phenomena"*, Conference on Electrical Insulation and Dielectric Phenomena (CEIDP) Montreal, Canada, 2012.

XI. *M. G. Andersson, M. Jarvid, A. Johansson, S. Gubanski, M. R. StJ. Foreman, C. Müller and M. R. Andersson, "Dielectric Strength of γ-Radiation Cross-Linked, High Vinyl-Content Polyethylene",* European Polymer Journal, vol. 64, pp 101-107, 2015.

Chapter 2

Background

This chapter presents an overview on the phenomenon of electrical treeing. The focus is on treeing in polyethylene (PE), and especially in cross-linked polyethylene (XLPE) for high voltage cable insulation, this material is being investigated in this project. As a thorough review of the phenomenon is provided in [3], only some relevant aspects are highlighted by presenting different factors affecting electrical tree inception, e. g. its growth and a resulting breakdown. Ways of improving polymeric insulation properties are discussed together with some comments on how research can further be advanced with the purpose of better qualifying newly developed materials. This is followed by describing various approaches on measuring and analysing experimental data, either for understanding the treeing phenomenon itself or for characterising insulation material qualities. Finally, relevant techniques to statistically present and understand treeing data employing Weibull statistics are discussed.

2.1 The Phenomenon of Electrical Treeing

Important degradation and breakdown mechanisms in high voltage cable insulation are associated with the phenomena of treeing. Two different types are distinguished, electrical and water treeing, the latter also known as electrochemical treeing. These are separate phenomena and only electrical treeing will be considered here, although water trees might act as points of initiation for electrical trees [4]. Observations on electrical treeing were published already in the 1950's [5]. Since then a substantial amount of research has been made on this subject; even so the topic is still not fully understood and relevant research activities are still much in demand.

Electrical trees originate at points with highly divergent electric fields, e. g. at surfaces of contaminants, protrusions, voids or at tips of water trees. Once initiated, they grow into branched or bush-like structures and continue growing until they eventually lead to a breakdown. Even though treeing is often linked to polyethylene cable insulation, other materials exposed to high electric field stress can also be affected, examples are polypropylene [6], epoxies [7], silicones [8], polyimide [9] or poly(methyl methacrylate) (PMMA) [10]. The electrical trees consist of hollow gas filled tubules, which penetrate the material whilst forming the tree-like structure. These tubules range between ~1 and ~30 µm in diameter [11]. Figure 2.1 shows an example of experimentally grown electrical tree in XLPE, initiated from an ultra-thin wire electrode.

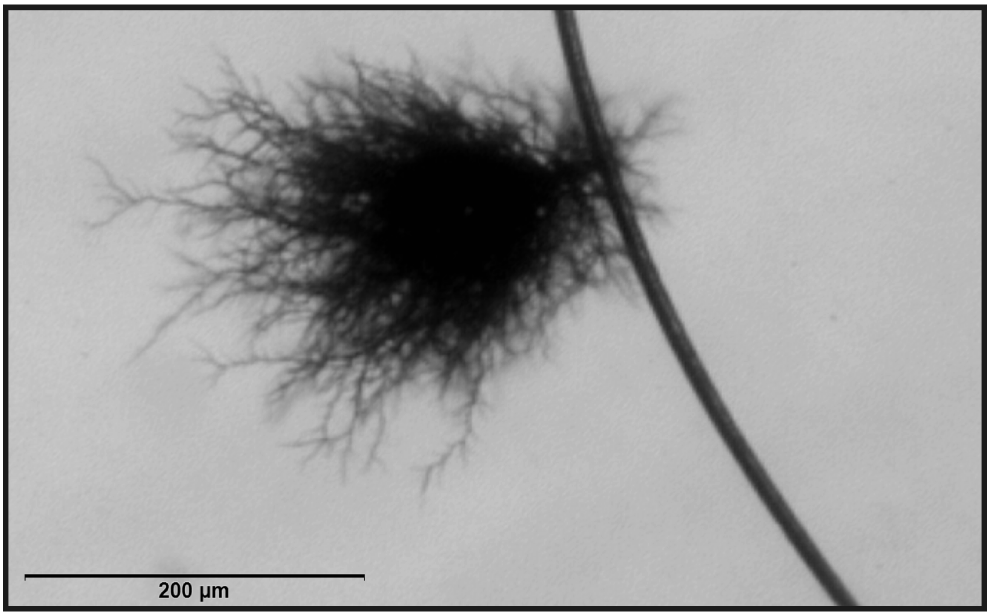

Figure 2.1 *Experimentally grown electrical tree in XLPE from a wire electrode of 10 µm in diameter under ramped AC voltage.*

2.1.1 Different Stages of the Treeing Process

The process of electrical treeing is generally divided into four separate stages; initiation, propagation, runaway and breakdown [12]. The initiation is preceded by an inception stage during which an emission of electroluminescence (EL) has been observed [13]. These stages are illustrated in Figure 2.2 and are further discussed in more detail.

The processes involved in the tree initiation are complex and still not fully understood, though there exist some different hypotheses related to this issue [14-16]. Laurent and Teyssedre [12] have postulated a stage process where the tree originates in a "void-free" material by excitation of molecules due to collisions with hot electrons or by charge recombination. This yields formation of nano-voids, where the mean free path of the charge carriers increases and a solid-gas interface appears. Further enlargement of such voids can now be caused by space charge induced electro-mechanical forces. Eventually, the voids reach a micrometer size and the degradation proceeds into a more severe stage, as gas discharges can now take place, an electrical tree is said to be incepted. When a void becomes able to retain partial discharges, at a size of approximately 10 μm in diameter [17], its boundaries start eroding. Hot electrons, UV light and thermal stress cause chain scission of the polymer matrix [12, 18]. The time required for this process can vary from some nanoseconds up to several weeks and is highly dependent on the type of applied electric stress. For inception to occur the electric stress needs to exceed a specific threshold level [19].

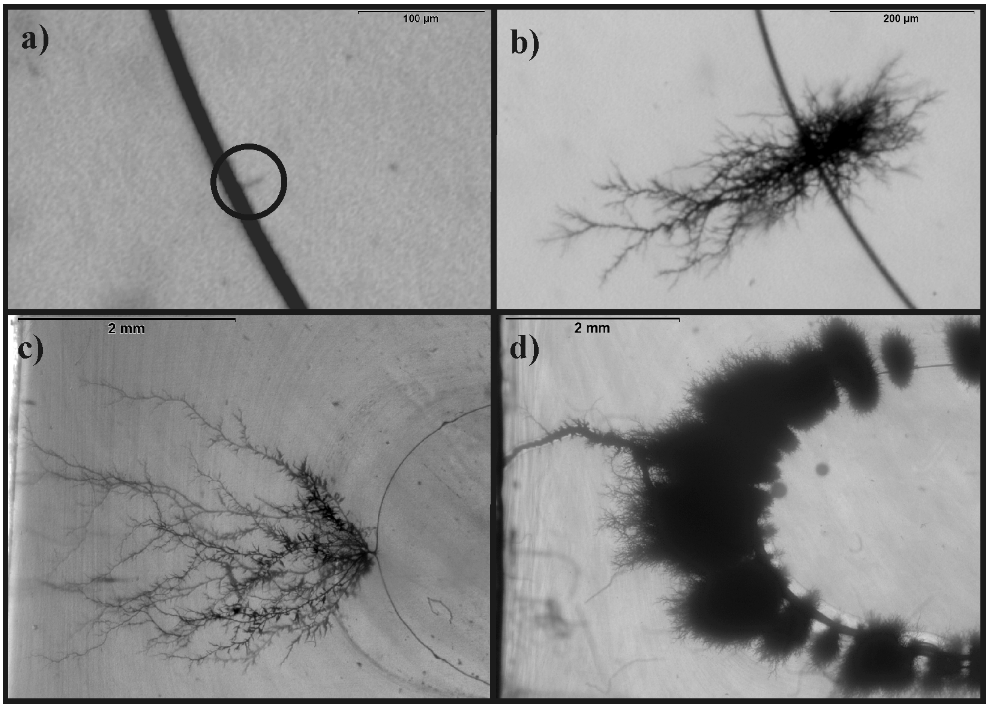

Figure 2.2 *Microscopic observations of the process of tree growth, shown with the stages of (a) initiation, (b) growth, (c) runaway and (d) breakdown. Trees are grown in XLPE with AC voltage conditions.*

Once the tree is initiated, it will start to propagate through the insulation, accompanied by partial discharges occurring in the created hollow tubules. The hot electrons of the plasma start deterioration processes in the dielectric at the tip of the tree, causing the tree channels to stretch. Furthermore tubules also start branching in a fractal-like manner. The rate of tree growth or propagation often changes with time. At the beginning the tree growth is usually fast, often followed by a period of a limited growth, a plateau region. A period of increased growth rate starts again thereafter. As various tree types may be formed, the growth rate can further depend on the type of tree formed.

Eventually the tree will reach a critical stage, where its growth rate increases rapidly, until it bridges the entire insulation thickness and causes a breakdown. According to Chen at al. [20] this occurs when the electrical field at the periphery of the branches reaches a value of around 100 MV/m. As one or maybe a couple of branches reach the opposite electrode, a gaseous path is formed and a complete breakdown of the insulation is close. The small width of the tubules may cause a delay of the breakdown for some time, until the tubules are widened sufficiently for an arc to be formed [17]. Another reason for such a delay can be related to the conductivity of tree tubules or perhaps even the pressure of the gaseous by-products inside them, as reported for polypropylene, where the time between bridging the entire insulation by a tree and the complete breakdown could take several hours [6, 21]. In the last stage the heat generated from the arc melts and carbonizes the discharge channel and the material loses its insulating ability.

2.1.2 Different Tree Types and Their Properties

Electrical trees have been classified into different categories depending on their appearance [22]. The most common division is between bush and branch trees. For distinguishing among them, a classification of fractal dimension (d_t) [23] may be used. Bush trees are, as the name suggests, denser in their structure with more branching and have a fractal dimension, $2 < d_t \leq 3$. Branch trees, on the other hand, exhibit a more sparse appearance with less branching and a fractal dimension less than two [11]. Examples of bush and branch trees are illustrated in Figure 2.3. More recently this distinction has evolved into a plenitude of types as well as combinations of the different types: pine, bush-branch, etc. [20, 24-26].

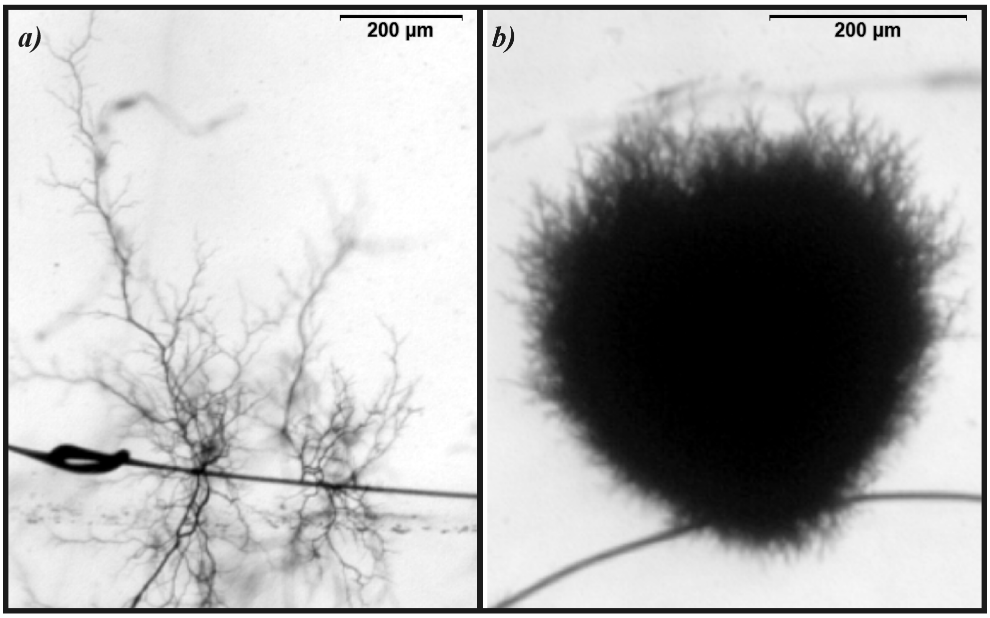

Figure 2.3 *Microscope pictures illustrating branch (a) and bush (b) type electrical trees, experimentally grown in XLPE under ramped AC voltage.*

As for the bush and branch trees, these have appeared to also have different properties [17]. The less dense structure of the branch tree shows different discharge behaviour in comparison to the bush trees, individual pulses are very short (1-2 ns) in time and the magnitude of the partial discharges ranges between 0.1 pC up to 1 nC during their growth. The rate of pulses is reported to remain nearly constant at ~200 pulses per second. The discharges do not bridge all the way to the branch tip, but rather widen the tubules and cause additional branching. Considering the bush tree, individual pulses are longer in time, they can reach magnitudes above 1 nC and levels of up to 2000 pulses per second have been reported. The partial discharges are believed to be concentrated in the body of the bush, creating a large amount of branching. However at the periphery of the tree, only minor damage is generated. The propagation of a bush tree is also slower compared to that of a branch tree. Whereas the larger discharges associated with branch trees cause the local breakdown to reach the tip of the tree channel resulting in further damage which increases tree growth. In many cases the two tree types are combined. The trees start of branch-like, at the plateau region a sharp change to the bush structure has been reported [11] and when the growth rate increases again a bush-branch tree is formed.

2.2 Factors Affecting Treeing Processes

A number of factors affect the process of treeing. The properties of the incepted trees depend on the type of the applied electrical stress, varying with AC, DC or impulse voltages. The related characteristic features, including findings regarding influence of voltages containing harmonics and PWM voltages, are summarised below. External factors, e. g. temperature and pressure additionally affect the treeing characteristics. Finally, material properties, such as material morphology as well as injection and presence of space charge are of importance.

2.2.1 Influence of Different Voltage Types

AC Voltage Conditions

As power frequency AC voltage is utilised in power systems world-wide, the effect of AC stress on electrical treeing has correspondingly been examined extensively. Since electrical treeing is a statistical process, treeing tests are preferably performed at low voltage ramping speed [27] that allows for the inception process to happen within a relatively narrow voltage span. The frequency of the applied voltage influences both the initiation voltage and the tree shape [28], for 50 Hz the trees are predominantly of branch type with mainly one leading channel that approaches the opposite ground plane. At 1 kHz the trees become much denser with several main channels bridging the insulation in addition to a multitude of smaller branches in the tree structure. The tree growth rate also appears to increase with higher frequency. Due to such a change in tree properties, it is not recommended to increase the voltage frequency for speeding up the testing. When, on the other hand, testing is performed at a constant AC voltage levels, the tree behaviour changes [20] with amplitude, at lower voltage levels the trees grow as predominantly branch structures, whereas when the voltage magnitude becomes higher, bush type trees are incepted. These different structures are also accompanied by significant variations in the growth rate and the propagation time. Table 2.1 summarises how different properties of AC stress as well as temperature affects tree initiation and growth.

Table 2.1 *List of some properties of electrical treeing under AC conditions*

AC voltage property	TIF or TIT	Grow rate	Tree type
Frequency ↗	↗	↗	more bush-type
Ramp rate ↗	↗	↗	more bush-type
Amplitude ↗	↘	↗	more bush-type
Temperature ↗	↘	↗	more branch-type

DC Voltage Conditions

Electrical trees appearing under DC stress behave differently from trees resulting from AC stress. However, for this case the research activities have not been equally extensive. The effect on treeing has been studied using:

(i) ramped DC voltage [29]
(ii) grounding after a DC voltage pre-stress [30]
(iii) polarity reversal after DC voltage pre-stress [31]
(iv) application of voltage pulses of opposite or the same polarity after DC voltage pre-stress [32, 33].

It was found that breakdown following a treeing process was higher for negative polarity as compared to positive one [31, 34], this was explained by the effect of injected space charges, the latter being more prominent in the case of negative voltage and thus in turn reducing the effective radius of the electrode and thereby increasing the electric field at its tip.For the DC case it has also been presented that a higher ramp rate reduces the tree inception level [31], an opposite dependence as compared for the case with AC voltage ramp rates. This tendency can be explained by homo charge injection, which becomes more prominent for the slower DC voltage ramping rate. Concerning the effect of DC voltage with superimposed impulses of the opposite polarity, the breakdown levels were found to be lower comparing to applying impulses alone [31]. For this cases a build-up of hetero charge at the needle tip is believed to increase the stress on the material at polarity reversal. The experiments with grounding a DC pre-stress voltage resulted in electrical treeing and breakdown at lower voltage as compared to the short term DC breakdown level [35]. This is also supported by results from tests with addition of antioxidants in XLPE [30], which showed that grounded DC of negative polarity resulted in lower voltages of tree inception. Table 2.2 summarises how different DC stress parameters affect tree initiation.

Table 2.2 *List of dependence on electrical tree initiation for DC conditions*

DC voltage property	TIF or TIT
Positive polarity	↘
Ramp rate ↗	↘
Amplitude ↗	↘

Further Types of Voltage Waveforms

As indicated above, treeing phenomena under impulse voltages has been investigated. Sekii [36] used impulse voltages of positive and negative polarity. The results for positive polarity showed a lower tree inception level, similarly as is the case for DC testing. It was further seen that positive impulses created longer tree channels and for each of the applied pulses the length increment was greater. The effect of needle electrode radius was in [37] investigated utilising impulse voltage stress and likewise for negative polarity the trees developed at a slower rate. Their appearance also differed depending on polarity. For needle radii smaller than 40 μm there was a pronounced polarity effect, while for larger needle radii the effect was lost, mainly because the field distribution changed from non-uniform to quasi-uniform. Impulse voltage was applied to pre-grown trees in [38], resulting in noticeably elongated and broadened channels stretching from the pre-grown trees, in case the latter were of bush type. When in contrary applying impulses to branch trees, their appearance remained unaffected. Tree inception for combinations with superimposed impulses on AC power frequency voltage was examined in [39]. It was shown that for low amplitudes of the AC voltage, the impulse voltage level needed for tree inception was relatively constant. For higher AC voltages the impulse tree inception voltage decreases with increasing the AC level.

Also with the increasing use of voltage shapes containing higher degrees of harmonic content, some recent investigations also covered the influence of harmonics on electrical treeing. Indications that tree growth becomes more extensive in such conditions are presented in [40]. Similar results demonstrating shorter times for tree inception at AC voltage with harmonic distortions are reported in [25].

2.2.2 Influence of Temperature and Pressure

Two parameters influencing electrical tree development are temperature and pressure. The effect of pressure on electrical tree initiation has not been extensively analysed so far. In [41] however, an attempt to evaluate this effect at an interface of a silicone cable joint is reported. A dependence of electrical tree inception voltage on hydrostatic pressure, ranging between one and fifty bar, showed a significant increase, whilst the growth rate increased only slightly. It was also discovered that branching developed stronger at higher hydrostatic pressure.

The influence of treeing properties with temperature has been more broadly covered. According to [17] the tree inception is only slightly dependent on temperatures, in the range between 25 and 70 °C. However, above this temperature range a strong drop in the inception time by an order of magnitude was observed, which remained stable up to the material's melting point. The authors also convey that branch type trees were typical at temperatures above 80 °C and they grew faster. A similar trend with lower tree inception levels at elevated temperature were reported in [42], for polyester and epoxy resins. At cryogenic temperature of 77 K trees are difficult to initiate, as the inception voltage is strongly increased [17, 43], the growth rate is reported to be low and before the trees become 0.5 mm in length the glassy polymer cracks.

2.2.3 Influence of Material Microstructure

The microstructure of a material, including degree of crystallinity and lamellae thickness, are also parameters to consider as they affect the treeing process. By decreasing the lamellae thickness, the amorphous regions in between are reduced, and tree initiation voltage is thus increased [44, 45]. Investigations comparing new cables with ones operated in service [46] revealed a slight decrease in tree initiation time but a clear decrease of growth rate for cables being in operation for 17 years. This effect was attributed to a resulting higher degree of crystallinity and decreased crystal size occurring from electrical and thermal stresses at cable operation. Tree growth rate and the coupled tree type has also been reported in [47] to depend on morphological factors.

Presence of mechanical stress or strain moreover affects the treeing process. In [48] the authors compared slowly cooled and quench cooled needle test objects, and the resulting mechanical stresses in the polyethylene was found to be higher in the quench cooled material. However, after allowing these objects to relax, treeing resistance became larger than for the slowly cooled objects. The difference in strain level was considered as the influencing factor. A local change of material microstructure may also be caused due to local heating associated with PD activity in tree channels [49].

2.2.4 Influence of Additives

Influencing the treeing initiation can naturally be used favourably to increase polymeric materials' resistance to treeing by introducing additives. Two main groups of additives are classified; chemical compounds known as "voltage stabilisers" and nano-size fillers (nano-particles). The concept of using voltage stabilisers for inhibiting electrical treeing in polymers has been around for several decades [50]. Recently new advances in this field [51] have been highlighted. It has been postulated that voltage stabilisers can dispose high-energy (hot) electrons in such a way that the polymer matrix is left unharmed. Ashcraft et al. [52] found a correlation between the efficiency of a voltage stabiliser and its ionization energy. Accordingly, the hot electrons that otherwise might cause electrical tree inception will on impact with a voltage stabiliser molecule cause it to ionize, this way creating a stable radical cation and releasing two non-harmful electrons of lower energy, as illustrated in Figure 2.4 (a). The stabiliser is designed to ionise at a lower energy compared to the polymer, thus free electrons are prevented from reaching levels of kinetic energy harmful to the bonds in the polymer chains. The stabiliser is also suggested to include the ability of healing already ionised polymer segments, see Figure 2.4 (b). The voltage stabiliser can possibly also be regenerated by combining with a free electron, see Figure 2.4 (c). Furthermore, a field-grading effect of voltage stabilisers is discussed in [53, 54], where it is proposed that polarisable stabilising compounds will be attracted by the enhanced electric field close to a defect, where it will increase the permittivity and thus reduce the electric field strength.

Several publications show that an addition of voltage stabilisers improves the resistance towards electrical treeing significantly [51, 55]. In addition, there are also a few commercially available antioxidants and ultraviolet (UV) stabilisers that are claimed to have electrical tree inhibiting properties [56]. However, in cases where similar structures have been evaluated using different types of measuring setups, the measured efficiency varies considerably and inquiries into the reasons behind the different results have generally not been made. An example is the evaluation of 2,4-dioctyloxybenzophenone where the different methods in [55] and [57] resulted in widely different stabilising effects. More information about factors influencing the stabilising effect, e.g. test conditions, is clearly needed. It is also desirable to expand the library of molecules functioning as voltage stabilisers and to better predict their effect in real life applications.

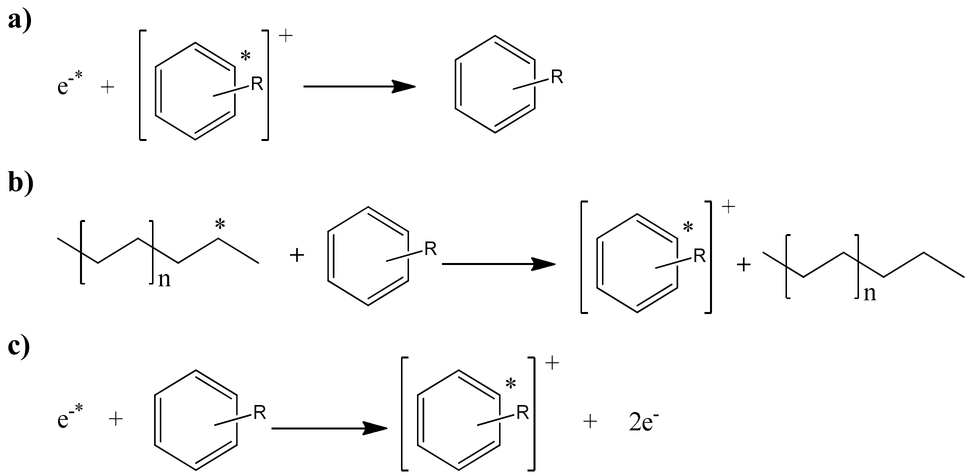

Figure 2.4 *Possible mechanisms of a voltage stabiliser; a) ionisation, b) healing already ionised polymer chains and c) regeneration.*

A second approach to improving the electrical properties of an insulating material is by addition of nano-sized particles to the polymer [58-61]. Yamano and IIzuka [62] showed that both the electrical tree inception level and especially the time to breakdown increases by addition of Al_2O_3 nano-particles together with phtalocyanine acid to a low density polyethylene (LDPE). The increase in TIV is ascribed to two main factors; absorbance of kinetic energy of electron carriers (similar to the case with stabilisers) and a local electric field distortion in the vicinity of the nano-particles. One of the challenges with adding nano-particles is however the need to accurately control their even dispersion in the polymer matrix, as this is found to highly influence the additive efficiency.

2.3 Object Types used in Treeing Tests

Before choosing an appropriate method for the electrical treeing study, many different factors need to be considered. Depending on the property to be explored as well as the properties of the material to be investigated itself. Several alternative options exist, regarding both the test object type and the tree detection method. All the methods have in common the utilisation of a sharp geometry of the high voltage electrode, required for introducing highly divergent electric stress in the test object. The electrode geometries utilized for treeing purposes include various modifications of needle-needle [63, 64] and needle-plane [26, 63-67] electrode types. Typically, steel needles with a tip radius of 3, 5 or 10 μm are used, though semiconducting protrusion electrodes have also been introduced [6, 22]. An alternative way for electrical treeing tests is the use of a wire-plane electrode configuration [55, 68].

The most common manner of initiating trees by using the needle electrodes is standardized in ASTM D3756-97 [27] and has thus yielded an extensive knowledge on their performance. For example, in [69] studies on the influence of several different electrode materials on the tree initiation showed a linear correlation between the tree initiation voltage and the work function of the oxide-covered electrode. The authors argued that charge injection is partly influenced by the oxide presence. Despite of this broad experience, a few concerns have been raised regarding the efficiency of needle electrodes, as the delicate needle tips can easily be damaged during the insertion, which causes their radii being difficult to control accurately. Voids and mechanical stress around the needle tips are also among the reported problems, which are likely to occur during the insertion or as a result of different thermal expansion coefficients of the metallic electrode as compared to the polymer [69].

Bamji et al. [70] have argued that using semiconducting protrusions provide a more realistic stress, as the insulating layer in a high voltage cable is not in contact with metal, but with semiconducting layers. Semiconducting protrusions were also used in [71] to incept electrical trees, although in this case with the purpose to study space charge injection into the polymer.

More recently an electrode arrangement utilizing an ultrathin tungsten wire instead of the needle [55, 68] has been introduced for the purpose of evaluating the resistance towards electrical treeing by improved insulation materials. The wire-plane configuration reduces some of the problems related to the needle electrode while creating additional benefits, such as a parallel formation of several trees in each tested object and exposure of a larger volume of the tested material [72], which in turn also allows for a larger amount of treeing data from each tested object.

2.4 Treeing Detection Methods

So far optical detection appears to be the most common and robust detection method for testing the resistance to electrical treeing in transparent or semi-transparent polymeric materials. This approach is intensively utilized also in this work. Microscopes equipped with CCD cameras usually provide excellent images. This way the different types of trees can easily be distinguished and a possibility to detect the tree growth in real time makes it easy to control the measurements. A novel technique to detect trees by using x-ray tomography imaging has recently been proposed [73]. As a result, trees can be visualised in three dimensions, even in non-transparent materials.

To further explore and understand the different stages of treeing, partial discharge (PD) measurements are often incorporated in the tests as a complimentary or as the main technique. Some results include differing PD patterns depending on the tree type [74], as is described earlier. It is also shown that PD patterns during the electrical treeing process can be linked to time-to-breakdown. PD amplitude might also indicate if tree channels are non-conducting or conducting (carbonised). The latter have been found to be characterised by apparent charges two to three orders of magnitude smaller as compared to discharges occurring in non-conducting trees, i.e. below the sensitivity of commercial PD detectors [75]. An alternative way to detect partial discharges in tree channels is by using UHF sensors, as demonstrated by Sarathi et al. [25]. Detecting electrical trees and estimating their properties through measurements of test object impedance has also been utilized [76]. This method relies on the fact that when an electrical tree appears within the test object, particularly when its channels become conductive, the impedance of the object changes due to altering of the electric field distribution.

2.5 Statistical Analyses of Treeing Data

Whereas different approaches are used for presenting and analysing the data of electrical treeing tests, a common way also proposed in standards [17, 27], is by means of the Weibull distribution [77]. This is an extreme value statistics where a chain fails through its weakest link. Breakdown models describing treeing phenomena using Weibull statistics have additionaly been developed by Hill and Dissado [78]. The three-parametric Weibull distribution is defined according to Equation 2.1.

$$F(x;\alpha,\beta,\gamma) = 1 - e^{-\left(\frac{x-\gamma}{\alpha}\right)^{\beta}} \;;\; x \geq \gamma \tag{2.1}$$

Here x represents the evaluated quantity. γ denotes the threshold value, this value must have a physical meaning as to why breakdown cannot occur below it. α describes the scale parameter, which represents how high above the threshold the probability of failure equal to 1/e or 63 percent. The voltage or field for this 63 % percentile is in this work denoted as V_{63} or E_{63}. This value is analogous to the mean value of the Gaussian distribution. β represents the shape value of the distribution. A graphic representation showing a cumulative Weibull probability plot is shown in Figure 2.5; the above named parameters are indicated in the figure. The same data are plotted as a density function in Figure 2.6, where the influence of the shape parameter, β, is clearer. A small β (<3) corresponds to a right-side tail (towards higher breakdown levels) in the density function and a high value (>3) corresponds to a tail stretching towards the left side.

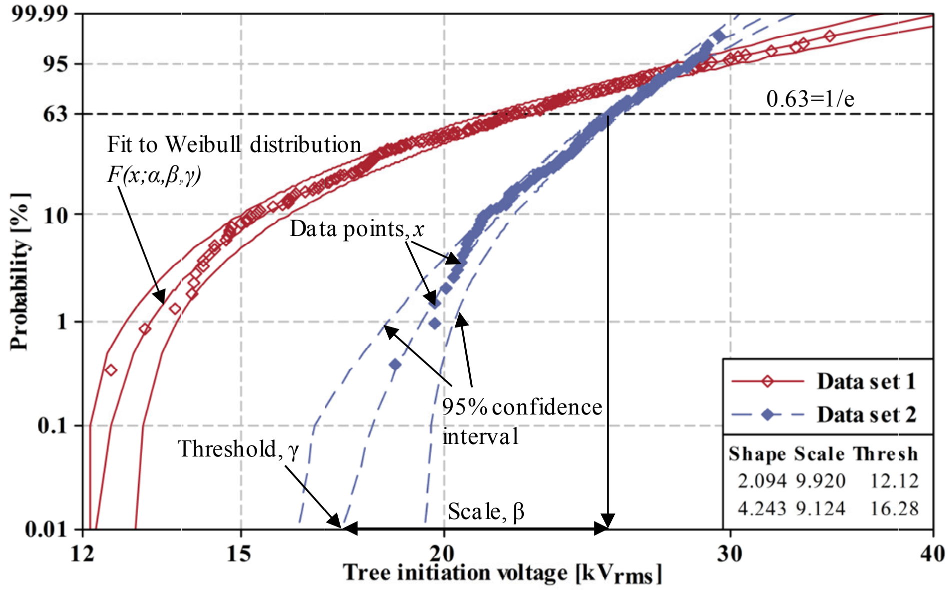

Figure 2.5 *Examples of three-parametric Weibull probabilities with shape, scale and threshold values indicated.*

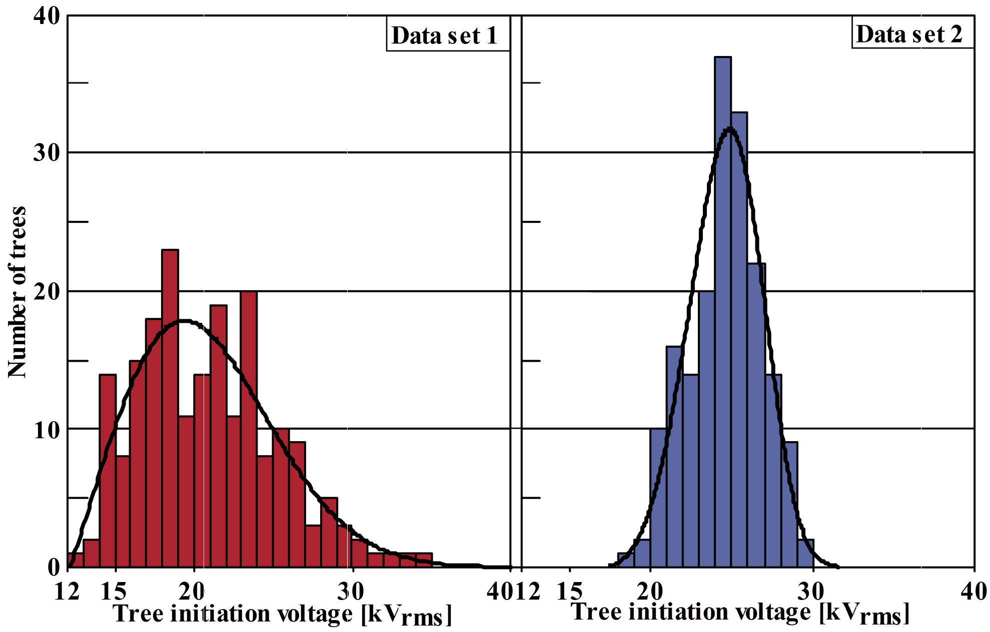

Figure 2.6 *Density functions for the two examples presented in Figure 2.5.*

A special case of the Weibull distribution utilises a threshold value set to zero, known as the two-parametric fit, which is often used if the data amount is insufficient to fit the three-parametric type. Different methods for fitting data to the Weibull distribution include the maximum-likelihood estimator (ML) and linear regression with least squares (LSR), together with more complex estimators [79] especially designed for smaller data sets. In this work the LSR method has been chosen using Minitab 16 statistical software, in which the goodness of fit is tested by analyses of the Anderson-Darling- (AD) and p-values.

Chapter 3

Evaluation on the Performance of Wire Objects and Multiple Treeing Analysis

In this chapter different properties of the wire test objects are discussed including possible ways to analyse the multitude of trees initiated in them. As wire-type objects have not been used widely, a deeper understanding of their behaviour is needed. This is made through comparative studies with the conventional needle-electrode test objects. The presented material attempts at filling this knowledge gap, where the design of the wire test objects is elucidated together with the results of tests performed on both needle and wire objects.

3.1 Design of Test Objects

Four different test object types have been studied. Among the wire-electrode types, the earlier developed design with a semiconducting tab as well as a newly developed object, without the tab, are compared, the latter being introduced within the framework of this project. As already indicated, they all utilise a sharp geometry of the tree inception electrode to achieve the highly divergent electric field strength in the dielectric material necessary to initiate the process of electrical tree growth. The examined four different object types are further on denoted as type A, B, C and

D. The objects of type A and B have a wire-plane electrode configuration. The needle-needle objects, C and D, are prepared according to the ASTM D3756 – 97(2010) standard [27]. Electrical treeing tests made with the A type object have previously been reported in [55, 68]. The B type object is a further development of object A during the beginning of the reported project. Figure 3.1 illustrates the four object types together with relevant dimensions; a photograph showing actual examples of the objects is also provided.

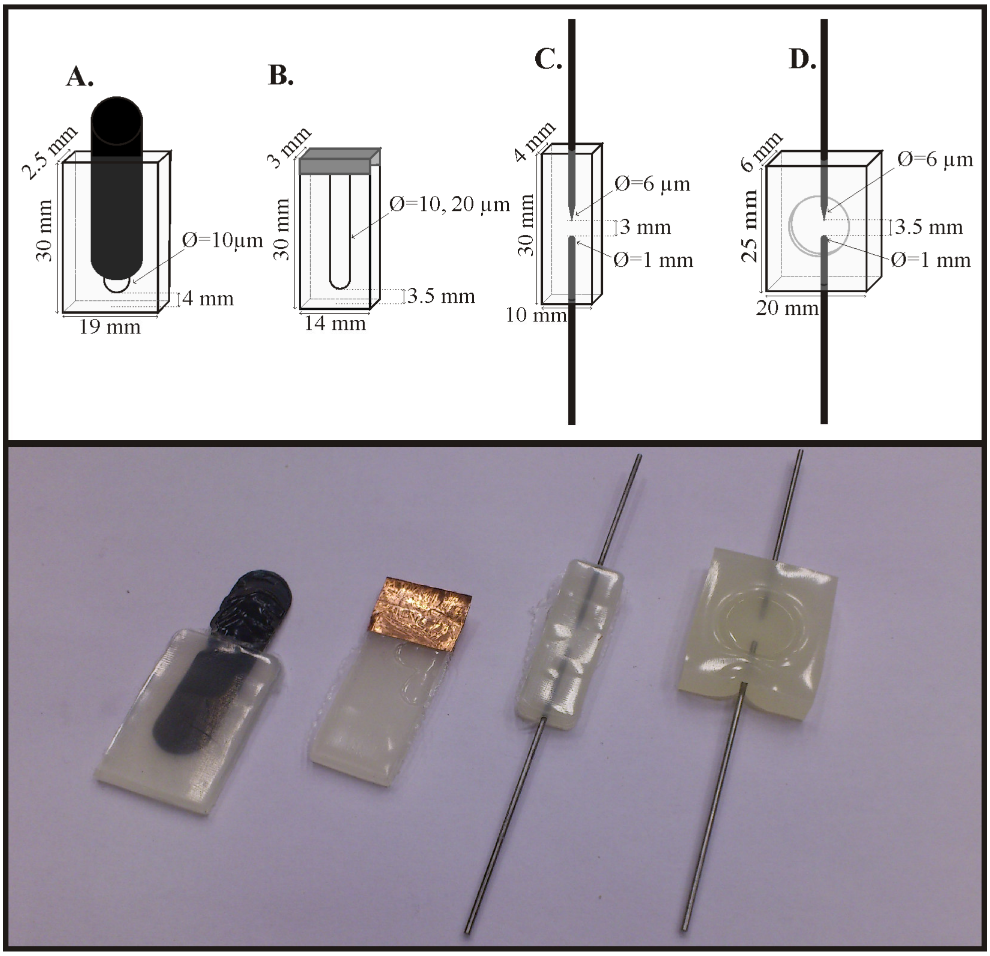

Figure 3.1 *Four investigated test object types; denoted A, B, C and D. The A and B type are designed with wire-plane geometry, whereas C and D are of the traditional needle-needle type.*

An ultra-thin tungsten wire, with a diameter of 10 or 20 μm, is used as the wire electrode. The A type object is made with the wire of 10 μm in diameter. The B type is however prepared in two sets; one with each of the wire diameters, thus it is further divided into $B_{10\mu m}$ and $B_{20\mu m}$ when this distinction is presented. Tungsten was selected as the electrode material for its hardness and high elastic modulus as well as for providing good electron emission ability. Stainless steel needles are used as electrodes in C and D objects, one needle having a sharply polished tip of a 3±1 μm radius at the end inclined at 30°. The second needle electrode has a semi-spherical tip with a radius of 0.5 mm. The objects are manufactured thin enough, enabling optical observation of electrical treeing. In this work only polyethylene has been investigated, which is semi-transparent, and the treeing is thus visible quite clearly in real-time. However by using electrical detection, as is introduced in Chapter 4, a transparent or semi-transparent material is no longer a prerequisite. The polyethylene with the trade name Borlink LS4201S was provided as LDPE resin by Borealis, Sweden and is characterised by a melt flow rate (MFR) of 2 g/10 min at 190 °C and 2.16 kg and a density of 922 kg/m^3. This resin, containing dicumyl peroxide and the antioxidant 6,6'-di-tert-butyl-4,4'- thiodi-m-cresol, has a low level of contaminants that may influence electrical measurements and is recommended for use in high voltage applications up to 220 kV. The tungsten wire was supplied by LUMA Metall AB, Sweden, while the steel needles were manufactured by Ogura Jewel Industry, Japan.

3.2 The Electric Field at the Electrode

To calculate the electric field distribution in the test objects, finite element simulations have been performed using Comsol Multiphysics software (vers. 4.2). The four investigated object types have been analysed by electrostatic simulations in 3D to estimate electric field strength in the vicinity of the electrode. The significant difference in dimensions between the electrode (µm) and the object (mm) requires a high number of mesh elements to resolve the electric field distribution. The size of the model can however be decreased by utilising symmetries and thus only a quarter of the objects needed to be modelled. The maximum electric field, at the electrode surface was then calculated.

A simplified field enhancement factor, K, has been introduced in [68] for approximating the maximum electric field at the wire electrode, according to Equation 3.1. By inserting the applied voltage, U, in kV, and K in mm^{-1}, the resulting electrical field, E_{max}, is given in kV/mm

$$E_{\max} = KU \tag{3.1}$$

The 3D simulations further revealed that for the wire-plane electrode arrangement the factor K remained approximately the same along the wire segment in which treeing is expected, not being particularly sensitive to the distance between the wire and the grounded plane.

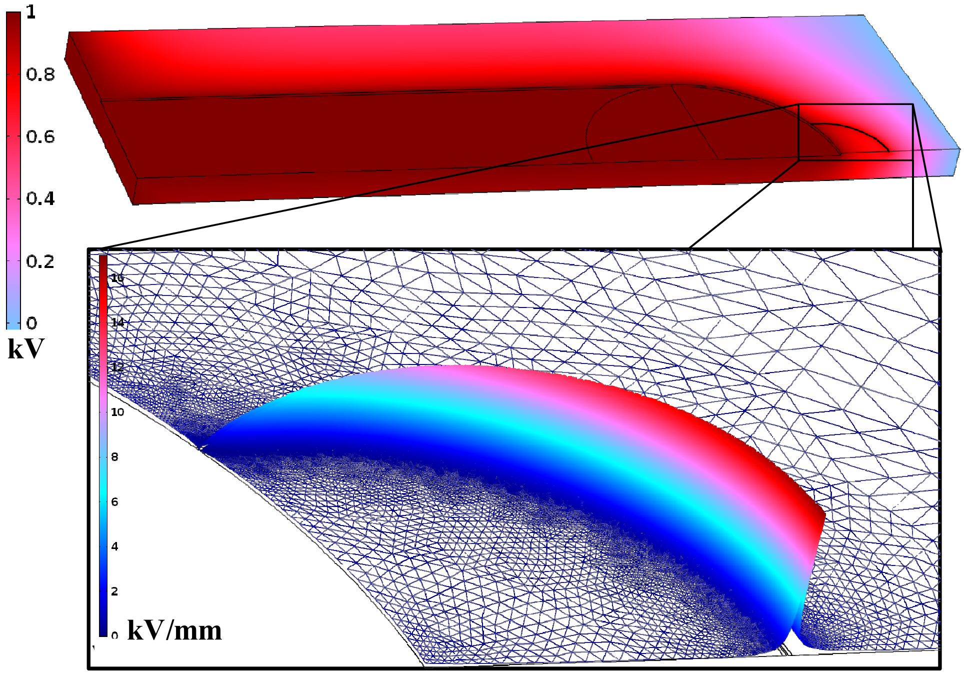

Figure 3.2 *3D simulations of the voltage distribution and the electrostatic field strength in a test object of type A.*

Comparison of the field enhancement factor, *K*, to basic analytical formulas

The electrical field correction functions found from the 3D numerical simulations are compared to analytical expressions for geometries approximating the different electrode systems in the test objects. For estimating the maximum electrical field strength at the tip of the sharp electrode in the double needle-electrode arrangement, $E_{max,DNT}$, an analytical expression derived by Griač et al [80] can be used. This approximation is based on an assumption that the needles can be represented by conducting hyperboloid surfaces and that the sharp electrode radius, r, is much smaller than the other geometries involved, i.e. the radius of the blunt needle, R, and the electrode separation, d. Equation 3.2 illustrates this dependence for an applied voltage U.

$$E_{\max,DNT} = \frac{2U}{r\ln\left[\frac{2d(1+2d/R)}{r}\right]} \tag{3.2}$$

The actual maximum field strength in the dielectric will however be modified due to injection of space charges, which depends on both the material of the electrode and the tested polymer [71, 81]. Taking this influence into consideration would require detailed models of the physical processes involved and further analyses involving this behaviour have not been made.

For obtaining the analytical expression describing the electric field strength, $E_{max,wire}$, in the wire-plane configuration a cylindrical conductor parallel to a plane has been considered [82] as defined by Equation 3.3. Here r stands for the wire electrode radius and d is its distance to the plane electrode. This formula, similarly to the former one, takes into account the geometrical factors only, without considering any space charge effects.

$$E_{\max,wire} = \frac{0.9U}{r\ln\left[\frac{(r+d)}{r}\right]} \tag{3.3}$$

The field enhancement factor, K, considered in Equation 3.1 has been evaluated from the 3D-numerical simulations for all the object types, including the needle-needle ones. For the needle type objects C and D, a good agreement with the analytical expressions describing the maximum electric field strength according to Equation 3.2 was found. From the simulations, K was found to be 70 and 68 mm^{-1} compared to the calculated values of 64 and 63 mm^{-1} using the analytical equation. These differences are due to a small variation in actual electrode distance. For the wire objects the analytical expression of Equation 3.3 was merely used as an indication, as its geometrical basis differs significantly from that of the A and B objects. In this case the simulations rendered values for K of 16, 21 and 12 mm^{-1} whereas the analytical expression provided values of 27, 27 and 15 mm^{-1}, for type A, $B_{10\mu m}$ and $B_{20\mu m}$ respectively. Concerning the objects of type A, the reduction of field enhancement factor from 21 to 16 mm^{-1} is caused by the proximity of the semiconducting tab, which in further investigations appeared to have a significant influence on the obtained treeing results (see more details in Section 3.5.2).

3.3 Preparation of Test Objects

The preparation procedure of the different test object types is described in this section. In order to make the material comparison as representative as possible the manufacturing process of the different object types has been kept practically identical. Following manufacturing, the objects were stored in sealed bags at room temperature until electrical testing. The time between the object preparation and electrical testing was within 30 days for all the batches.

3.3.1 Moulding and Cross-Linking Procedure

The preparation process consists of several stages; the material is first ground, thereafter follows a melt-forming of thin plaques. These steps are followed by preparation and placement of the electrodes, except for the D objects, where the needle electrodes are inserted in the last stage. The prepared objects are now ready for cross linking of the polyethylene material. Microscopy is finally utilized to ensure that defect samples are removed.

Grinding and melt-forming

Pellets of the high voltage grade low density polyethylene are cooled in liquid nitrogen and ground into a powder in a Retsch grinder with a sieve of 500 µm for achieving an even material in the finished objects, without distinct boundaries. In the next step, for the objects of A and B type, two plaques of polyethylene are prepared for the wire electrode to be placed in between. These plaques are cast from the polyethylene powder in metallic moulds, specially constructed for the purpose. To melt the powder into the desired shape without initiating material cross linking, the temperature needs to be kept at relatively low level. The temperature and press force scheme for preparing these plaques is illustrated in Figure 3.3. The press force is 2 kN at the start of the process with a temperature of 130 °C. After three minutes the force is raised to 200 kN and kept for three minutes before the temperature is decreased to ambient (~20 °C) during fifteen minutes, where after also the press force is removed.

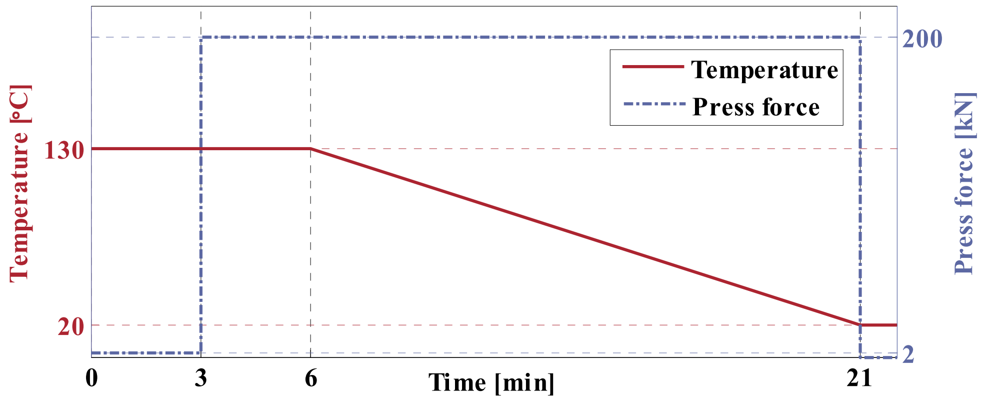

Figure 3.3 *Temperature and press force cycle during the primary moulding of plaques for object types A and B.*

Preparation and insertion of electrodes

The A type objects utilize a semi-conducting tab to provide a connection point between the high voltage supply and the wire electrode. These tabs are prepared of a cross-linked polyethylene with addition of carbon black which renders them semi-conducting. Onto each tab a tungsten wire of 10 µm diameter is manually sewn, forming a loop protruding from the end of the tab. The tab, with the attached tungsten wire, is thereafter placed between two plaques prepared in the previous step. In preparing the B objects the wire is attached to a piece of copper tape with electrically conducting glue. The wire is fixed in its place between the plaques and the copper tape is fastened. Both types of objects are then again placed in metallic moulds, ready for cross linking. Figure 3.4 shows how the different parts of A and B type objects are arranged before cross linking.

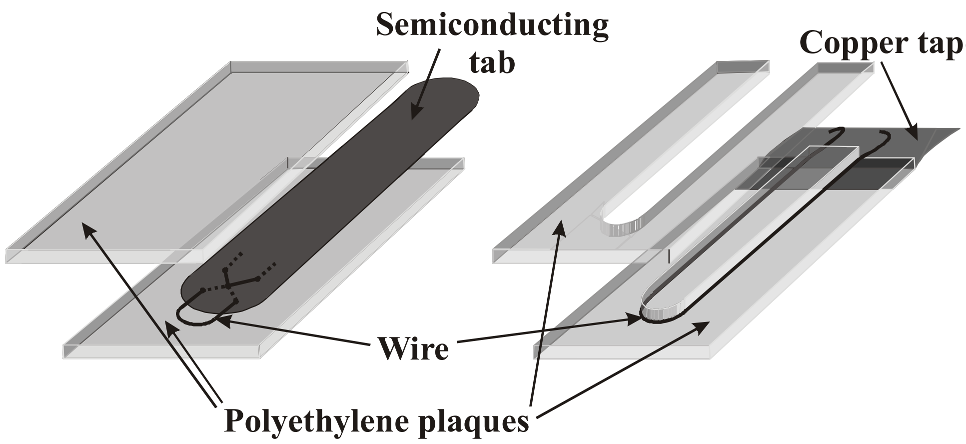

Figure 3.4 *Sketch of A and B type objects illustrating how the wire electrode is positioned between the pre-made plaques of polyethylene.*

Regarding the needle objects, the needles are first examined under a microscope to make sure that the geometric requirements are fulfilled prior to their insertion. When preparing the C type objects needles are melted in the polyethylene powder in a special mould and thereafter the whole assembly is cross linked. In contrast, for D objects material blocks of suitable size are first manufactured and cross linked and the needle insertion is done after this stage.

Cross-linking process

The temperature and press force cycle used for the cross-linking process is illustrated in Figure 3.5. A force of 2 kN and a temperature of 130 °C is used during the first 15 minutes. Thereafter both press force and temperature is ramped during 15 minutes up to 200 kN and 180 °C, respectively. This press force is kept for the remaining part of the process. At the same time, the temperature is kept at 180 °C for another 15 minutes, whereafter it decreases during the following 30 minutes.

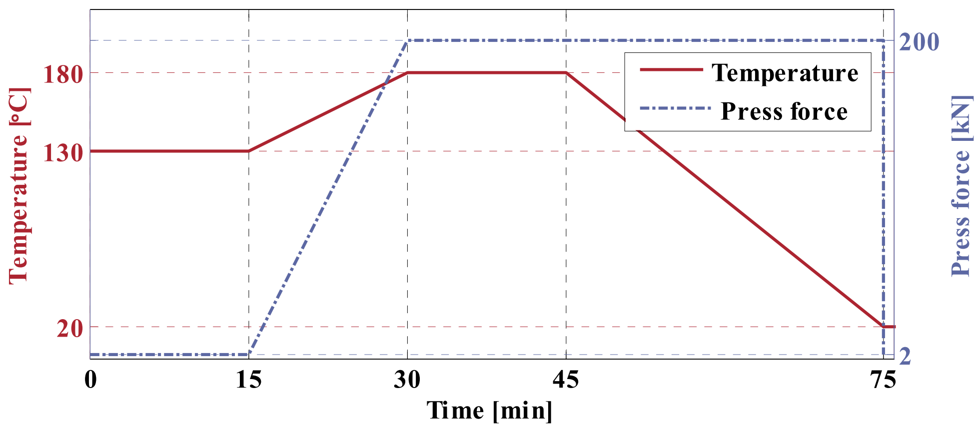

Figure 3.5 *Temperature and press force cycle during the cross linking of all object types.*

Needle insertion in D type objects

After cutting blocks of 20 x 25 mm^2 from a 6 mm thick XLPE plaque prepared according to the cross-linking process described above, these are placed in a needle insertion jig and pre-heated for 90 minutes at 125 °C. Thereafter the needles are slowly inserted at this temperature. Following the insertion the temperature is kept for another 30 minutes to release internal stresses within the material, after which the oven is turned off and the setup is left to cool slowly overnight.

3.3.2 Degassing Process

The dicumyl peroxide-induced cross-linking process of polyethylene releases reaction by-products such as; methane, acetophenone and cumylalcohol [83]. Presence of these by-products usually results in a higher resistance to electrical treeing [17, 83]. However, with time the by-products migrate out from the material and evaporate. To make the tests reliable and repetitive, this process is speeded up by degassing the cross-linked test objects, in a vacuum oven at pressure less than 1 mbar for five days at a temperature of 55 °C.

To investigate the amount of by-products remaining after degassing, IR spectroscopy and HLPC chromatography tests were performed on the investigated material [84], these showed that the remaining amount of by-products after five days of degassing was around 0.1 %.

3.4 Test Procedure

Tree initiation voltage or field (TIV, TIF) has been obtained for measuring the XLPE's resistance towards electrical treeing. All objects have been tested at ambient conditions using constantly ramped sinusoidal voltage. Before and after the electrical testing, optical microscopy was used to identify and remove objects having visible defects. The visual inspection has been made with both non-polarized and polarized light for identifying birefringence patterns that indicate presence of strain in the material.

3.4.1 Electrical Setup for Treeing

The electrical measurements for tree initiation voltage were performed in a setup as illustrated in Figure 3.6. A 20 kVA variable step-up transformer with a maximum voltage output of 75 kV_{rms} was applied as the voltage source. A constant voltage ramp rates of 500 V_{rms}/s was employed. To limit short circuit currents in case of breakdown in or across the test object a water resistor of approximately 200 kΩ was connected in series with the test object. Voltage measurements were made using a resistive voltage divider connected to a DAQ device (NI USB-4431) at sampling rate of 1 kHz.

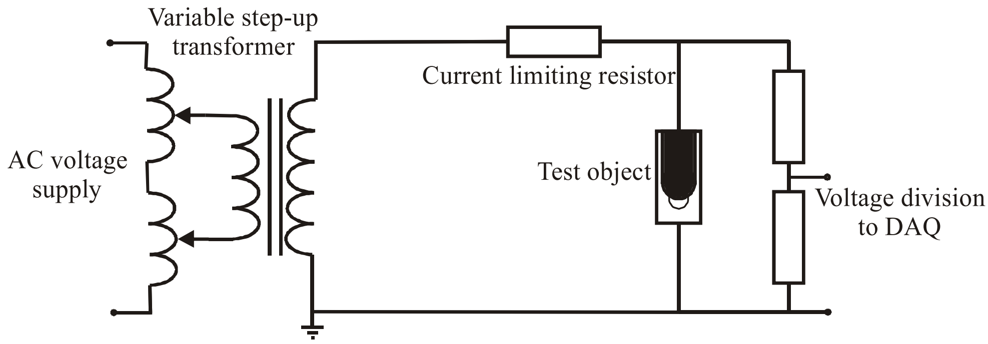

Figure 3.6 *Schematic view of the electrical testing circuit.*

3.4.2 Detection Methodology

During testing the object was placed in a glass tank filled with transformer oil, preventing a flashover across the surface of the test object, as illustrated in Figure 3.7. The oil also provided a similar refractive index to the polyethylene enhancing the visibility of the electrical trees.

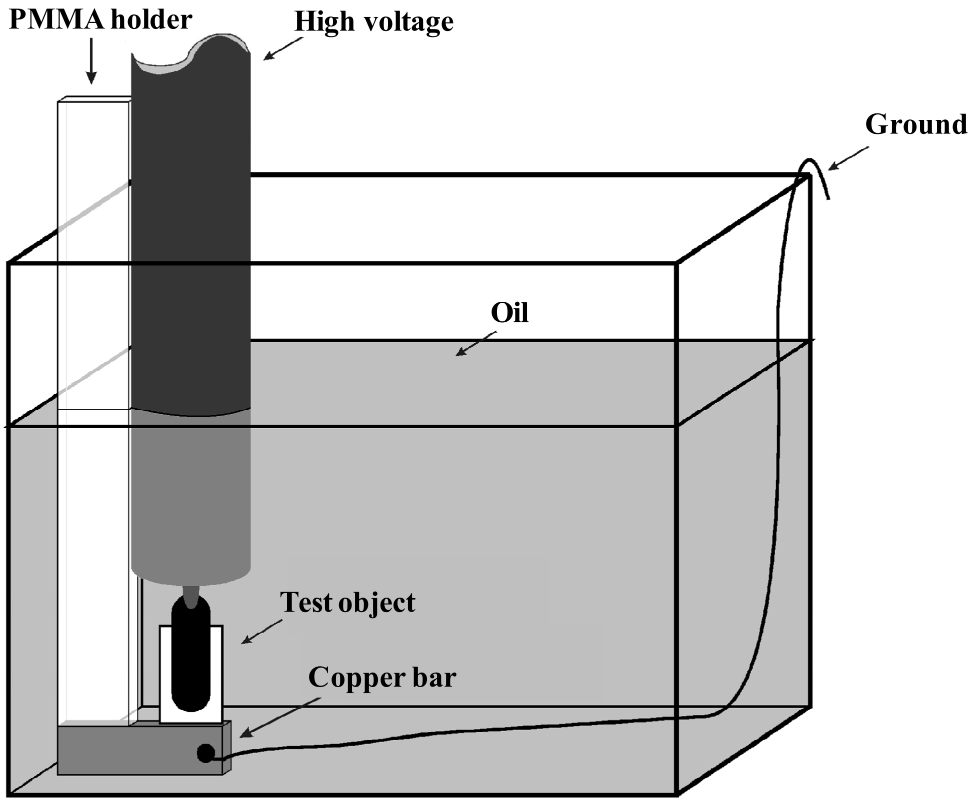

Figure 3.7 *Sample holder - the test object is placed between high voltage connection and grounded copper bar in a glass tank filled with transformer oil.*

A CCD camera, capturing 25 frames per second at a resolution of 768 x 576 pixels per frame, was utilized for detection of the trees. The CCD camera was positioned in front of the test object which was lit from behind. The oil was kept at ambient temperature (19-22 °C). The treeing process was examined both in real-time and recorded to be studied in more detail after the tests. By analysing the recorded videos the time of each tree initiation could be noted and correlated to the corresponding voltage level. This voltage is throughout this thesis considered as the tree initiation voltage, even though in reality the tree starts growing before it can be observed with the CCD camera. The exact level of treeing initiation is however not of great importance when comparing between different materials and this systematic error is further reduced in the measurements with the optical microscope of a higher resolution, introduced in Chapters 4 and 5.

3.5 Analyses on Wire Type Objects

With the introduction of the wire electrode, a larger volume of the dielectric is exposed to the highly divergent electric field as compared to the needle electrode. From this follows that several electric trees initiate at the electrode, in each of the tested objects, as is illustrated in Figure 3.8.

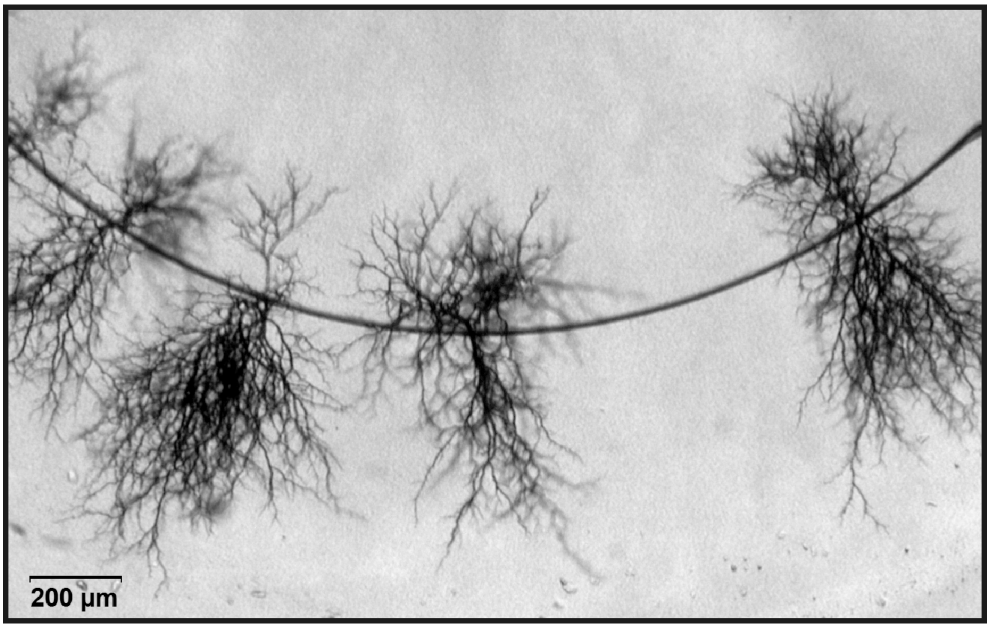

Figure 3.8 *Multiple trees growing from the wire object.*

This is perhaps the most prominent feature of the wire-type object, as opposed to the traditional needle type where only a single tree is formed. In order to further understand and make better use of the treeing processes yielded in the test objects, a deeper analysis is made on this behaviour. The appearance of many trees will naturally provide more data, however some consideration on how to interpret and present this information is necessary. The data interpretation is simpler for the traditional needle due to the single obtained data point per test object. With multiple trees present in every object there is a need for a more sophisticated approach for the statistical analyses. The plenitude of obtained data should be utilised in an as beneficial manner as possible. A suggestion on how to achieve this is presented below together with a detailed evaluation and verification on its suitability. This work has so far mainly been focused on the initiation of the treeing phenomenon, as for material testing purposes the growth and runaway processes can be considered less significant, especially considering that breakdown is usually only a matter of time once the tree has first appeared.

3.5.1 Multiple Treeing Analysis

Prior to this statistical analysis, data from trees growing close to defects of the wire have been censored. At these positions the electrode geometry becomes distorted and therefore also the electric field stress leading to incomparable results. These data points mainly relate to trees initiated at twisted or curled parts of the wire electrode, henceforth labelled as kinks, a deeper study of the reasons behind kink appearance and their influence on the treeing process is presented in Section 3.5.5.

Initial investigations have been made by dividing the trees chronologically by the order of appearance; i.e. the initiation voltage of the first tree in each of the objects are grouped together, the second tree in each object is grouped and so on up to number seven. Hereafter fewer trees are incepted, even in the $B_{10\mu m}$ object. Figure 3.9 shows the tree initiation voltage of the chronologically ordered trees. It is clearly observed that the A-type object has produced significantly fewer trees compared to the two B-type objects; the cause hereof is further explored in Section 3.5.2. Some statistical outliers are present for the first tree of both the B-type objects, even though no apparent reason for them initiating at these low levels could be discovered by the microscope observations performed before and after the testing. Hence it cannot be proved whether the outliers are the result of some imperfections in the objects and should be removed from the analysis or if they are simply statistical outliers, indicating the threshold level of treeing initiation in the dielectric. In any case, this is an advantage with the wire object with regard to the needle type, where the multitude of treeing initiations shows outliers more clearly.

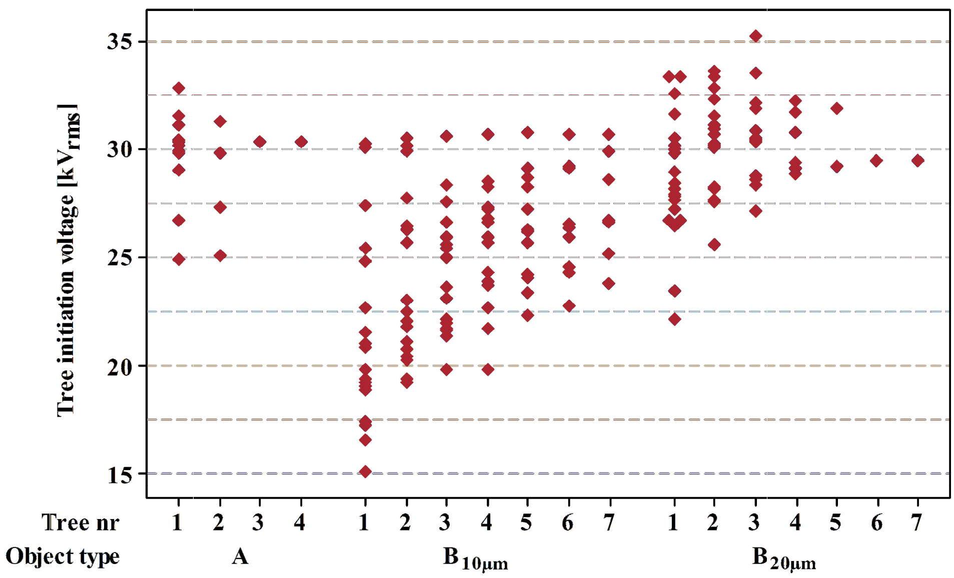

Figure 3.9 *Chronologically ordered tree initiation voltage levels for the individual trees.*

In contrast to the needle objects, where the high electric field is limited to the tip of the needle and the tree growth is forced to this location; along a wire electrode the tree can incept at a multitude of points and will to a higher extent find weak spots of the material. Concerning treeing in B-type objects, Figure 3.9 further reveals similar initiation voltage magnitudes for the first number of trees; at around the fifth tree, however, a larger difference in the voltage level of the lowest initiation is noticeable. For even higher tree numbers they will gather more and more at the maximum voltage used during testing and in doing so the focus is also moved from the threshold level.

Another way of presenting the results from the multitude of trees is by fitting the chronological data to a Weibull distribution; here three-parametric Weibull plots for trees of $B_{10\mu m}$ object numbered 1 to 7 are presented in Figure 3.10. In addition a collected fit for trees 1 to 4 is also shown. A question now arises on how to include all the obtained data in a suitable way in the final statistical evaluation. Just adapting the simplest manner possible and including all (up to twenty or more) the trees appearing, could perhaps be misleading. One drawback would be a more spread data distribution, moving the focus from the important threshold value. As it was observed that the first four trees are initiated on more or less equal terms, the conclusion is that these can be grouped together for the actual evaluation; this provides plenty of data from the testing while not putting the integrity of the overall results at risk.

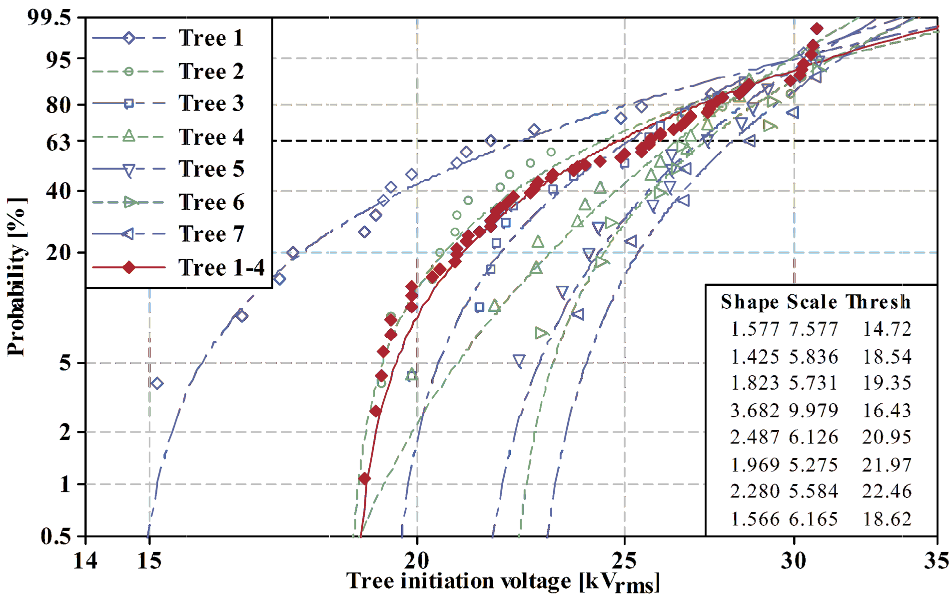

Figure 3.10 *Three-parametric Weibull fits for chronologically ordered trees in B10µm objects together with the collected fit for tree numbers 1 to 4 in each object (with the four lowest values in the series censored)*

A comparison between the different object types is shown in Figure 3.11. It can be noted that the removal of the semi-conducting tab from the test object results in a strongly reduced tree initiation voltage level, which is an advantage for practical measurements, especially concerning accurate electrical detection of PD activity in the objects. These results are also in line with the results of numerical simulations, from which the field reducing role of the semiconducting tab was revealed. It can also be noted that the shape values differ quite significantly between the $B_{10\mu m}$ and $B_{20\mu m}$ objects. For the thinner electrode the tree initiation became spread over a substantially large voltage range, an explanation to this effect would require further investigations.

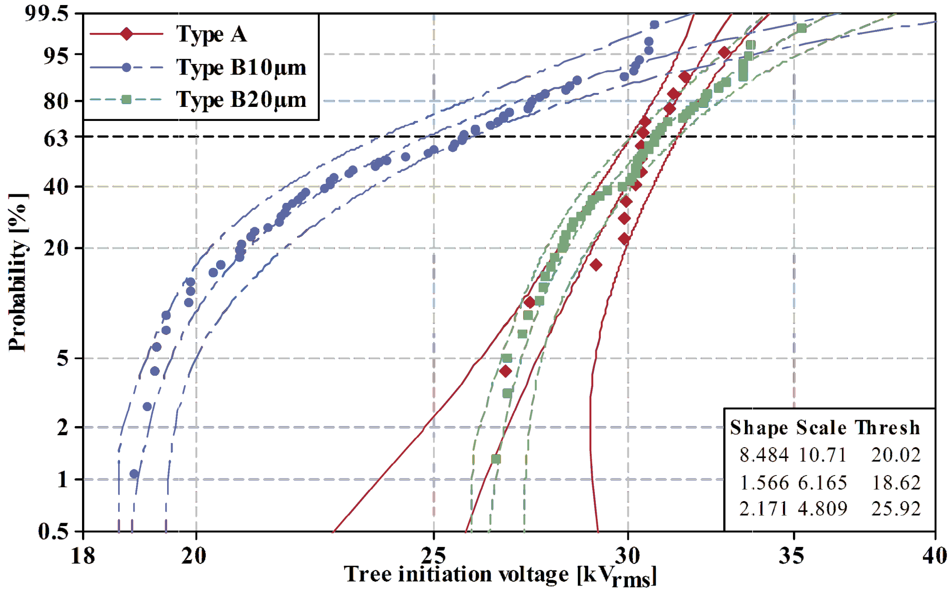

Figure 3.11 *Three-parametric Weibull distributions of tree initiation voltage for the collected first four trees in A and B type objects, together with the parameter values and the 95 % confidence interval of the fit.*

3.5.2 Object A – Influence of the Semi-Conducting Tab

For understanding the reasons behind the rather limited number of trees appearing in the objects of type A, further examinations were made. An effect of the wire position in relation to the semiconducting tab, i.e. how far away from the semi-conducting tab the wire electrode extends, became evident. Achieving objects with uniform loop shapes is not an easy task since the XLPE flows during the object preparation process, moving the wire away from its original position in an uncontrollable way. Thus two distances were measured for each of the tested objects; the wire loop extension from the tip of the semiconducting tab and the shortest distance between the wire and the ground plane, both represented in Figure 3.12 (where distance between tab and ground electrode and wire and ground are explicitly measured). These distances were thereafter correlated with the data of tree initiation voltage.

Figure 3.13 shows the initiation voltage as a function of distance between the semiconducting tab and the outmost part of the wire electrode. A clear dependence can be noticed; small wire loops yield higher tree initiation voltages, indicating that the tab does impede tree initiation by screening the field enhancement at the wire electrode. It was also observed that no trees incepted close to the semi-conducting tab.

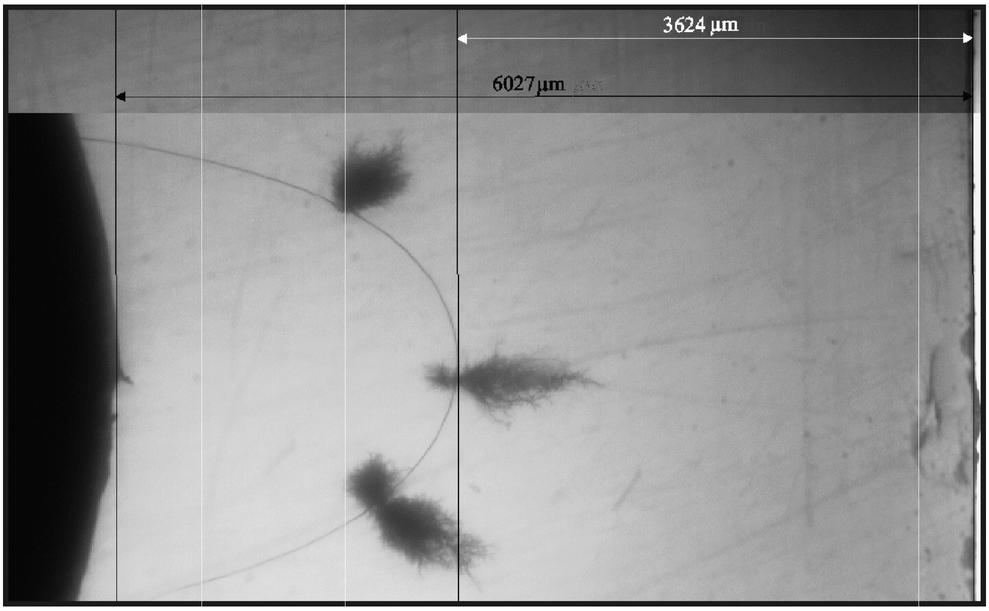

Figure 3.12 *Definition of wire electrode positioning in A-type objects.*

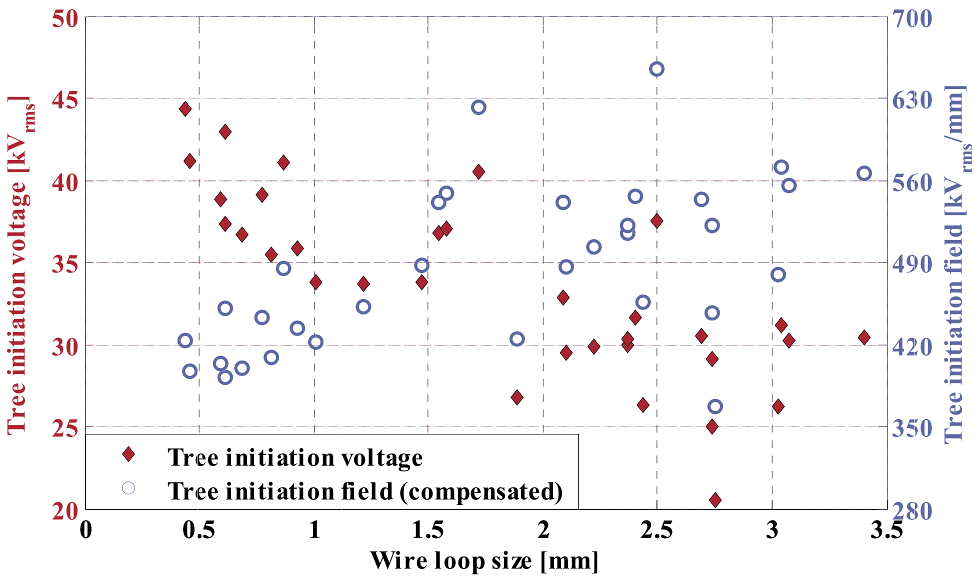

Figure 3.13 *Tree initiation voltage as a function of distance between semiconducting tab and wire electrode. The compensated values of tree initiation field are shifted according to the function determined from Figure 3.14.*

The FEM simulations, described in Section 3.2 gave further insight on how the maximum electric field strength at the wire surface decreases as the wire to tab distance becomes shorter. The numerical calculations were made on the resulting electrostatic field in an A-type object for thirteen various loop sizes, ranging between 0.5 and 3.5 mm. The results corresponded well with the measured trend; the semiconducting tab shields the electric field in its close vicinity, leading to lower field strength at the wire surface for the shorter wire loops. The maximum of the electric field at the wire surface, as plotted in Figure 3.14, acquires field strength furthest away from the tab and closest to the ground plane. This graph shows the thirteen data points obtained from the numerical simulation; these are then fitted to a simple second order equation also presented in the figure. When the measured raw data from Figure 3.13 are corrected with the defined relation, the tree initiation voltage levels become less influenced by the distance to the semiconducting tab, especially for distances between 1 and 3.5 mm. To limit the influence of tab effect, only objects with wire loops extending 2.5±1 mm were further considered, while still leaving enough data for comparisons as the one shown in Figure 3.11.

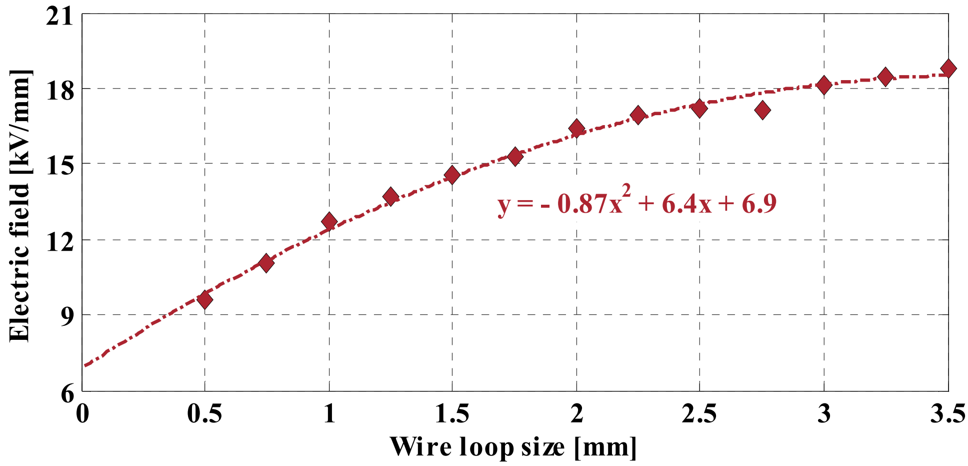

Figure 3.14 *Calculated maximum electric field strength at the wire as a function of the tab-to-wire distance.*

A similar field analysis was also made for the electrode-to-ground distances, varying between 2 and 5 mm. A correlation in this case is not so evident, even though a small trend can be noticed in Figure 3.15, indicating that this parameter is not so critical for controlling the accuracy of the treeing initiation tests.

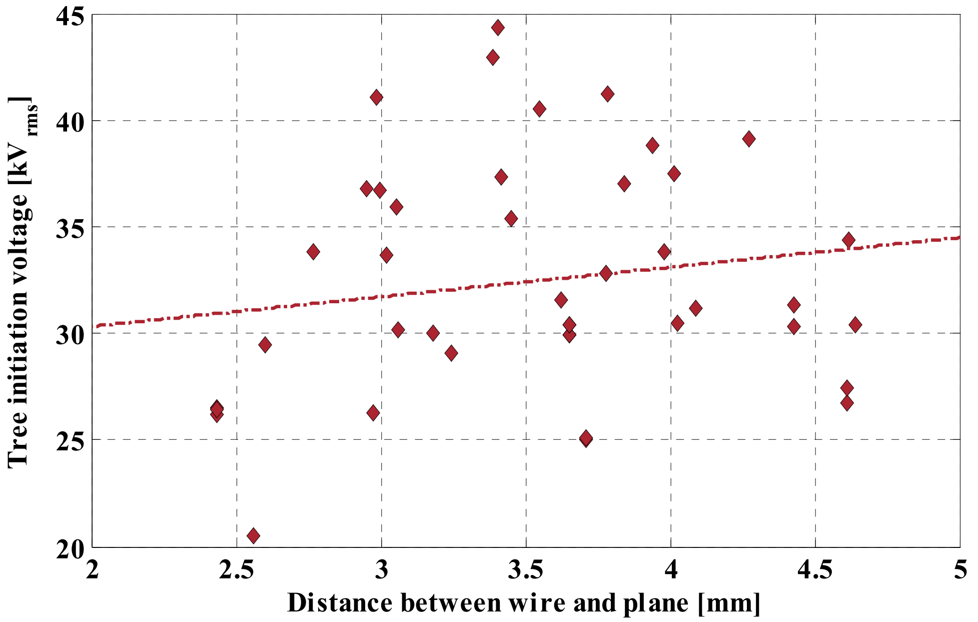

Figure 3.15 *Dependence on the wire-to-ground distance on tree initiation voltage in A-type objects.*

A further inconvenience, albeit of a different nature, with the use of semiconducting electrodes, is that in cases of a complete breakdown, carbon black particles disperse in the surrounding transformer oil, significantly reducing the visibility whilst also changing its dielectric properties. Therefore the oil needs to be changed and both the container and the object holder need to be cleaned thoroughly after each such occasion.

3.5.3 Object B - Newly Developed Object without Tab

For improving the above reported problems the B-type object, without the semiconducting tab, was further developed. To verify its superiority as regards less dependence on the field enhancement due to variations in the electrode positioning, the tree initiation voltage and field enhancement at the electrode were further examined. The wire-to-plane distance was examined for both $B_{10\mu m}$ and $B_{20\mu m}$. In Figure 3.16 the observed tree initiation voltage are ordered by the wire to ground distance. As determined, a lack of such dependence can be noticed and the allowed distance variations were set to 3.5±1mm. The 3D-simulations also showed a similar behaviour, only a very small change in the electric field strength was found when varying the distance between the electrodes.

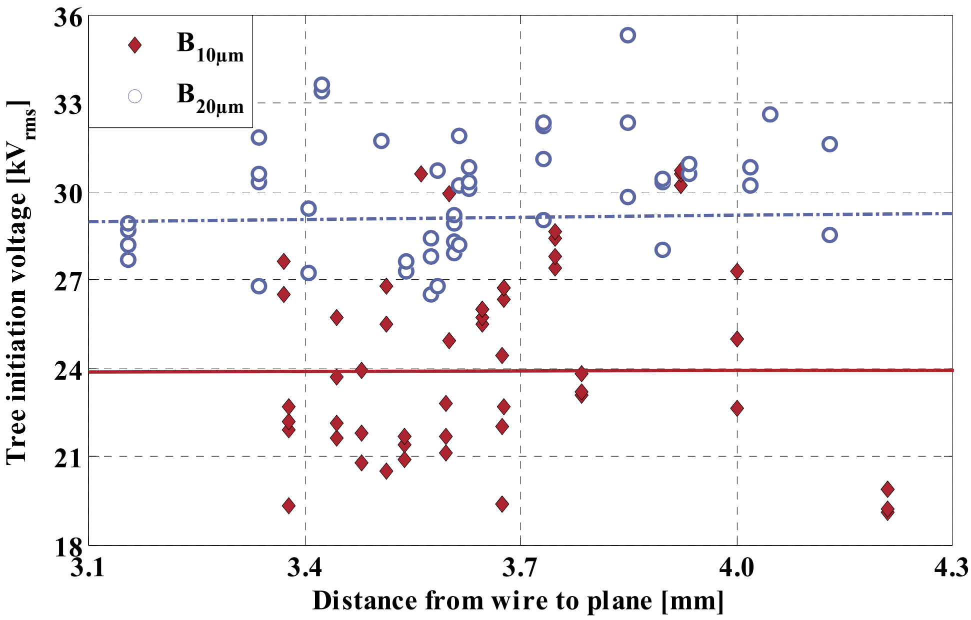

Figure 3.16 *Dependence of tree initiation voltage on wire-to-ground distance for for 10 and 20 µm B-type objects.*

Also the influence of tree position on the wire was analysed. It was done by relating the angle at which the tree appears, or for the trees located further than 2 mm away from the tip of the wire loop by its distance. Figure 3.17 shows how this distinction is made, 0° is placed at the tip of the curvature and for reference reasons 90° is positioned at the parallel line made at a distance of 2000 µm from the curvature tip, which was the designed wire loop width. For trees appearing on the straighter parts of the wire, above this line, a division is instead made by their distance from the line.

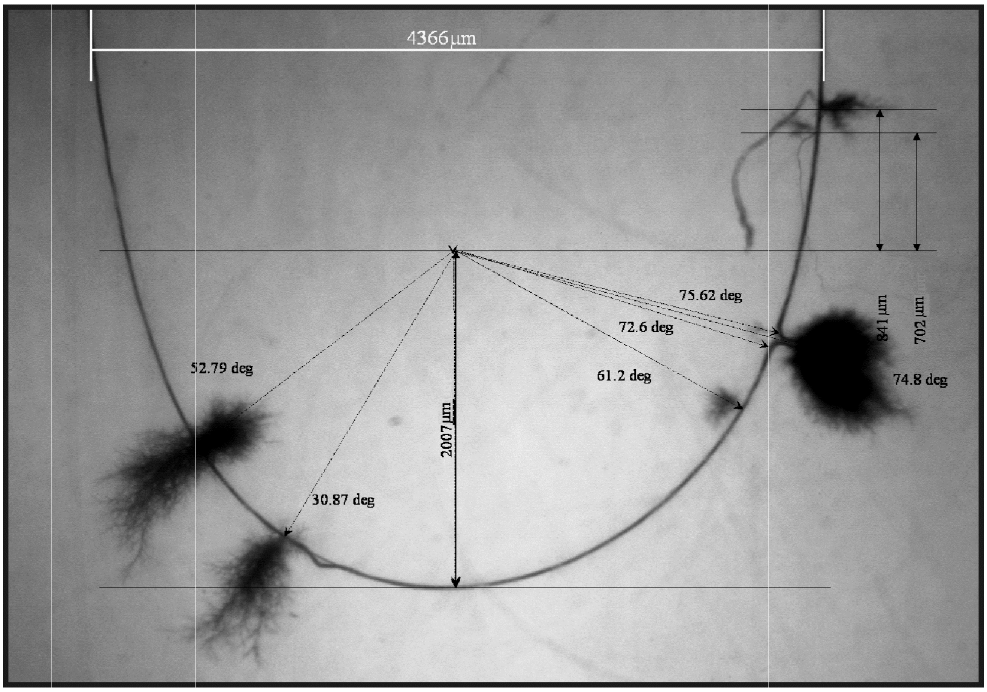

Figure 3.17 *Definition of tree position on wire electrode loop in B type objects.*

The performed tests revealed no signs of dependence on the initiation voltage on the tree position, as presented in Figure 3.18. There is some decrease in number of trees initiated at the wire as the distance to the ground electrode increases. It should however be noted that this decrease is somewhat smaller in reality as some more trees incepted at longer distances, not included in the view of the CCD camera. Thus the initiation voltage levels of these trees remain unknown and are as a consequence not included in the analysis. The collected number of trees at different distances is presented in Figure 3.19.

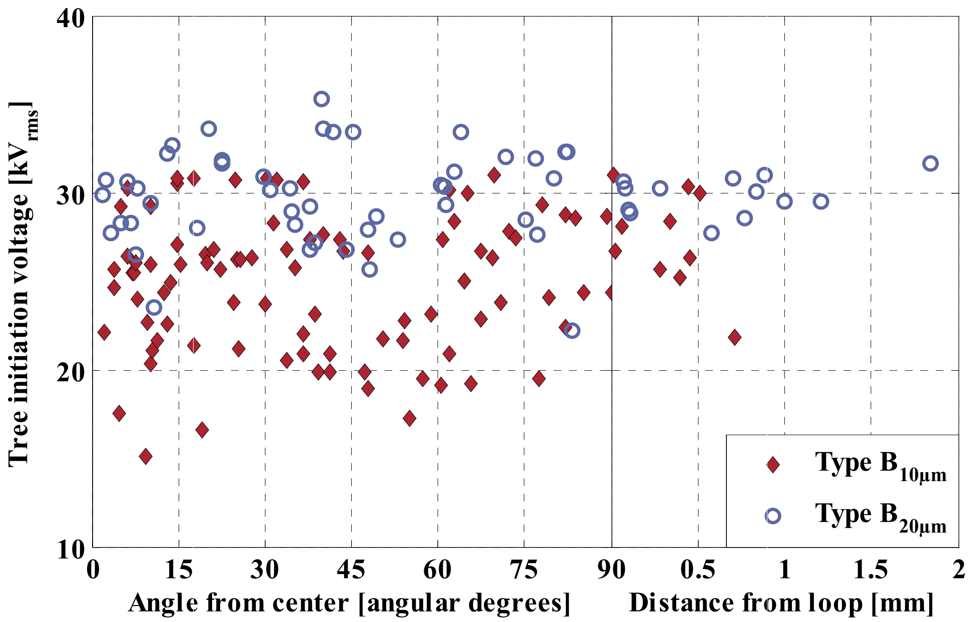

Figure 3.18 *Treeing initiation voltage as a function of position on the wire electrode.*

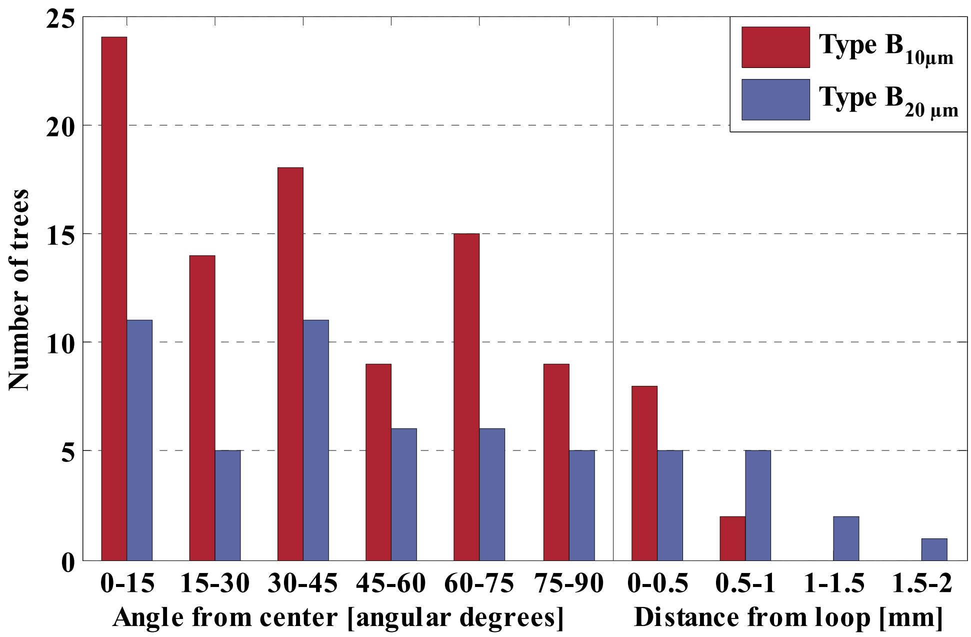

Figure 3.19 *Number of trees appearing at various positions o the wire electrode.*

A last consideration was made to conclude if the trees were independent of each other; this is related to a question if the position of a newly incepted tree can be affected by the locations of already growing trees. The trees proved to appear randomly at the electrode, independent on the previous treeing instances, as illustrated in Figure 3.20. It is therefore assumed for further analyses that all the trees do practically incept on equal terms, despite of their position along the wire and small geometry deviations in the prepared objects.

Figure 3.20 *Order of appearance of electric trees in* $B_{10\mu m}$ *type object (the figure is constructed from a video sequence).*

3.5.4 Comparison of Electric Field Strength at Initiation

The field enhancement factors were utilized to compare the electrical tree initiation field. For this also the correction factor of the dependence on the tab-to-wire distance was taken into account. The resulting three-parameter Weibull fits are illustrated in Figure 3.21. As seen, a shift between the object types is evident, in the A-type objects the trees initiated at similar voltage levels to those of the B-type objects with 20 μm wire, compare with Figure 3.11. In the case when comparing the field strength in the different objects types with the same electrode dimension, the results overlap. Part of the explanation of the decrease in electrical field strength for 20 μm objects could be the difference in material volume exposed to the strong field and the increased probability of finding weaker material points, especially for the first trees appearing. Another reason behind this behaviour could be related to space charge injection [71, 81], this might influence the correlation factor K between voltage and electric field introduced in Section 3.2, especially for sharper geometries, which corresponds to the shift towards higher fields in Figure 3.21. However, this effect still requires deeper clarification.

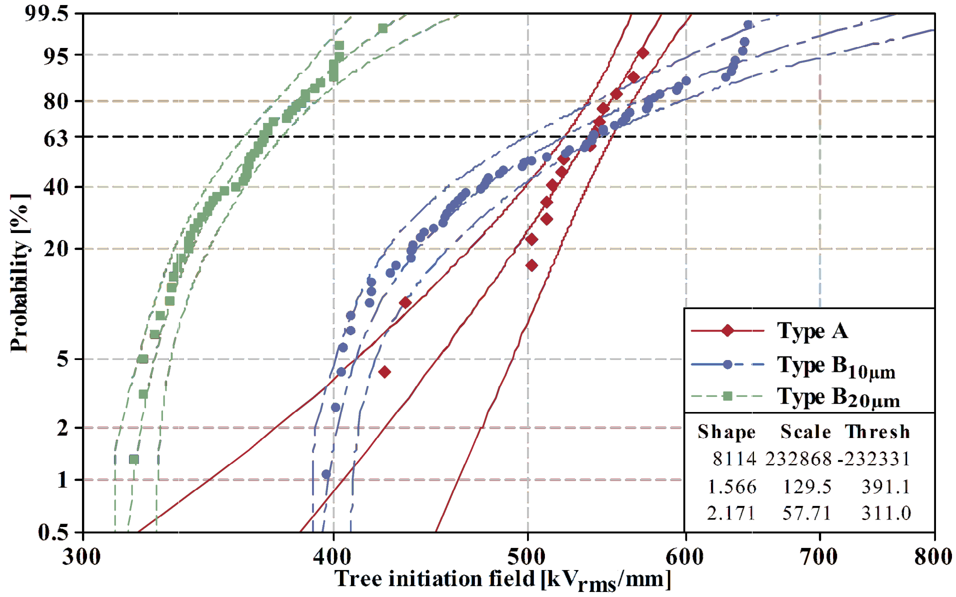

Figure 3.21 *Three parametric Weibull distribution for the calculated field strength at tree initiation for the wire objects of types A and B.*

3.5.5 The Appearance of Kinks and their Influence

The main disadvantage with the wire electrode is its tendency to form kinks, modifying the electrode geometry and thus also changing the electric stress in the test objects. The kinks have been found to appear and develop during the object manufacturing. One important factor is the largely varying thermal expansion coefficients for polyethylene and tungsten, causing stress at their interface during the temperature cycling. Cross linking takes place at around 180 °C, where the peroxides are active, and thereafter the objects are cooled to room temperature. Despite the fact that this was always done at high pressure and at a controlled rate, kinks appeared in most objects. When cooling at a faster rate by use of metal blocks, cooled to 10-20 °C below zero, the kinks were found to be reduced in both number and sharpness, however they grew back again during the degassing process, as seen in Figure 3.22, showing a kink in a test object checked under microscope at 24 h intervals during the degassing at 55 °C.

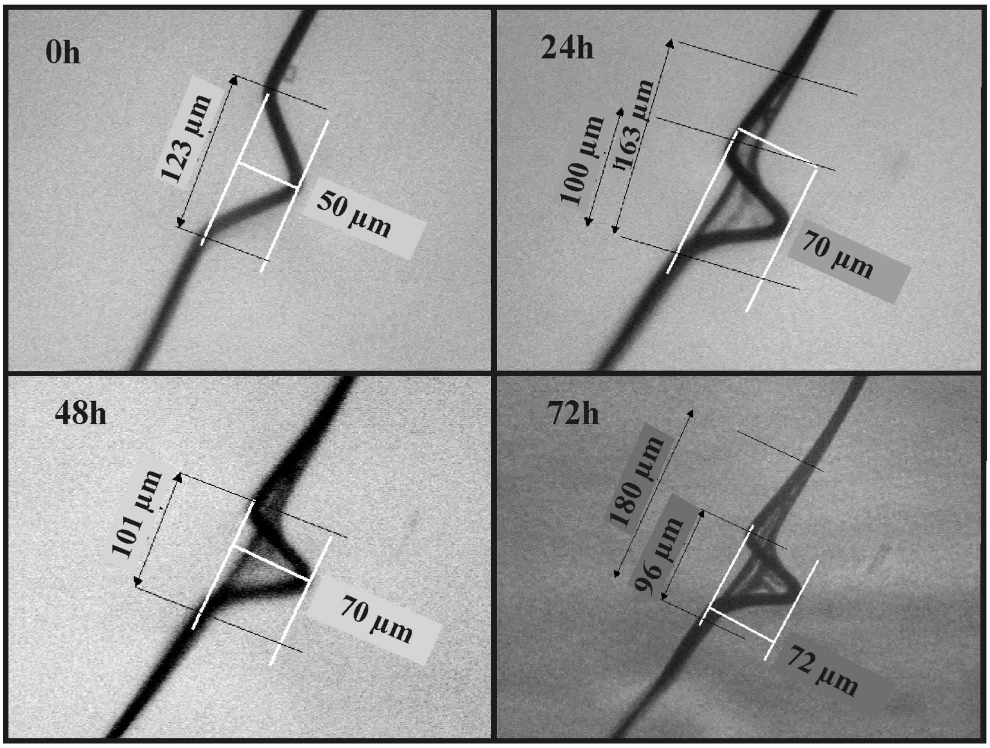

Figure 3.22 *Kink development during the degassing process at 55 °C*

The material in the vicinity of the wire electrode has also been checked using polarised light; a typical result is shown in Figure 3.23. As seen from the birefringence patterns, mechanical stress is present in the polyethylene close to the kink formation, which might influence the electrical treeing inception at these points. On the other hand, no such stress is observed elsewhere along the non-deformed parts of the wire.

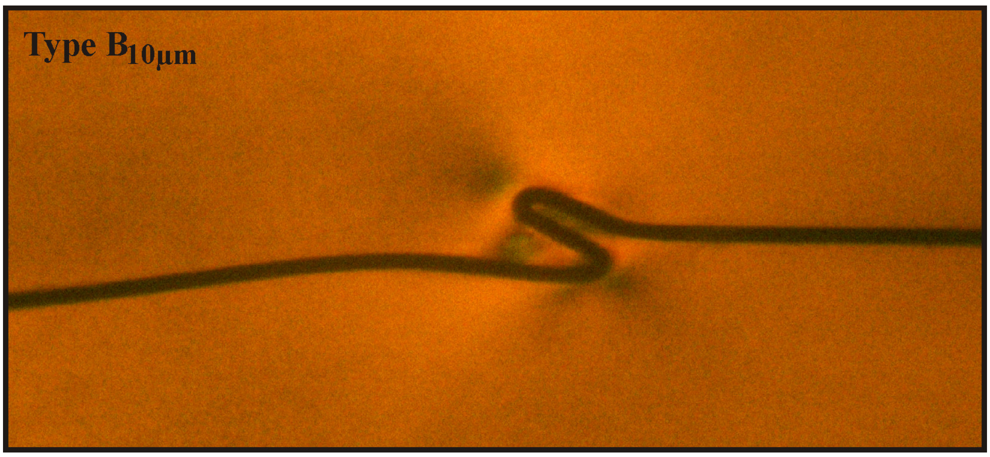

Figure 3.23 *Birefringence close to a kink indicating built-in stress in the material.*

Having concluded that the removal of kinks seems quite unlikely, the influence on treeing inception is further analysed. Figure 3.24 shows the Weibull distribution of three following cases: one fit on the first tree at a kink, the second shows tree initiation of the first tree in objects where this first tree occurred at the wire and the third distribution shows the first tree at the wire after kink censoring. As expected the trees growing from a kink initiated at a lower voltage levels, although it is not a rule that kinks hosted the first tree in all the objects. As trees growing at kinks are removed from further analyses, the most important feature is that the first trees at the wire electrode initiate at similar voltage levels, independent on whether a previous tree has started at a kink or not. This further strengthens the hypothesis that trees on the wire incept on close to equal terms.

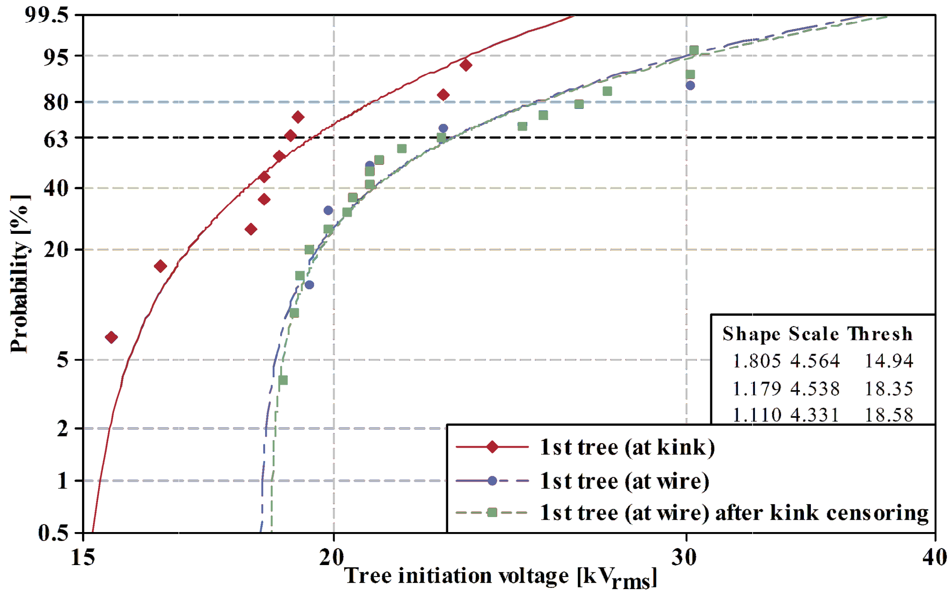

Figure 3.24 *Weibull plots showing tree inception level at kinks and at wire.*

3.6 Comparison with Needle Objects

As indicated earlier, comparisons between the two different needle-needle type objects were made for analysing their advantages and disadvantages in comparison to the used objects with wire electrodes. The very fine tip of the needle can easily be damaged during handling and insertion into the polymer. All the needles used in the experiments were carefully checked and several damaged needle were unfortunately found among them. In eight out of eighteen needles, deviations of the tip curvature were found; the crooked needle in the Figure 3.25 shows one of the more severe cases. During this check also the diameter of the needles was controlled and they were found to vary rather evenly, between the allowed limits of 3±1 µm. Test objects with needle radii outside these limits have been discarded from the results.

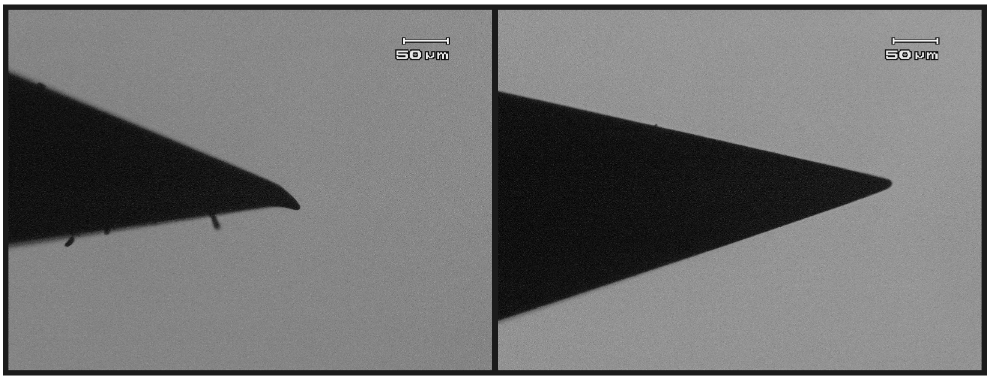

Figure 3.25 *Example of needle electrodes with damaged and proper tip.*

A presence of mechanical stress was also found in the tested polyethylene material by checking the objects using polarised light. Two typical examples of C and D objects are presented in Figure 3.26, note that the images are not to scale. For the D objects, where the needles where inserted into the already cross-linked material clear birefringence patterns can be observed at the needle tip, indicating frozen in mechanical stress in the polyethylene. For the C type objects, no such patterns could be found at the tip of the needle, though some birefringence can still be identified in the material bulk.

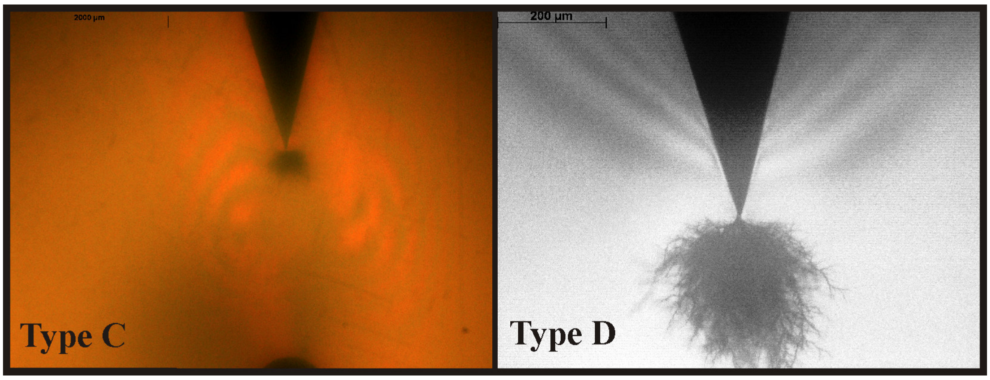

Figure 3.26 *Typical birefringence patterns found in C and D objects.*

The mechanical stress also had an impact on the tree initiation voltage, as illustrated in the Weibull plot of Figure 3.27, where the unfilled squares represent data from needle objects of type D with birefringence patterns close to the needle tip. It can be noted that these objects generally had trees initiated at lower voltages as compared to the objects where no mechanical stress could be distinguished.

The above named disadvantages of the needle type objects should however be weighted to other qualities. Knowing the exact location of tree growth allows for higher magnification of the optical methods. This is also a prerequisite when attempting to capture electroluminescent signals during the tree inception stage. The appearance of a single tree can also be an advantage for qualitative electrical measurements of e.g. PD activity in the electrical tree, as it is evident from which point it originates.

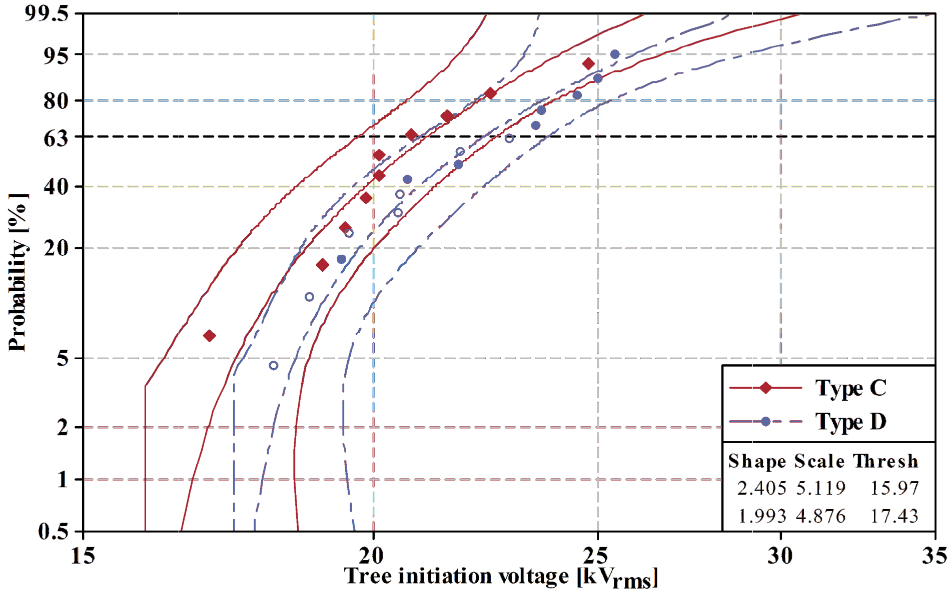

Figure 3.27 *Two parametric Weibull distributions of tree inception voltage in C and D object types.*

3.7 Material Structure

Some further observations of tested objects were made by using scanning electron microscopy (SEM), where the morphology of the polyethylene as well as the appearance of the bare tungsten wire electrode could be observed. As displayed in Figure 3.28, the wire has evenly distributed sub-micrometer ridges along its length and also some minor metal particles were encountered on its surface. As the noticed ridges are consistent in size and also smaller than the wire diameter by more than an order of magnitude, they are not believed to influence the test object performance for tree initiation test.

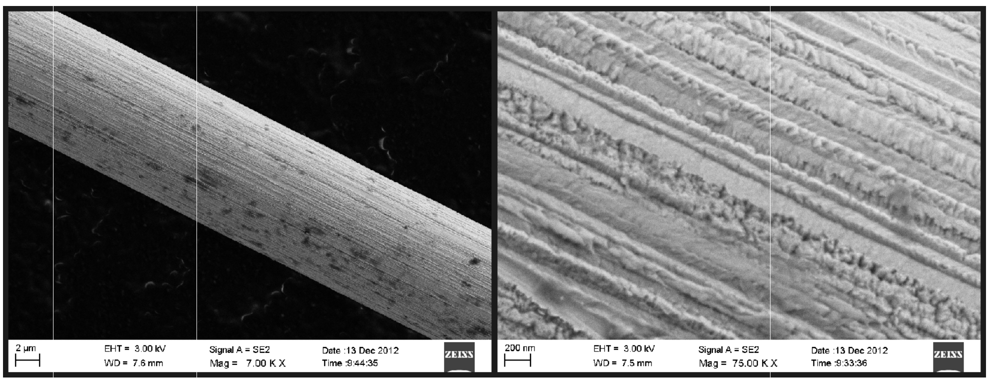

Figure 3.28 *SEM view of wire electrode prior to object preparation.*

SEM was also used to inspect test objects, before and after testing, to examine if any difference in the bulk could be distinguished in different parts of the object, especially to clarify if any change material morphology appeared to occur in the proximity of the wire electrode. Before the SEM observations of the test objects, they were first cooled in liquid nitrogen before splitting them into two halves, exposing the wire electrode and the surrounding bulk of the material. The split objects were thereafter etched and sputtered with gold before the study. As exemplified in Figure 3.29 no clear difference in the morphology of the polyethylene could be distinguished close to the wire electrode or elsewhere in the objects. An examination on the crystal regions in XLPE showed no significant variation in size. Further the contact between the electrode and the insulation appears satisfactory; an imprint of the sub-micrometer ridges in the polymer is noted in the channel, where the wire was positioned. As seen in the figure the tungsten wire has been forced out of its original position during the splitting of the object.

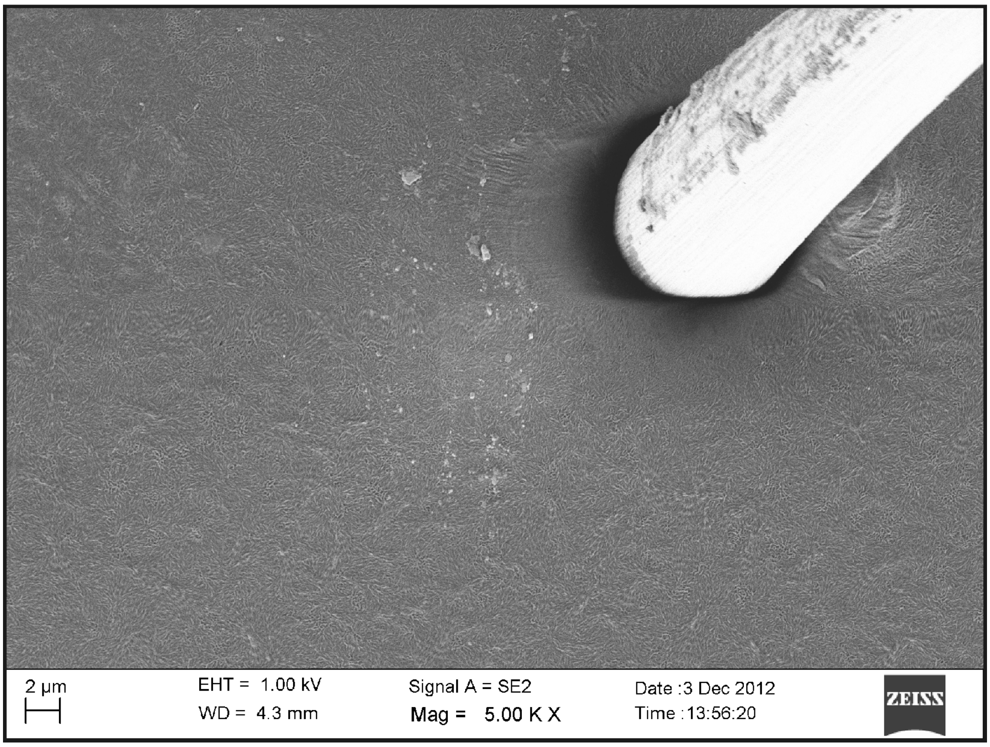

Figure 3.29 *SEM picture of the XLPE close to the wire and further out in the material bulk.*

Chapter 4

Correlation of Electrical and Optical Treeing Observations

In the previous chapter it was verified that the wire object functions in the desired way and having decided upon how to statistically analyse the visually obtained treeing data, further testing has focused on how treeing can be detected and studied with additional electrical measurements of the partial discharge activity in the tree channels. The properties of the obtained PD signals are analysed and these are compared to the optical observations, mainly with respect to tree initiation voltage and the number of incepted trees. Tests have been performed for the reference XLPE and for the same material with addition of a voltage stabiliser. These results are then utilized in a method to determine a material's resistance to treeing without depending on optical observations. Effect of stray capacitance on the treeing process is also investigated, as is the effect from constant amplitude of the AC voltage stress.

4.1 Test Procedure

To facilitate the treeing analyses, the ramp speed of the applied voltage has been lowered by an order of magnitude, which provides for both a better accuracy in the determination of tree initiation as well as more data traces in which to study PD activity. Some small modifications in the object preparation and to the test setup were introduced as described in the following section, though the testing mainly followed the same procedure as described in Chapter 3.

A non-commercial stabiliser, 4,4'-didodecyloxybenzil (in this work also denoted as Et_{12}), with the chemical structure seen in Figure 4.1, has been tested along with reference XLPE, without stabiliser addition. This particular stabiliser was originally chosen for a more detailed study on stabiliser performance as its benzil core exhibits promising properties with respect to its ionization potential. Alkyl chains have been bound to the core for providing better miscibility with polyethylene. The stabiliser was first dissolved in 300 ml of dichloromethane (DCM) and mixed with the polyethylene powder by shaking it in an erlenmeyer flask during approximately one hour. The solvent was then removed by placing the mixture in a rotary evaporator for around one hour at a pressure of 800 to 900 mbar. An additional drying was thereafter performed in a vacuum oven for 12 hours at 40 °C. Test objects of type B with the 10 μm wire electrode were manufactured from the XLPE with and without the stabiliser, following the earlier described procedure. Four different loadings of the stabiliser were studied, 10, 20, 30 and 40 mmol/kg of polyethylene, which respectively corresponds to approximately 0.56, 1.12, 1.68, and 2.24 wt%.

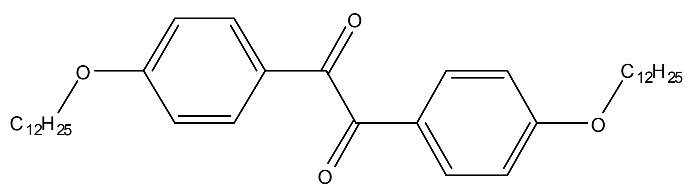

Figure 4.1 *Chemical structure of the added stabiliser, 4,4'-didodecyloxybenzil.*

4.2 New Test Setup

The following modifications have been implemented in the test setup, as are illustrated in Figure. The transformer has been exchanged for another one allowing slower ramp rates, between 20 and 160 V_{rms}/s and a PD measurement system, based on the principles described in [85, 86], is introduced. The selected PD detection method is chosen due to its efficiency in separating the PD signal from the applied voltage with only some simple electrical components. It has the PD decoupler connected in parallel to the test object, which protects the data acquisition system in case of occasional breakdown of the object. The PD decoupler comprises a 95.66 pF capacitor, C_{pd}, a 51 Ω resistor, R_{pd}, as well as a 1.80 meter long coaxial cable with the screen grounded in both sides. The resistor and capacitor create a high-pass filter, suppressing the applied sinusoidal voltage without affecting the high frequent PD signal. The coaxial cable acts as a resonant amplifier for the high frequency content of the signal, thus amplifying the PD signal. Furthermore, a Pearson current monitor, model 2877 with a bandwidth of 200 MHz providing a ratio of 1 V for a current of 1 A, is positioned around the ground wire connected to the test object, allowing for measurements of the current in the object during treeing. The PD detector, the Pearson current monitor and the voltage divider are connected to a Tektronix DPO4000 oscilloscope with 8 bits resolution and a bandwidth 350 MHz with a maximum sampling rate of 2.5 GHz. However to limit the data amount the PD traces are sampled at a rate of 50 MS/s. The signal traces (each 20 ms long), corresponding to one period of the applied sinusoidal voltage, are collected and stored in a computer. The time between each set of traces is set to 2 seconds. The testing was performed for four different 50 Hz AC voltage ramp rates; 20, 40, 80 and 160 V_{rms}/s.

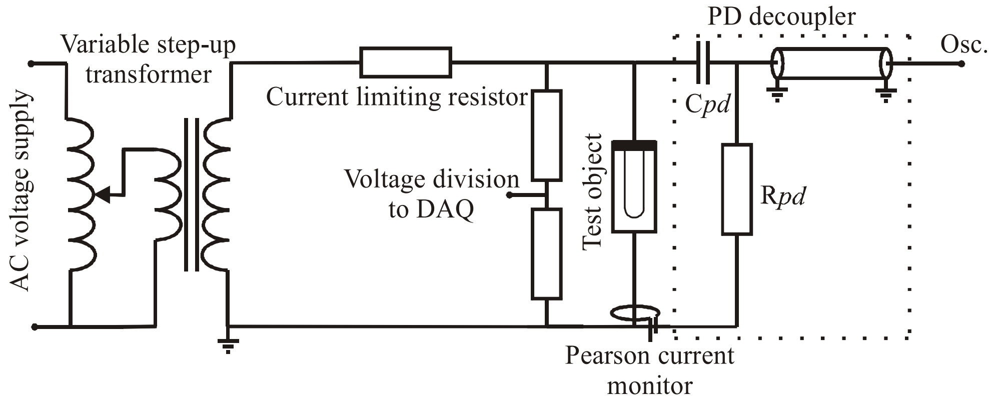

Figure 4.2 *Modified set-up with PD decoupler and Pearson current monitor.*

The CCD camera used in the tests presented earlier in Chapter 3 has been exchanged by a stereomicroscope equipped with another CCD camera, recording the process at 3.7 frames per second at a resolution of 2048 x 1532 pixels. This allows for detection of trees smaller than 10 μm and makes the determination of tree initiation significantly more accurate. The electrical tree initiation tests were performed in transformer oil in a custom made container, as shown in Figure 4.3.

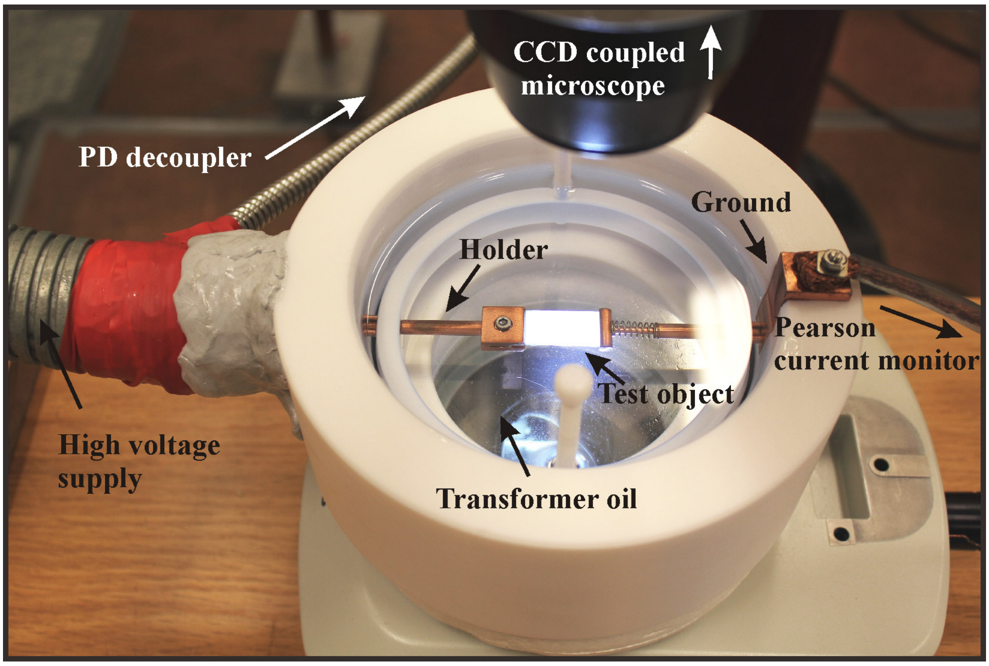

Figure 4.3 *New optical detection set-up for the treeing experiments, showing a microscope coupled to a CCD camera and the new object holder designed for the purpose.*

4.3 Properties of the PD Detection System

Not having access to an electrically shielded room for these measurements implies that some issues with background noise and disturbances in the signal have been encountered. Different types of noise could be distinguished and Figure 4.4 shows the background noise originating from the surrounding environment, which resulted in a peak-to-peak noise level of about 25 mV. This limits the trigger level used for detecting PDs in this work. Furthermore, the stepper motor regulating the voltage ramp produces a background noise of a similar range, though precaution has been made to shield and limit it. Unfortunately, a non-identified source has additionally produced considerably larger disturbance, appearing occasionally, thus destroying the measured signal and rendering PD detection impossible in some tests. If this happens in only a few signal traces of the test, these are simply removed from the analyses; otherwise the electrical detection from that test object has to be discarded. Due to these disturbances some tests series could not be analysed, however an adequate amount of data was obtained to perform a characterisation of the treeing process to a certain extent.

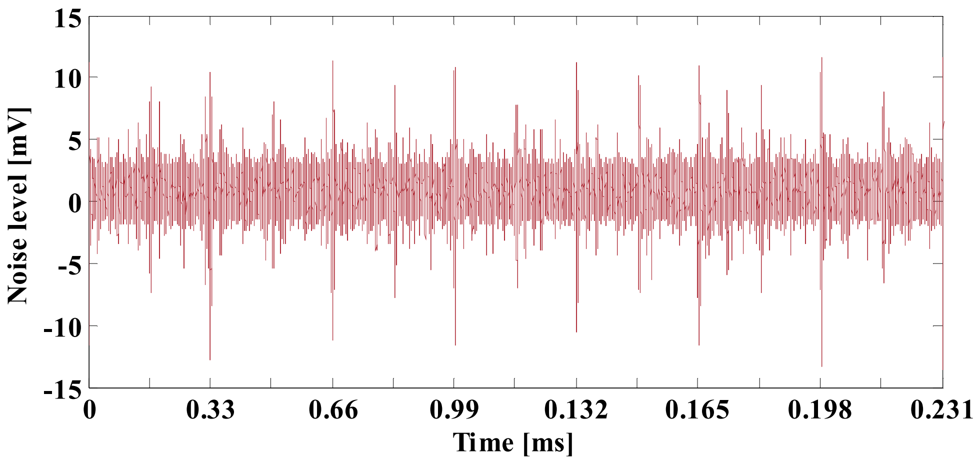

Figure 4.4 *Periodic background noise, without high voltage applied to the test set-up, limiting the detection trigger level.*

To estimate the charge of the measured PDs, calibrations were made with Haefly PD calibrator type 451 applying PD signals of 200, 100, 50 and 20 pC to the test setup in parallel to the test object. The resulting traces from this calibration are shown in Figure 4.5, with the signal from 20 pC charge omitted as it is below the noise level. As seen the sampling rate of 50 MS/s is not enough to resolve the oscillations in the applied PD pulse and accordingly the accuracy in the peak values of the detected PD becomes affected. The sampling frequency is however high enough, to detect the occurring PDs. Recreation of the apparent charge of the PD by integration of the voltage will thus not be accurate, due to both the poor sampling rate and the background noise. Therefore a simpler approach of correlating the peak-to peak value of the signal is chosen as an indicator of the PD amplitude. For the three cases of 200, 100 and 50 pC; the corresponding peak-to-peak voltages are 212, 100 and 52 mV, respectively. A linear relation can be observed between the voltage amplitude and the charge and 1 mV in the measured PD signal represents about 1 pC in the magnitude of the partial discharge. The presented results will be provided as peak-to-peak values in V, as more focus is put here on differences in the PD activity rather than on the determination of their physical behaviour.

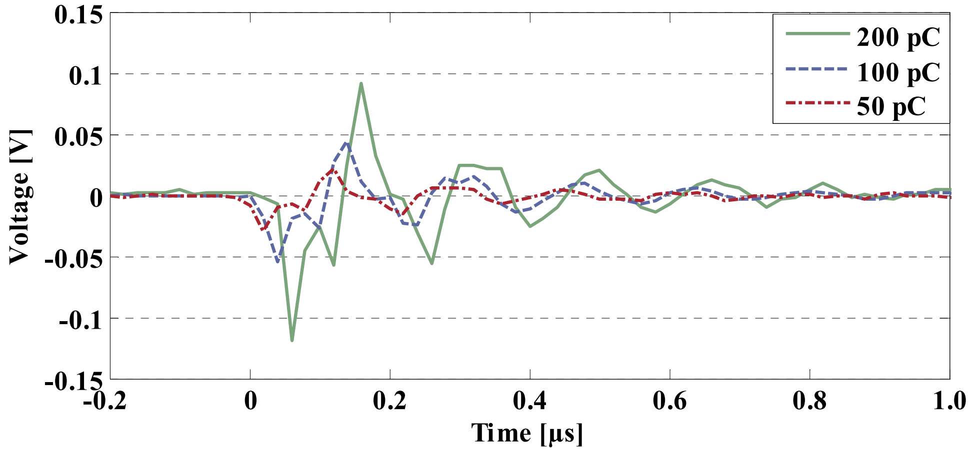

Figure 4.5 *Signals from calibration pulses of 50, 100 and 200 pC connected in parallel with the test object.*

The 50 Hz sinusoidal voltage is sufficiently suppressed for direct PD detection. However, to minimise the influence of noise and the voltage ramp to allow also for detection of weaker PDs an accumulated sum is subtracted from the measured signal according to Equations 4.1 and 4.2, as introduced in [85].

$$u_{acc}(t, c-1) = \frac{u_M(t, c-1) + n u_{acc}(t, c-2)}{n+1} \tag{4.1}$$

where u_M is the measured signal by the oscilloscope, u_{acc} the accumulated sum from the earlier signal traces and n is set to the number traces chosen to average over. c is the recorded cycle number and t is time. For these test series n is set to 120 when applying the 20 V/s ramp speed and set to 20 for the faster ramp rates where the voltage remnant varies more between two consecutive traces, c.

$$u_{diff}(t, c) = u_M(t, c) - u_{acc}(t, c-1) \tag{4.2}$$

where u_{diff} is the difference between the captured voltage trace and the accumulated sum from the previous recorded traces. Due to the stochastic nature of PDs, both the phase locked disturbances and the remnant from the applied voltage are limited. Figure 4.6 illustrates how the signal-to-noise ratio is somewhat improved by removal of the low frequency contributions from the applied voltage. The described approach has been implemented in LabView, based on the acquisition software used in [85, 86].

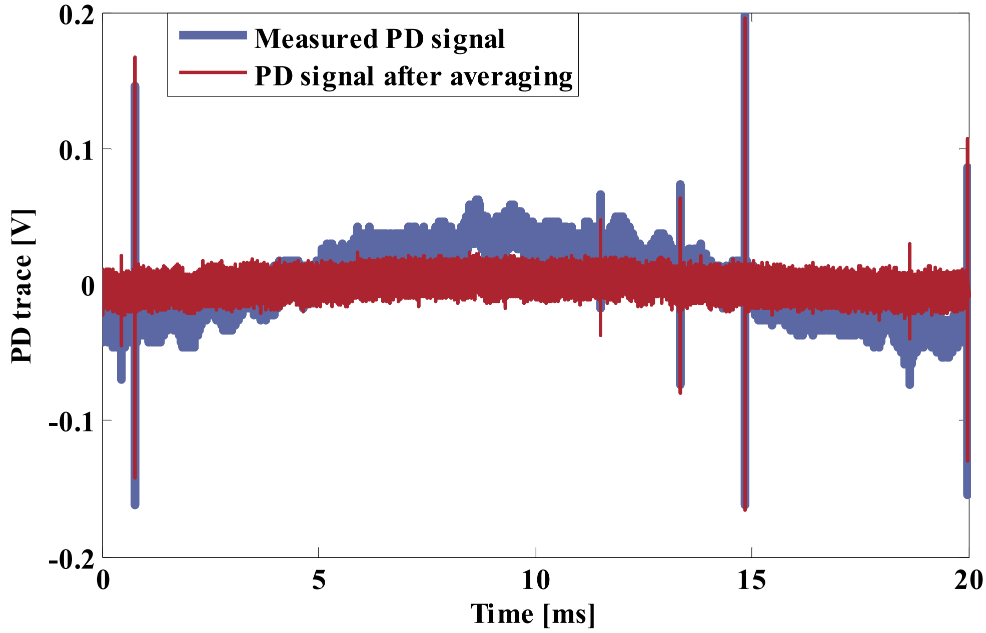

Figure 4.6 *PD signal traces (u_M and u_{diff}) and before and after the averaging, removing the voltage remnant from the applied voltage.*

U_{diff} is then employed in detecting the PDs by using a simple threshold, PD_{trig}, value of the peak-to-peak voltage. The PD_{trig} level has been set to 0.035 V for the PD decoupler trace and to 0.002 V for the Pearson current monitor. Two traces originating from the same PD are displayed in Figure 4.7 together with the different trigger levels (note that both the current signal and its trigger level are amplified ten times in the figure for comparison purposes). The low sample rate limits the accuracy of the PD amplitude estimation. However by increasing it, the time between two consecutively captured traces is increased also, thus the 50 MS/s rate was chosen as a suitable trade-off.

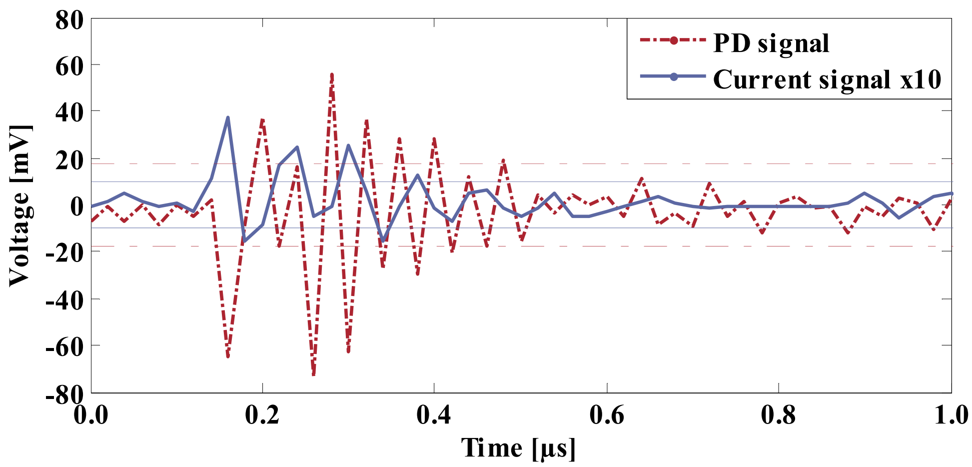

Figure 4.7 *Recorded PD and current signals, together with indicated detection trigger levels. Note that the current signal has been magnified ten times.*

In theory, the relation between both measured PD amplitudes for the two employed detectors should be closely linear. Figure 4.8 shows a phase-resolved pattern of PD amplitude (PRPDA) detected for a single test object during a complete voltage ramp by means of both the detectors. To enable the comparison, the voltage measured by the Pearson current monitor is scaled with a factor of 24.24 (estimated from Figure 4.7). Some deviations can be noticed, both as lower and higher values (indicated in the highlighted box), which can probably be attributed to the low sampling rate. It can further be noted that the PD decoupler allowed detection of smaller PDs.

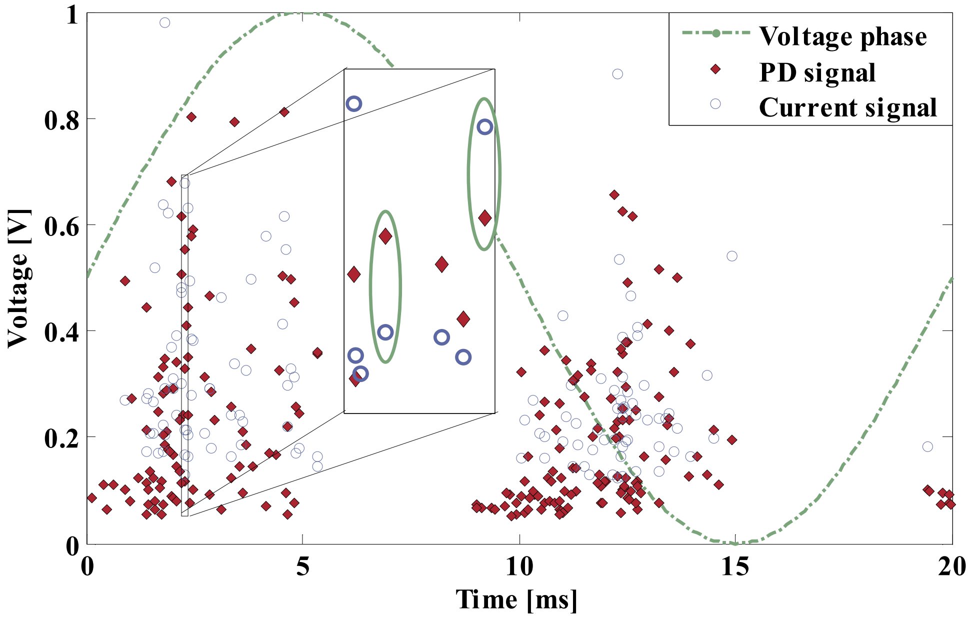

Figure 4.8 *PRPDA pattern detected in the same test object by PD decoupler and Pearson current monitor while the applied voltage is ramped up. As seen, the amplitudes do not scale with a constant.*

The presented data indicate for some advantages of the PD decoupler approach. Therefore, in the following no more results obtained by means of the current monitor will be presented.

4.4 Characteristics of PD Behaviour

In order to correlate the optical detection of the treeing processes with analyses of the in parallel ongoing PD activities, aspects and possible approaches were investigated. These are presented in this section.

4.4.1 PD versus Optical Detection with Respect to Initiation Voltage

In real-time, the results of optical observations and electrical detections appeared quite simultaneously. However, when analyzing the video recordings frame by frame, it appeared that the optical evidence of the inception could be observed somewhat before the PD signals were detected above the noise level. Figure 4.9 elucidates this correlation by comparing the tree initiation detected with the optical system to that of the PD decoupler for the different investigated ramp rates.

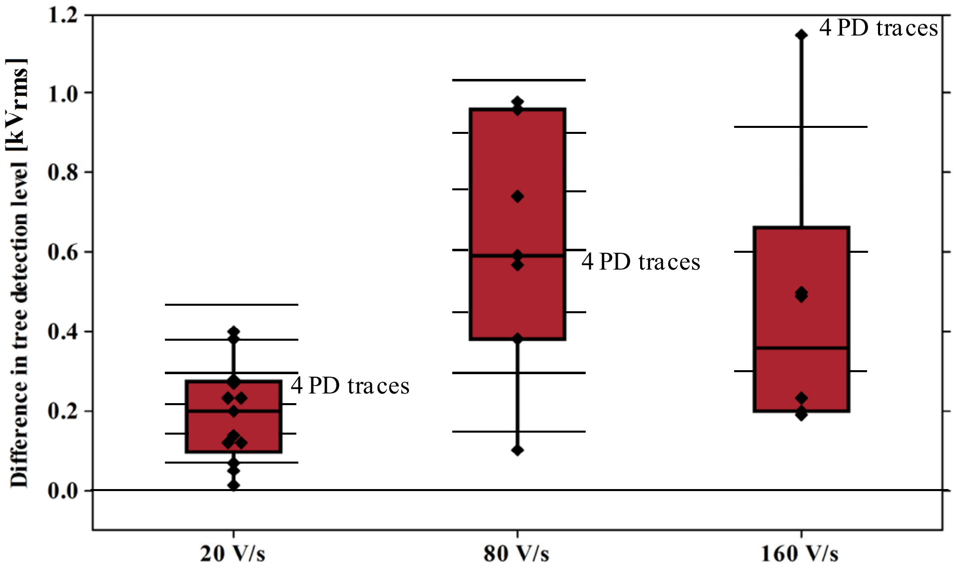

Figure 4.9 *Box plot illustrating the difference in tree initiation voltage for trees measured by PD decoupler as compared to the results of optical observations. The 0 kV level corresponds to the optically detected tree initiation voltage.*

The voltage level where the first tree is optically detected is set in the figure as zero voltage level. The difference between this voltage and the level of the first detected PD is plotted in form of the raw data as well as fitted to a box plot, with the mean and the 75 percentiles indicated. In addition the voltage steps between the captured cycles are indicated by black lines. As the time between recorded traces is constant, i.e. 1.7 s, the step in the applied voltage is larger between traces for the higher ramp rates. It can be observed from the figure that the lowest ramp rate shows least difference between the optical and the electrical detections, with a mean value of the difference at around 0.2 kV and a maximum deviation slightly higher than 0.4 kV. For the intermediate voltage ramp rate these values are respectively 0.6 and 1.0 kV, though for the fastest ramp rate the mean value is reduced to 0.3 kV even though the maximum deviation is still high, close to 1.2 kV. The reduction in the mean value for the fastest ramp rate could be a result of the too low number of data points, however it could also be related to the fact that trees at the higher ramp rates initiate at higher voltage levels and grow more rapidly, probably producing larger PDs from the beginning. It can also be noticed that for all ramp rates, some of the optically detected inceptions are detected electrically during the subsequently recorded PD trace. In other cases a few traces are needed before the inception is electrically seen. For the two lower ramp rates, at most six to seven traces were needed, while for the fastest ramp rate up to four traces. The fact that not all trees can be detected in the subsequently captured PD trace is mainly attributed to the signal to noise ratio, the PDs may be weak and hidden in the noise. It might also be the case that PDs do not occur at every sinusoidal period, and as the system is limited to recording cycles every 1.7 s, i.e. every 85th cycle, no PD may exist in the tree channel during the first recorded cycle or cycles.

4.4.2 PD Activity versus Voltage Magnitude and Number of Trees

To elucidate how the PD activity depends on the treeing process in the test object a few parameters were analyzed. These are the number of PDs, as well as their maximum, summed and average PD amplitudes per sinusoidal period. Figure 4.10 illustrated a treeing progress in a test object, similar tendencies were observed in a majority of the test objects. The inception of each newly appearing tree and the rate of growth of the previous trees are seen in the pictures together with the corresponding initiation voltage level. To simplify the following analysis only the five first trees are illustrated.

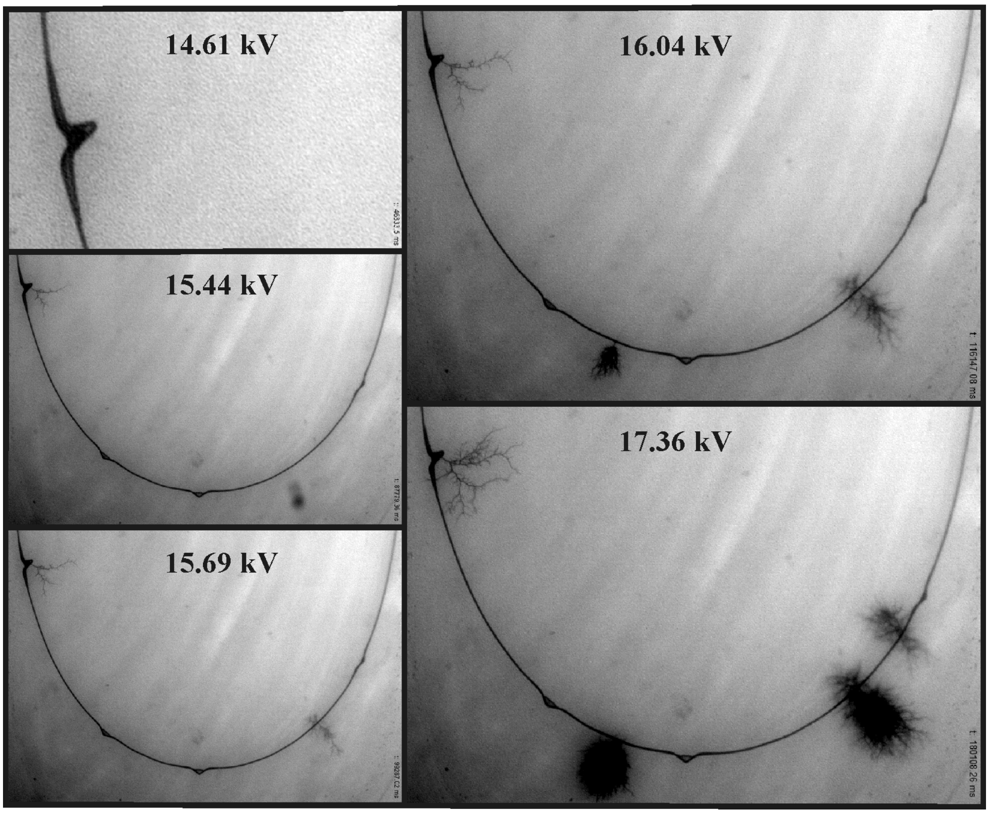

Figure 4.10 *Sequence of images illustrating initiation and development of electrical trees and voltage levels for five first trees appearing in the same test object.*

The raw PD data presented in Figures 4.11, 4.13, 4.14 and 4.15 reveal existence of a considerable variation of the measured parameters. To simplify the analysis a floating average, $PDnum_f$ for each data series was calculated according to Equation 4.3. $PDnum$ is the number of PDs in each trace and n is the number of subsequent traces used for the calculation. It has to be remembered that the ramp rate increases the voltage amplitude between each captured trace. Therefore different values of the cycle number n are utilized for the different ramp rates (according to Table 4.1) to ensure a good fit with the measured voltage. Accordingly, floating averages are also calculated for the summed, maximum and average PD amplitudes.

$$PDnum_{f,i+1} = \frac{PDnum_i + nPDnum_{i-1}}{n+1} \tag{4.3}$$

Table 4.1 *Values of n used for calculating the floating mean for the different ramp rates.*

Ramp rate (V_{rms}/s)	Cycle number, *n*
20	6
80	3
160	2

The measured behaviour of the different PD parameters are shown for the case illustrated in Figure 4.10. To simplify the comparison between electrical and optical detection, the initiation voltage for each tree is indicated on the x-axes in Figures 4.11, 4.13, 4.14 and 4.15. First the number of PDs detected per period is presented, in Figure 4.11. One may observe an apparent increase in number of PDs after the appearance of next electrical tree. This is further stressed by including slopes of the Number of PDs in the figure, displaying noticeable changes in the steepness.

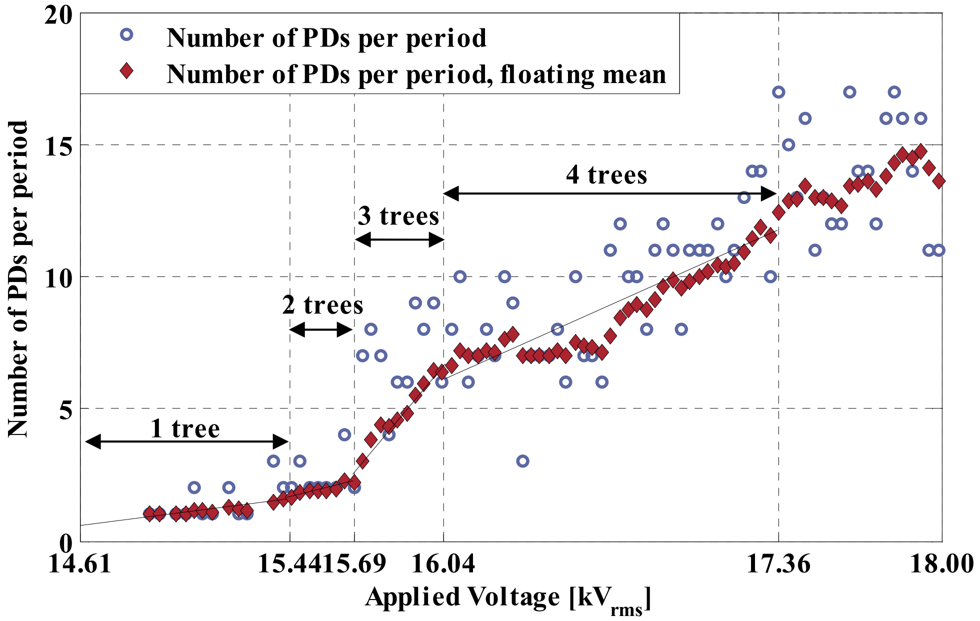

Figure 4.11 *Number of detected PDs per cycle for the test object illustrated in Figure 4.10. The indicated lines correspond to the case with one, two, three and four trees growing from the wire electrode. The tree initiation voltage levels for these first five trees are marked along the x-axis.*

The presented approach to identify appearance of new trees based on the PD data was utilized on several test objects. Figure 4.12 shows a comparison of such results for a test series (15 objects). A tendency for increase in the number of detected PDs, as represented by the increasing slope, suggests that this type of analysis provides a possibility to follow the inception of new trees in the insulation.

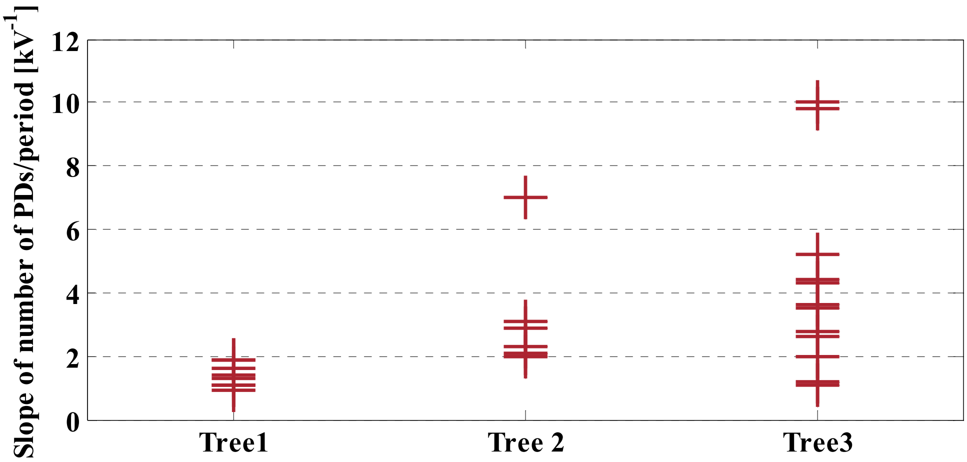

Figure 4.12 *Slope of the number of PDs per period for the first three trees appearing along the wire electrode in 15 studied test objects.*

The next considered parameter is the summed PD amplitude, which shows a correlation between the applied voltage level and the number of trees (Figure 4.13). Here a similarity to the data presented in Figure 4.11 is seen. A larger summed PD magnitude can be observed as the number of trees increases. This relation between the number and the total amount of detected PDs has been observed through all the tests employed in this study. However since the resolution employed in this investigation is limited, the evaluation of the number of PDs detected is probably a more accurate measure at this stage.

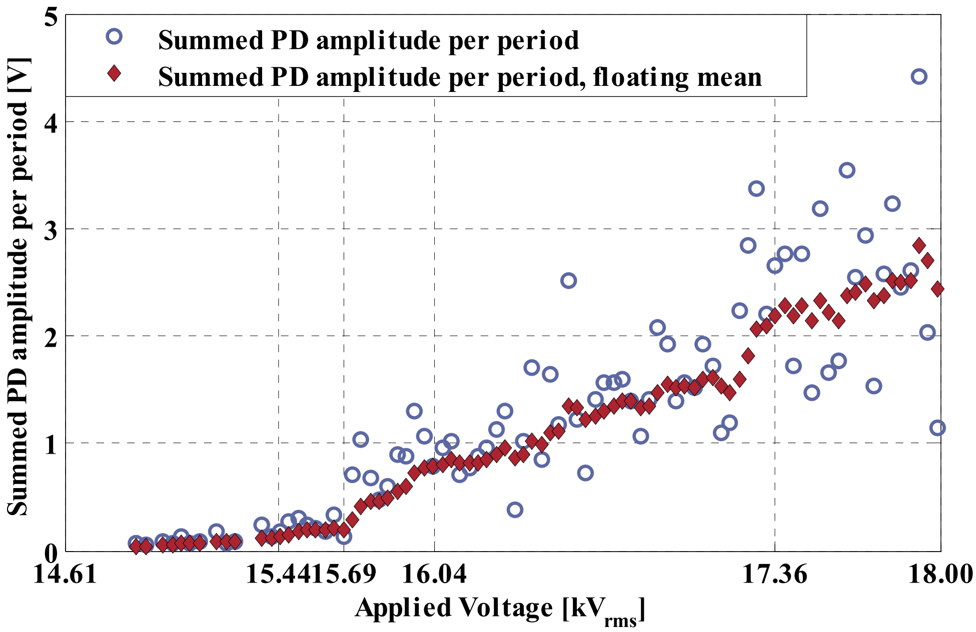

Figure 4.13 *Summed PD amplitude per cycle, for the test object illustrated in Figure 4.10. The TIV for the first five trees are marked along the x-axis.*

The relatively stable relation between the number of detected PDs and the summed PD amplitude suggests that the average amplitude should be relatively constant, which is further illustrated in Figure 4.14. An additional observation based on several data series suggests that the average PD amplitude converges to 0.2 V, independently of the ramp speed and eventual addition of voltage stabiliser to the investigated XLPE. When reaching this level of PD amplitude, all the test objects had exhibited intensive tree growth (Figure 4.10 at 17.36 kV). Finally the maximum PD amplitude detected in each period is plotted in Figure 4.15.

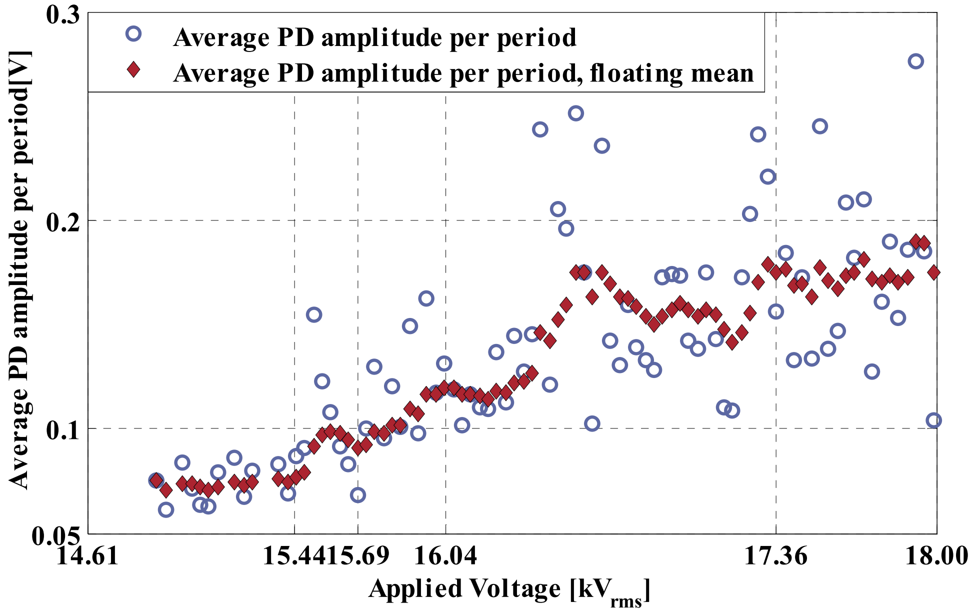

Figure 4.14 *Average PD amplitude per period, for the test object illustrated in Figure 4.10. The TIV for the first five trees are marked along the x-axis.*

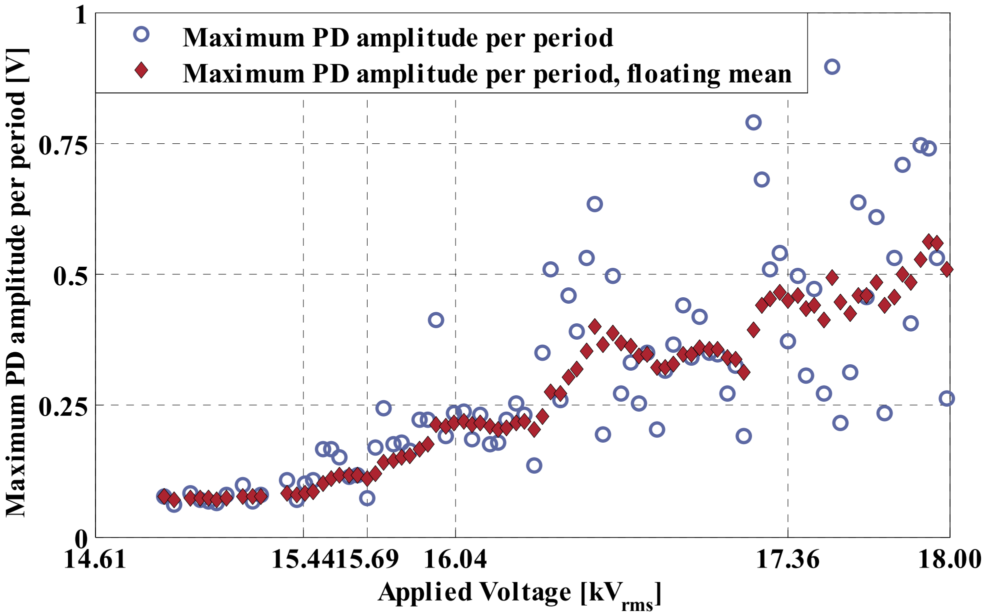

Figure 4.15 *The maximum PD amplitude per cycle, for the test object illustrated in Figure 4.10. The TIV for the first five trees are marked along the x-axis.*

The most apparent observation is that the amplitude increases together with applied voltage level. A natural assumption is that this is caused by both the gradual growth of the tree channels in volume as well as the voltage increase.

4.5 Correlation of PD Activity to the Number of Incepted Trees

So far the gradual changes in PD characteristics have been evaluated for increasing number of trees. In this section the data values of the relevant parameters discussed in previous section are compared at test completion. First it is concluded that the number of PDs per period are related to the number of trees found in the samples. As shown in Figure 4.16, a fairly linear correlation between the number of PDs and the amount of trees can be observed.

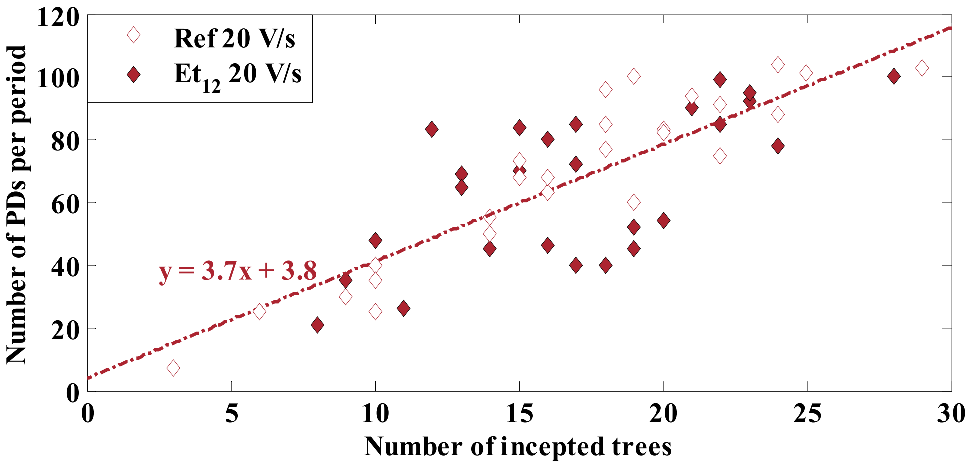

Figure 4.16 *Number of PDs versus number of incepted trees found after test completion. The data is fitted to a linear function.*

The same approach was used on the summed PD data, which according to previous observations regarding the converging average amplitudes, should closely follow the relation between the number of PDs and the number of trees. Figure 4.17 indicates that this correlation indeed takes place. From this also the number of PDs follows the summed PD amplitude, presented in Figure 4.18. The presented observations enable the evaluation of new materials' resistance to treeing. However additional tests are still necessary to further explore how to use the PD characteristics in an optimal way.

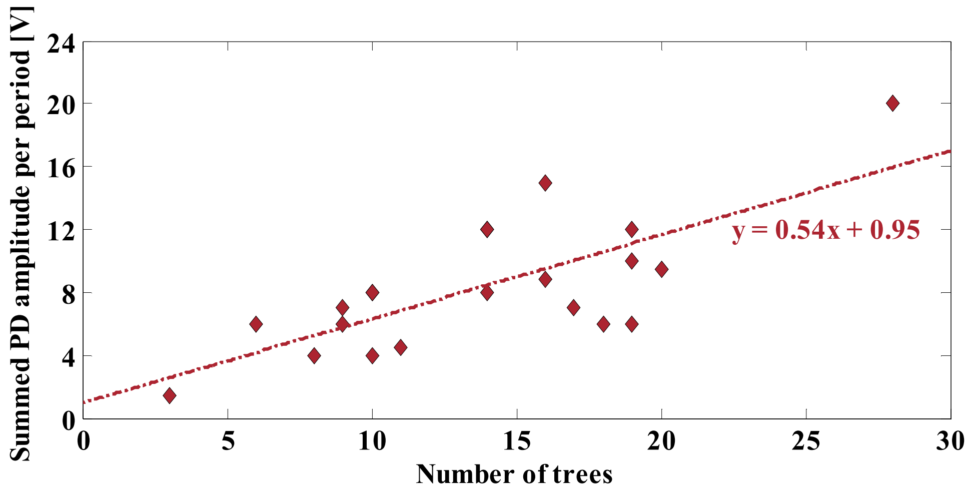

Figure 4.17 *Summed PD amplitude per period versus the number of incepted trees at completed test, fitted to a linear function.*

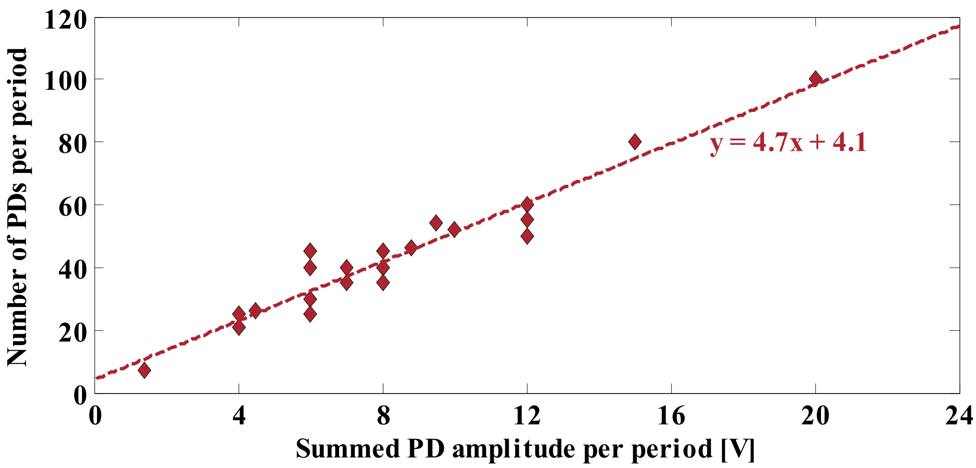

Figure 4.18 *Number of PDs per period as a function of the aggregated PD amplitude per period.*

The tree inhibiting effect caused by introduction of the stabiliser into the XLPE should be reflected in the information provided through PD analyses. To enable such a comparison, the results of analyses are presented in Weibull statistics plots; the optical measurements of the initiation voltage level for the first four trees are fitted to a three-parametric Weibull distribution, see Figure 4.16. As a first approximation, the data for the four trees observed optically are compared with the expected number of PDs presuming five trees are incepted, assuming that a few have originated from defects. It is assumed, based on the approximation from Figure 4.16 that 22 PDs per period are by average corresponding to the formation of five trees. The voltage level at which this number of PDs are detected is retrieved as the tree initiation voltage of the investigated test objects. Three-parametric Weibull distributions from both the optical and the proposed electrical detection method of test series for the reference as well as the stabilised material are illustrated in Figure 4.19, together with the fit using optical detection. As can be observed the stabilised material shows higher resistance to electrical treeing and this behaviour is also reflected in the PD data, as expected. This suggests that the electrical approach can be employed to evaluate different materials based on the electrical measurements only.

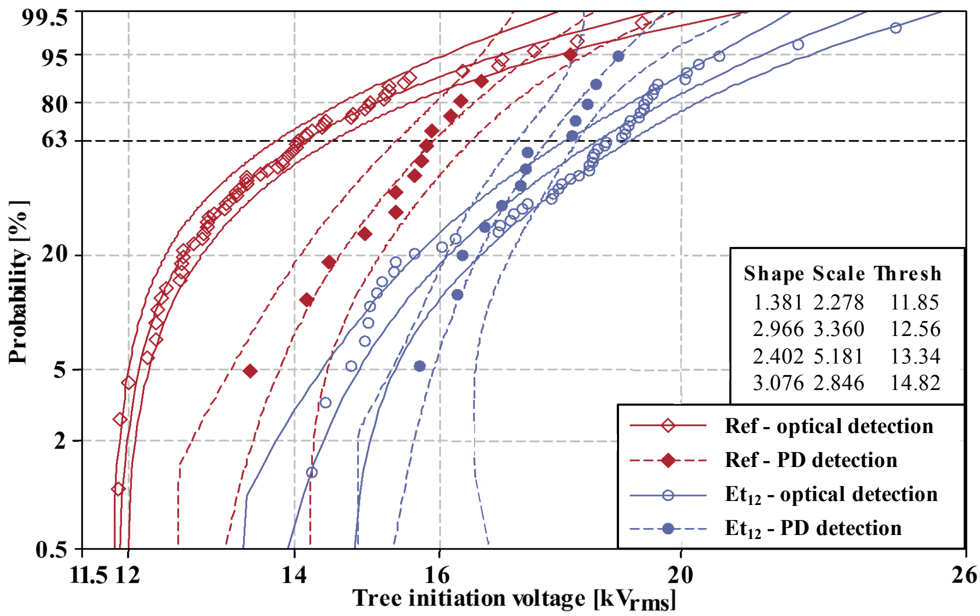

Figure 4.19 *Three-parametric Weibull fit of tree initiation voltage for the two materials compared. Fits are presented for both the optical data and from the PD measurements.*

4.6 Influence of Test Object Orientation

So far the relation between the measured PD characteristics and the tree initiation voltage and growth has been presented. An attempt to increase the sensitivity of the measured PD signals is now discussed for a case of switching the test object orientation, i.e. by forcing the trees to incept at the wire electrode while remaining at a ground potential. The used connection of the test object in the setup presented in Figure 4.3 is made with the sample holder mounted in the opposite direction, maintaining the PD measurement circuit always coupled to the high voltage side. In theory, the electric field distribution should remain independent of the object orientation if not considering capacitive couplings to surroundings. The latter can be represented in form of parasitic capacitances as represented in Figure 4.20. Reversing the object polarity would also be advantageous if attempting to measure the change of object capacitance during the treeing process [87].

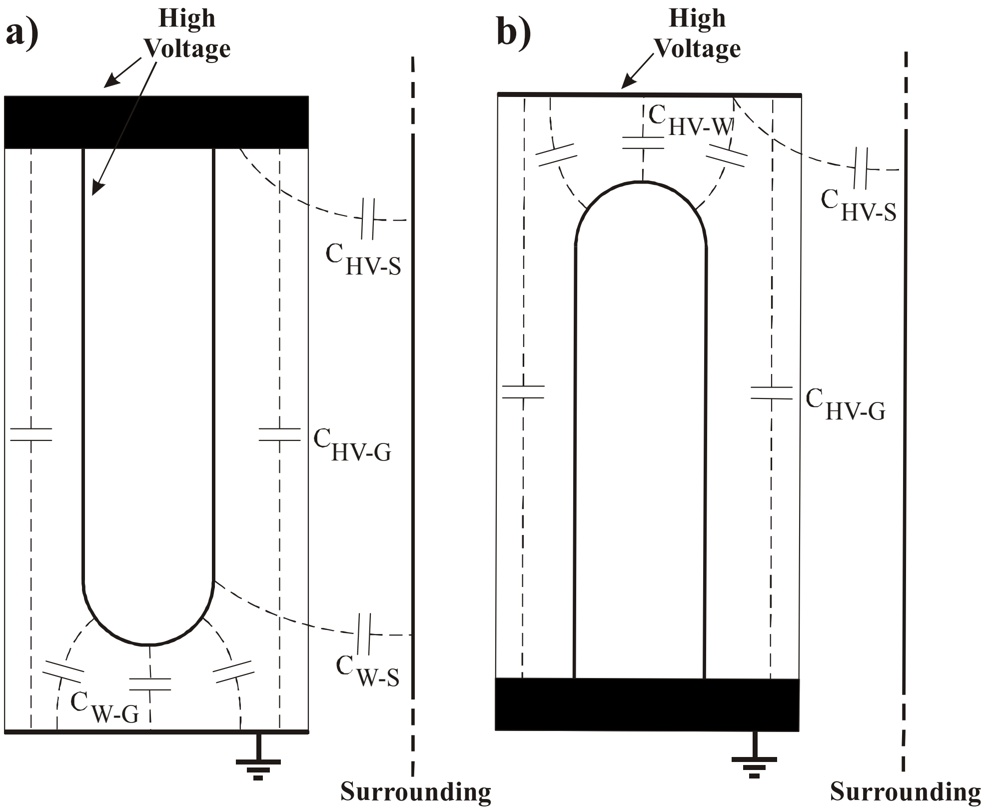

Figure 4.20 *Stray capacitances between the two electrodes and to the surrounding, influencing the field distribution.*

To evaluate this method, six test objects with reference XLPE for both cases were subjected to treeing test; this is repeated also for the stabilised XLPE. In Figure 4.21 two test objects are illustrated showing that the electrical tree growth is affected by switching the test object orientation, an obvious observation is that fewer and less developed trees can be observed for the objects with a grounded wire. It is therefore suggested suggesting that the influence of the stray capacitances on the actual electric field distribution is significant. This was further supported by numerical simulations, similar to those described in Section 3.2, where the grounded surrounding is implemented into the model as a distributed capacitance with zero potential at a given distance from the object surface. By using a distance of 5 cm, which well corresponds to the geometrical arrangement in the test setup, the maximum electric field at the wire becomes lowered by 20 % when applying high voltage potential to the plane electrode.

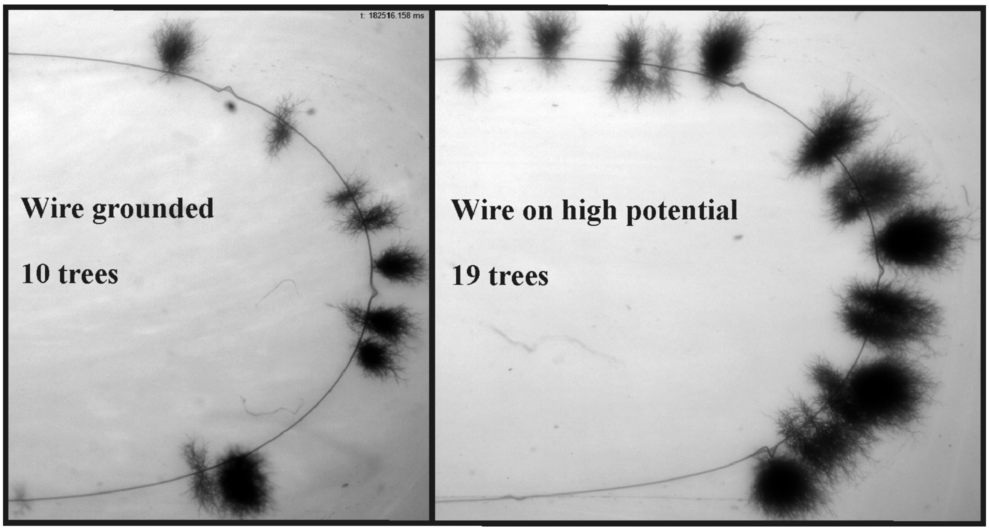

Figure 4.21 *Typical behaviour of type and number of trees for test objects with wire electrode connected high voltage or ground potentials. The images display all trees appearing after finished measurement at 21 kV.*

As concluded earlier, the number of detected PDs was considered an important indicator to evaluate the number of trees present in the insulation material. When performing such evaluation for the two test objects illustrated in Figure 4.21, the same tendency is found. It is illustrated in Figure 4.22 where the comparison is made up to the maximum voltage level, thus including the all incepted and growing trees.

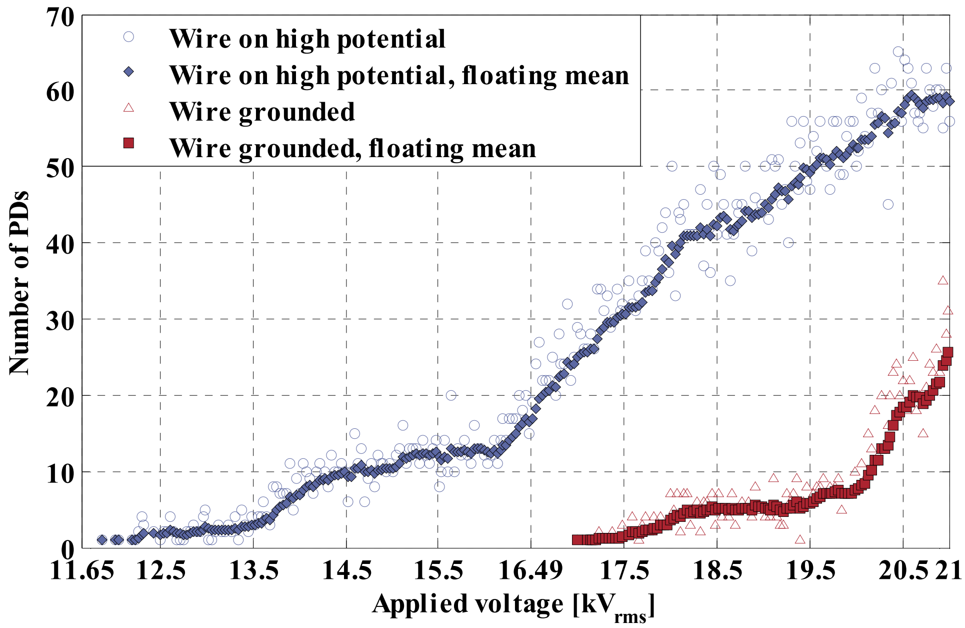

Figure 4.22 *Number of PDs measured for the two objects illustrated in Figure 4.21. The first trees incepted at 11.65 kV for the wire on high voltage potential and at 16.49 kV for the grounded wire.*

It was earlier concluded that the relation between the number of detected PDs and the summed PD amplitude was close to constant due to the converging average PD amplitude. When comparing these characteristics in Figure 4.23 for the case with change object orientation, it appears that the same trend is followed, i.e. the PD amplitude of 0.2 V is the limiting level.

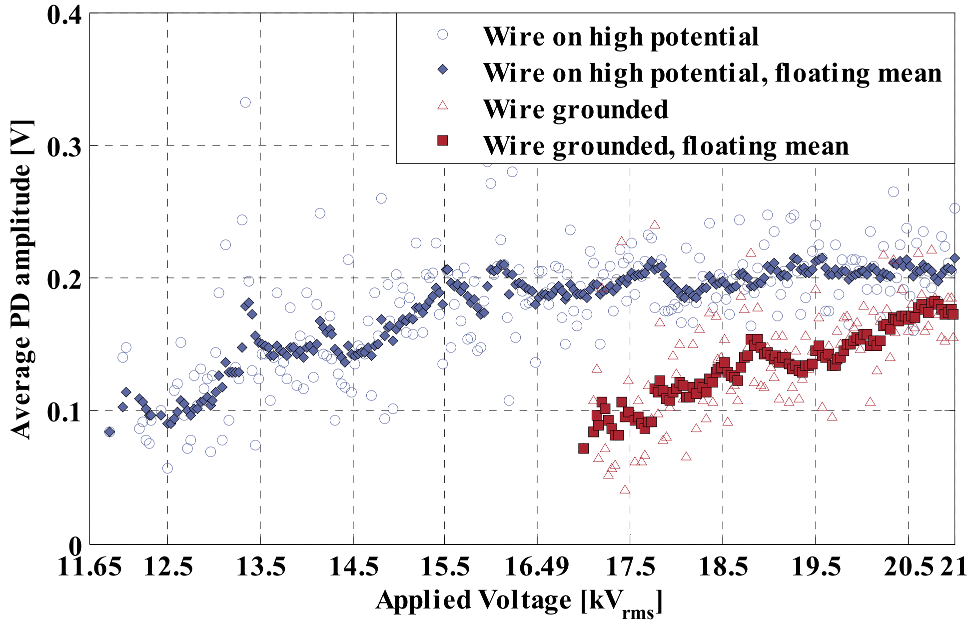

Figure 4.23 *Average PD amplitude for the two test objects illustrated in Figure 4.21.*

The natural conclusion from to the above presented observations is that the relation between the summed PD amplitude and the voltage level should follow the same tendency as discussed earlier. It thus should be closely related to the number of PDs detected. Which indeed is also the case, as illustrated in Figure 4.24.

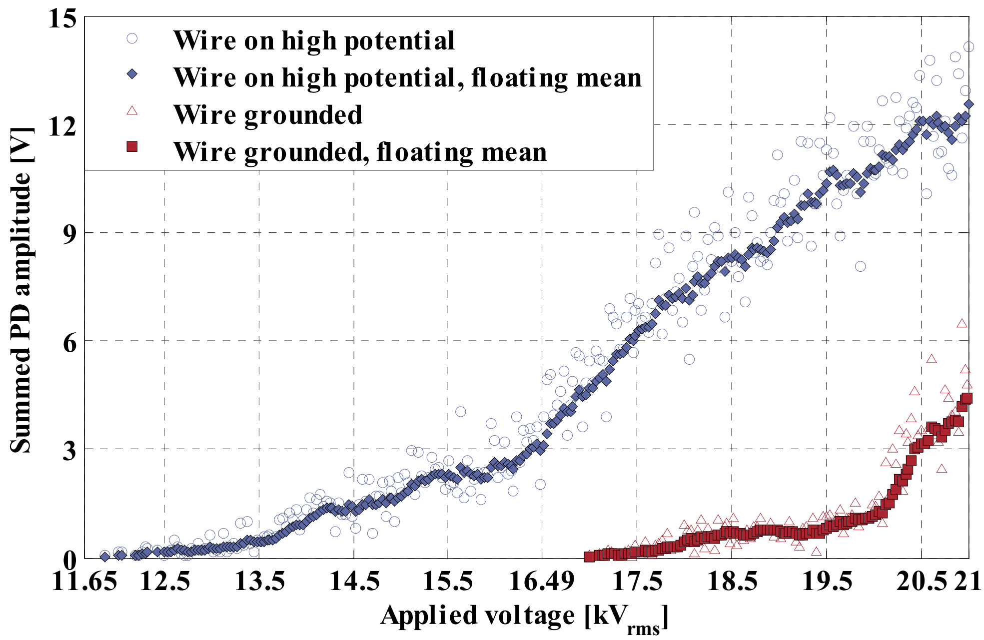

Figure 4.24 *Summed PD amplitude for the test objects illustrated in Figure 4.21.*

The final comparison between the maximum PD amplitude detected per cycle is shown in Figure 4.25. Here it is again clear that less can be said about the tendency of treeing, apart from the observation that the PD amplitude increases for higher voltage levels. It can be observed that the maximum PD amplitude, for the object with ground potential on the wire electrode, has not reached the same value at 21 kV. This implies that a multitude of branches increases the probability of large PDs, as the tree growth is less extensive for this case.

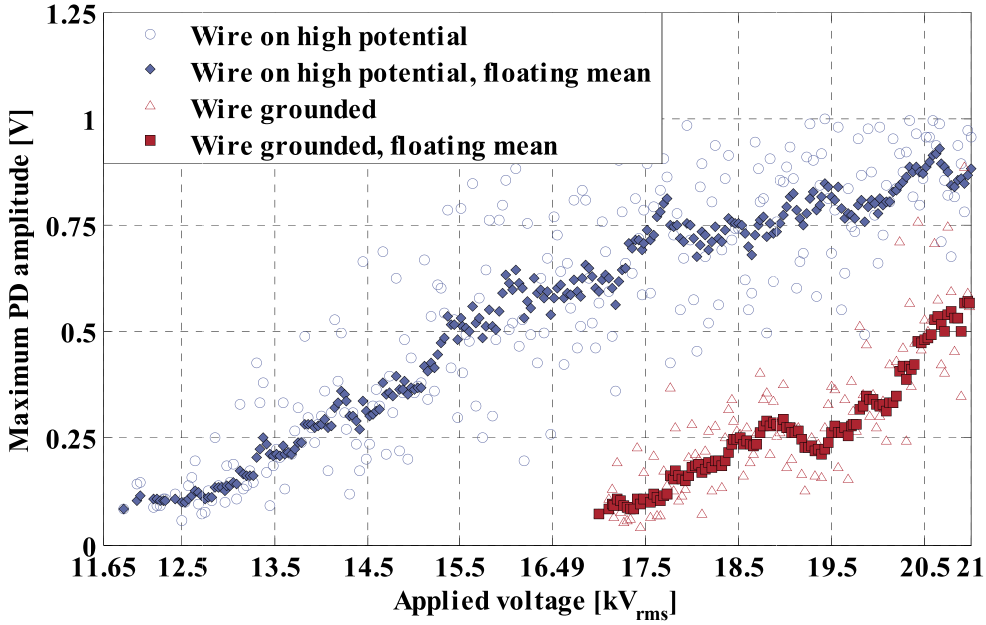

Figure 4.25 *Maximum PD amplitude for the test objects illustrated in Figure 4.21.*

Apart from comparing the PD characteristics and number of trees for the cases of having the wire either grounded or at high potential, a statistical analysis of the tree inception voltage was also made. The resulting Weibull distributions are plotted in Figure 4.26. For the reference an increase in tree initiation voltage is clear, for the stabilised material no such tendency is found, with a larger number of data would be needed for further clarification.

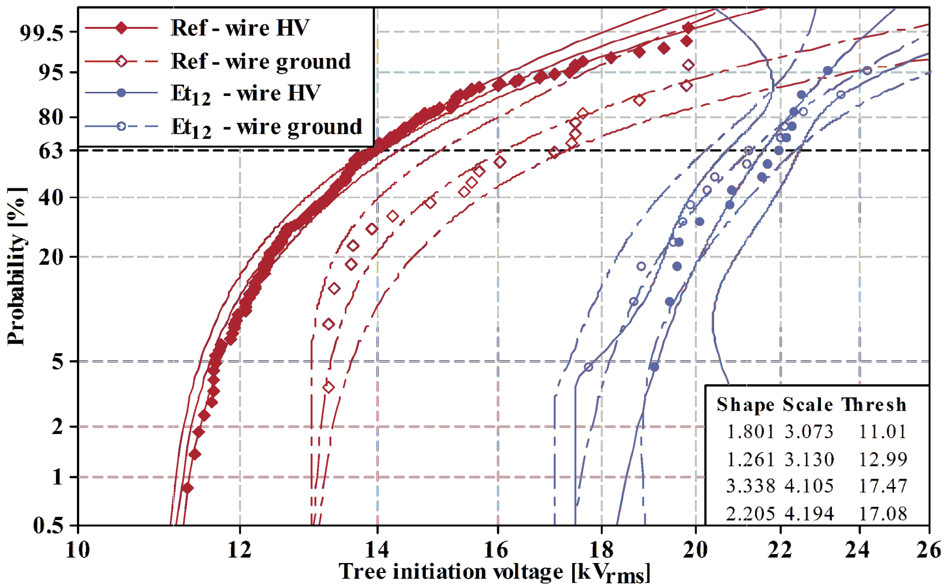

Figure 4.26 *Weibull plot of TIV comparing the configurations with ground and high potential on the wire electrode for both stabilised and reference material.*

4.7 Effect of Constant AC Voltage

To limit the influence of difference in voltage level at tree inception and during growth, further tests have been performed using a constant voltage level. The voltage was ramped with 160V/s to a constant level where it is kept during 3000 s. This level was chosen according to the optically obtained threshold values from Figure 4.19. Two different levels are used for comparison: 11 and 14 kV, however it was found that 11 kV was too low for inception of treeing in the stabilised XLPE. Six test objects were tested for the remaining different cases. Figure 4.27 shows a three-parametric Weibull distribution comparing tree initiation for both voltage levels and the two materials. Note that the x-axis represents time of initiation, as opposed to the tree initiation voltage magnitude used in the other Weibull plots. As can be seen trees appear later for the higher level of applied voltage, there is also a tendency that trees appear later for the stabilised XLPE, this could also be considered the case for 11 kV, where trees did not appear at all during the 3000 s. The difference in number of incepted trees is even clearer, with only 9 trees in the stabilised material comparing to the 42 incepted trees in the reference for 14 kV, 0 and 28 respectively for 11 kV. This concludes that the voltage stabilising effects evident during ramped AC voltage, from Figure 4.19, are also reflected in the lower number of trees and time until inception for the constant AC voltage tests.

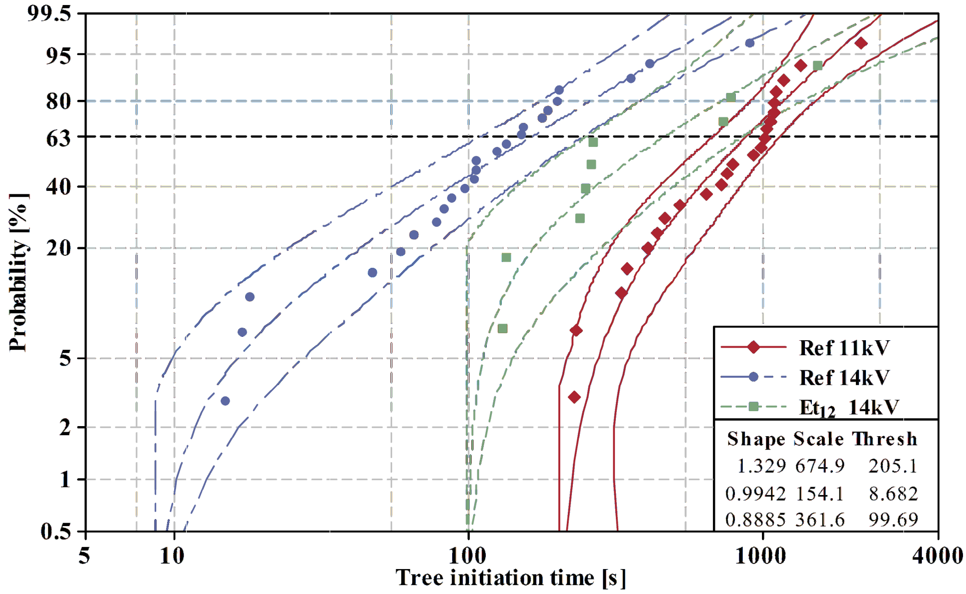

Figure 4.27 *Weibull plot of tree initiation time for reference and stabilised XLPE tested at constant AC voltage amplitude.*

Further, a difference in tree structure was apparent, as is illustrated in Figure 4.28. At the previously described ramped AC treeing tests, even though the tree types vary, typically bow-type and quite dense bush trees appear. For the constant voltage test, which was instead kept for a longer duration of time, pine-like trees (with tiny branches) began to appear together with trees having longer branches extending from the wire, as shown in the figure. These pine-like trees where never appearing for ramped AC test, i.e. at no stage during their growth. The tree growth rate was also measured for the both materials at 14 kV, no difference in growth rate existed between the two materials though in the early stages of a tree the growth rate was higher.

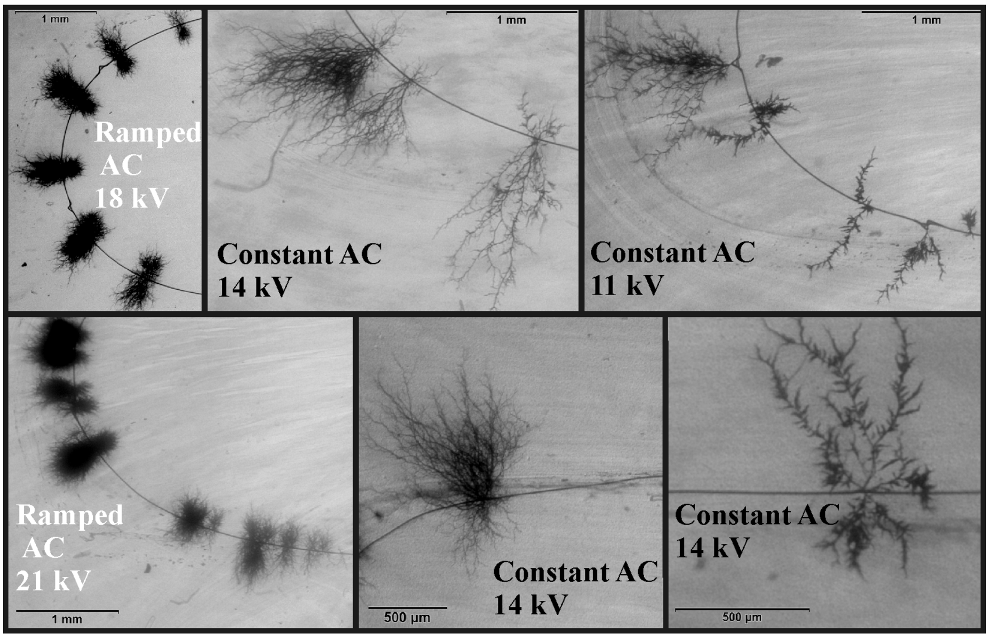

Figure 4.28 *Microscope images showing difference in tree structure for ramped and constant AC voltage. The top rows illustrates referens XLPE, the bottom row depict XLPE with addition of Et_{12}. The pine-like structure appearing at constant voltage levels was not present at ramped AC voltage, not even during the start of tree growth at lower levels. The voltage level indicated for the trees at ramped AC is the level during which the images are captured.*

4.8 Effect of Gas Release – Tree Puncture in the Test Object

In several objects one of the growing trees punctures the insulation. If this occurs to one of the trees close to the ground electrode, then a complete breakdown occurs at the interface between XLPE and oil. If on the other hand a tree punctures the insulation further away from the ground electrode the oil holds as insulation and the test can continue. For these incidents (six in total) a dramatic change in tree structure and growth rate is observed. The branches of the punctured trees increase their growth exceptionally, as compared to the neighbouring non-punctured ones. The pressure of the enclosed gas in the tree tubules is assumed to be linked the tree growth. As is seen in Figure 4.29 the punctured tree also has a much more branch-like appearance as compared to the neighbouring trees which have been exposed to the same voltage. These branches of the punctured tree are also considerably longer, stretching far into the insulation.

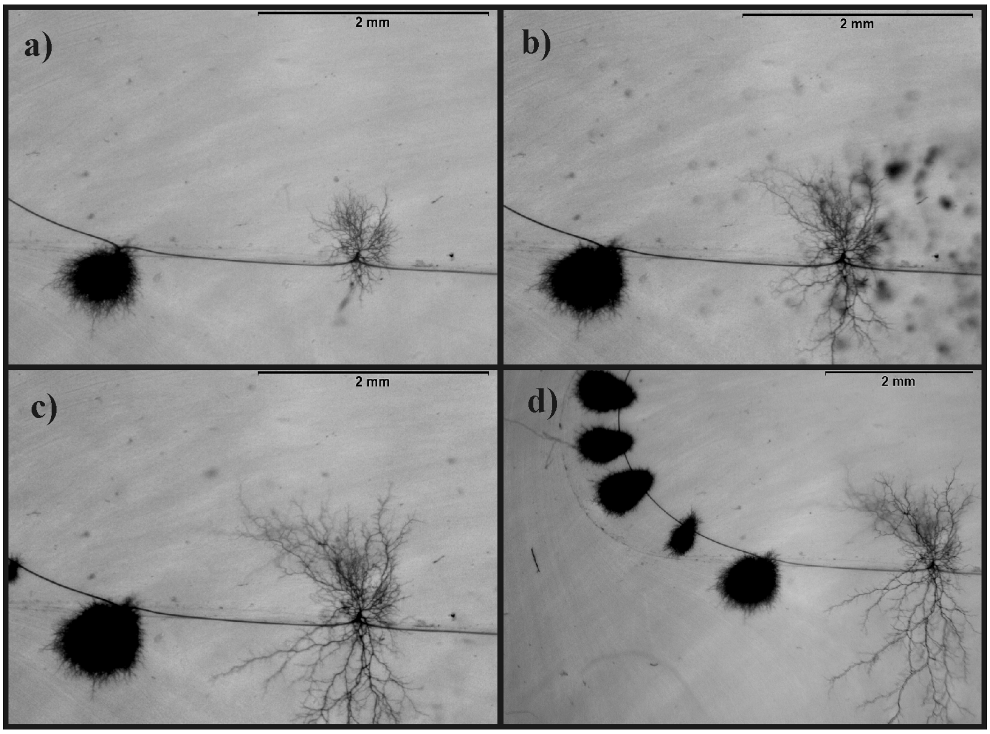

Figure 4.29 *Tree development after the tree to the right growths through the test samples and the gas is released from the tree channels. This tree is more widespread, with very branchlike structure. a) shows two trees at the time of puncture, b), c) and d) show the appearance with 100 s intervals. In b) the gas being released from the tree tubules can be observed as bubbles.*

Chapter 5

Performance of Voltage Stabilisers

To evaluate how to increase the treeing resistance of XLPE, a number of stabilisers have been tested and evaluated. Presented first in this chapter is a more extensive analysis of the addition of 4,4'-didocyloxybenzil (Et_{12}), as used in Chapter 4. This is followed by investigations on several other stabilisers belonging to the same group (benzils). These results are further presented in Publication VI. In addition the stabilising effect is related to the electron affinity of the used molecules. The design and synthesis of the tested stabilisers as well as the related molecular modelling was mainly made by Markus Jarvid and is in detail presented in his doctoral thesis [2] as well as in the listed publications from Chapter 1.2. Results from tests of the stabilising effect of fullerenes are presented in Publication VII. A number of thiaxanthone- and melamine-type stabilisers were also tested and accounted for in Publication VIII. Publication IX relates the molecular properties of the stabilisers to the tree inhibiting efficiency.

5.1 Annealing of Test Objects

To ensure a coherent procedure of the evaluation of materials with and without voltage stabilisers, all the test objects were heat treated after the preparation and degassing in an oven for five minutes at 130°C and then the oven was turned off and its temperature decreased to ambient, shown in Figure 5.1. As earlier investigations have revealed, the treeing inception voltage can be affected by annealing of the test object material [47, 48]. The electrical treeing tests were consequently performed on the following day; some additional tests were also made after 85 and 130 days of sample stored in aluminium bags at ambient temperature.

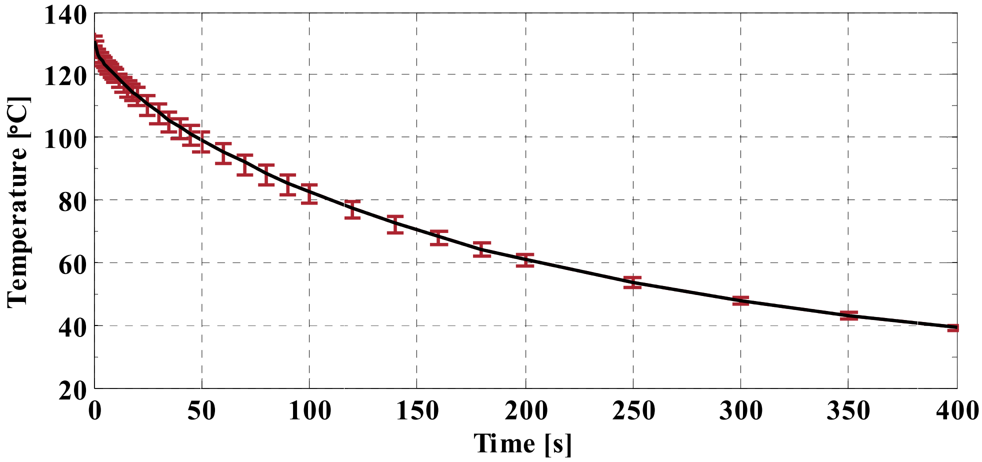

Figure 5.1 *Measured temperature decay during the heat treatment.*

5.2 Benzil-Type Voltage Stabilisers

5.2.1 4,4'-Didocyloxybenzil - Effect of Ramp Rate

So far the influence of different ramp rates has not been discussed in detail, apart for the comparison between the electrical and optical detection of the first appearing tree. As illustrated in Figures 5.2 and 5.3, the test ramp rate implicates a considerable influence on the voltage level of incepted trees.

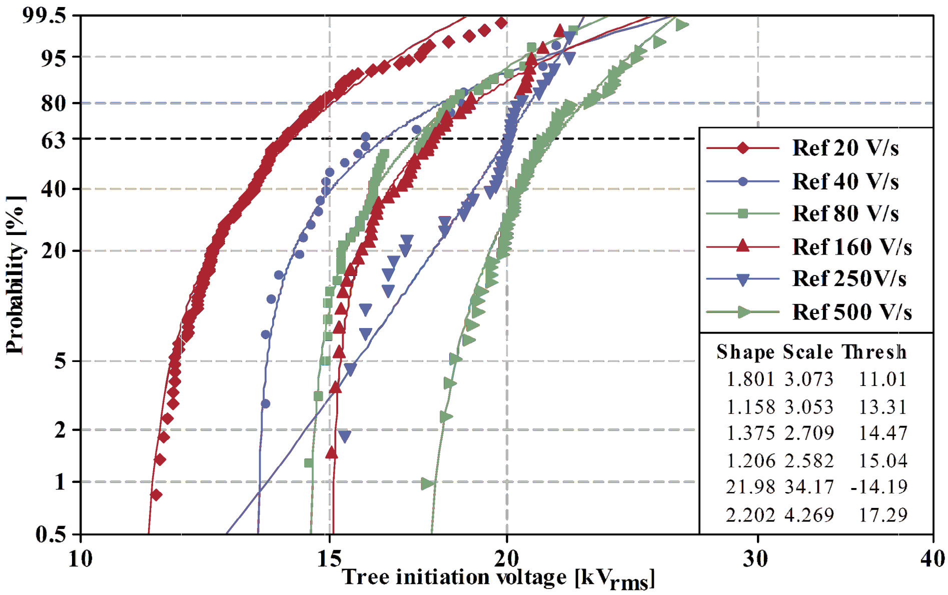

Figure 5.2 *Effect of ramp rate on tree initiation voltage in the reference material. The inception voltage increases with the ramp rate.*

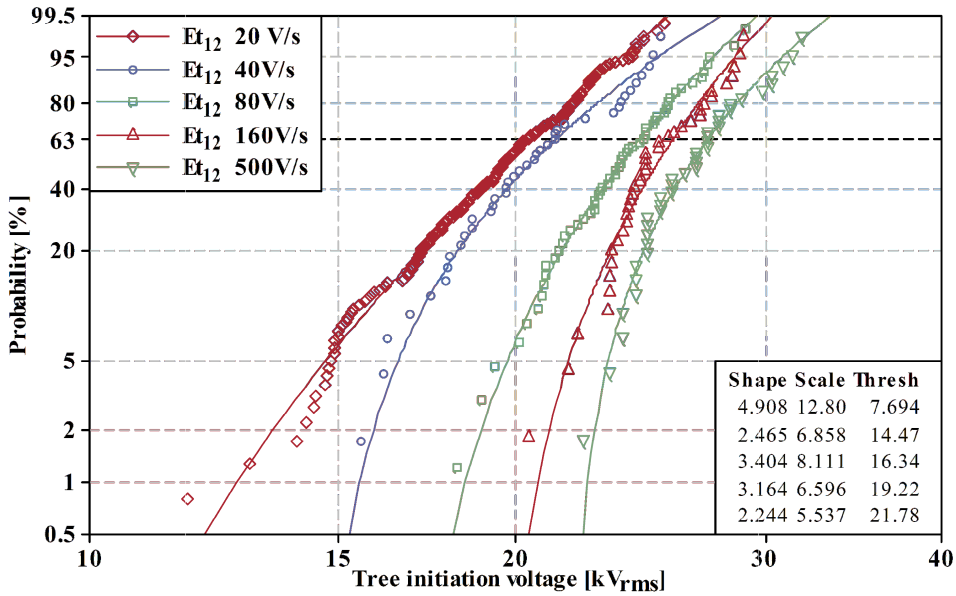

Figure 5.3 *Effect of ramp rate on tree initiation voltage in the stabilised material. The inception voltage increases with the ramp rate, as it does for the reference XLPE in Figure 5.2.*

This effect is apparent, for both the reference and the stabilised XLPE. The illustrated Weibull distributions show that a higher ramp rate increases the initiation voltage considerably for both materials. For in all ramp speeds the advantageous effect of the stabilisation remains. The relative increase in E_{63} percentile remains high (45.5, 30.3, 42.3 46.5 and 26.7 %) for the stabilised XLPE in comparison to the reference material for all the ramp rates between 20 and 500 V_{rms}/s, as listed in Figure 5.3.

5.2.2 4,4'-Didocyloxybenzil – Effect of Concentration

In order to study how the stabilisers tree inhibiting effect depends on the amount added to the polyethylene, concentrations of 10, 20, 30 and 40 mmol/kg have been tested. As shown in Figure 5.4 there is a clear increase from 10 to 20 mmol/kg, and a slight increase to 30 mmol/kg. Thereafter the treeing initiation level remains more or less equal for the higher concentrations, it is expected that this is due to the solubility limit in XLPE. Figure 5.5 shows the positive effect, with the number of appearing trees reducing at higher concentrations. These images all show the appearance when the ramped voltage has reached 20 kV_{rms}, this level is also marked in Figure 5.4

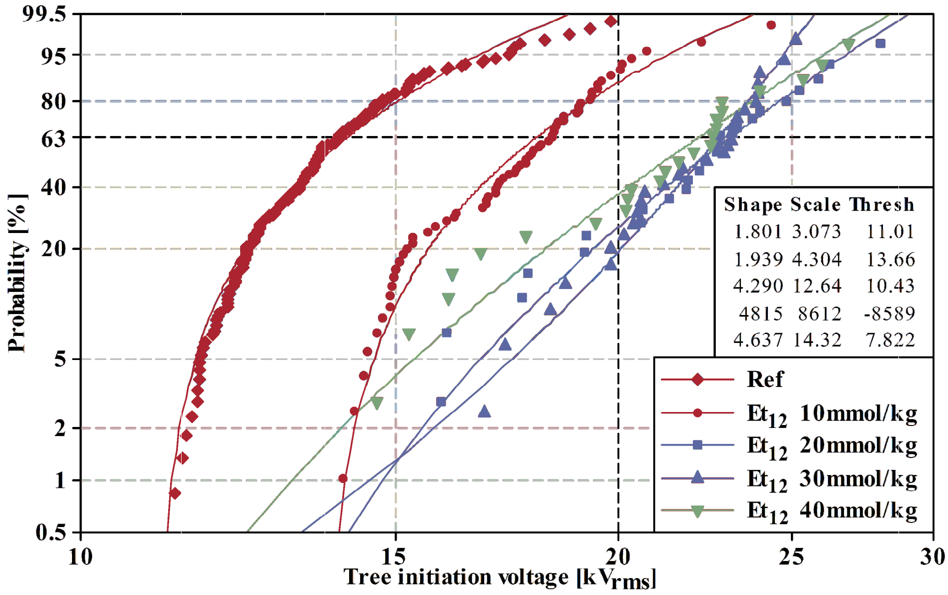

Figure 5.4 *Effect on tree initiation voltage by the amount of added stabiliser.*

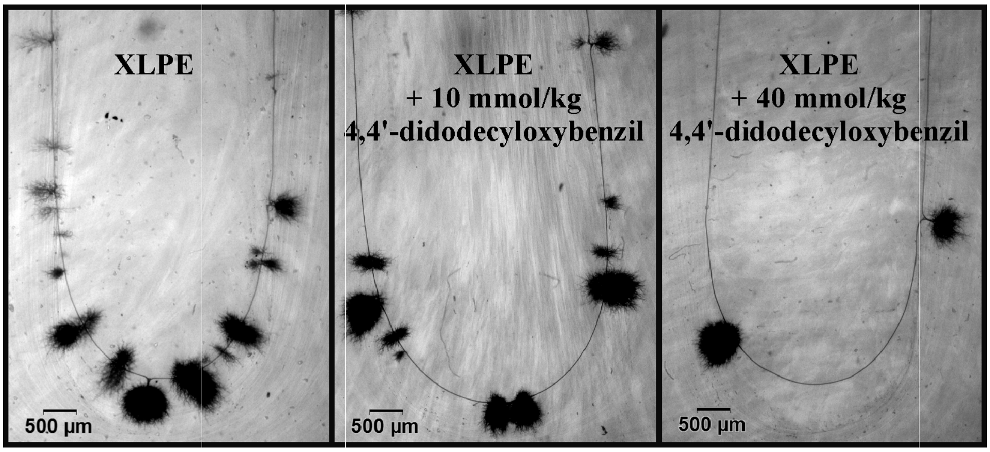

Figure 5.5 *Difference in tree growth at 20 kV$_{rms}$ for XLPE without and with 10 and 40 mmol/kg addition of 4,4'-didocyloxybenzil.*

5.2.3 4,4'-Didocyloxybenzil – Effect of Annealing

Some test objects have been stored for around 85 and 130 days prior to successive testing. After the first 85 days the efficiency of the voltage stabiliser has increased substantially, as reflected in the Weibull distributions in Figure 5.6. The additional 45 days has resulted in a weak further increase in tree initiation voltage, though the involved processes seem to have stagnated. For the reference XLPE this behaviour is not the case, after annealing the tree initiation voltage has become slightly lower, although still within the same voltage range. The relevant aspect is however here is to ascertain if it increased, which it has shown not to.

Figure 5.7 shows the increase in E_{63} percentile for all the annealed batches of objects containing different concentrations of Et_{12}, indicating a clear trend in increased resistance to treeing with time. This trend also appeared for other tested stabilisers. It is being speculated that migration of the stabiliser in the material is the main cause behind this increased strength. Filling of micro-voids can also be considered as an additional explanation.

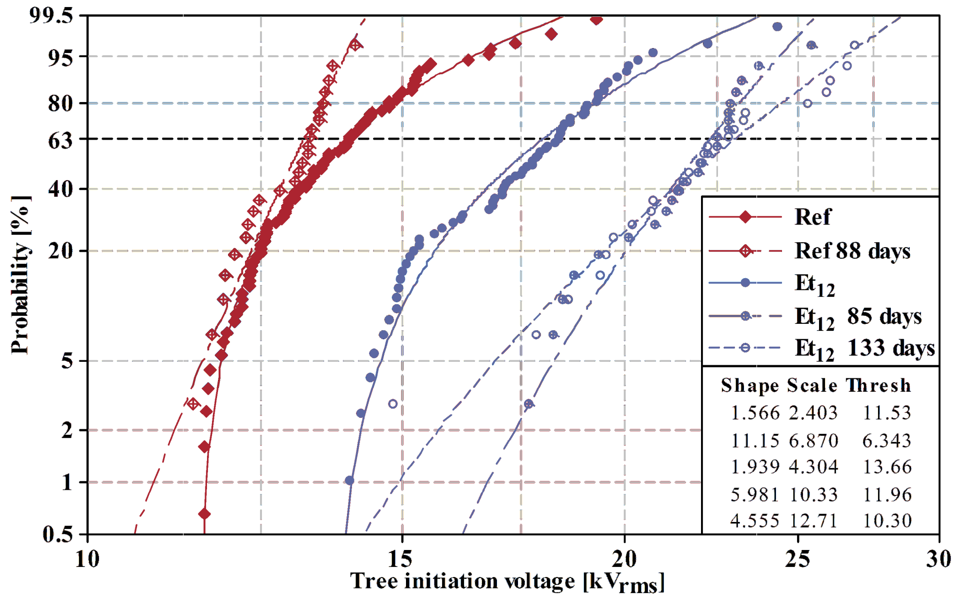

Figure 5.6 *Effect of 85 and 130 days of annealing on tree initiation voltage.*

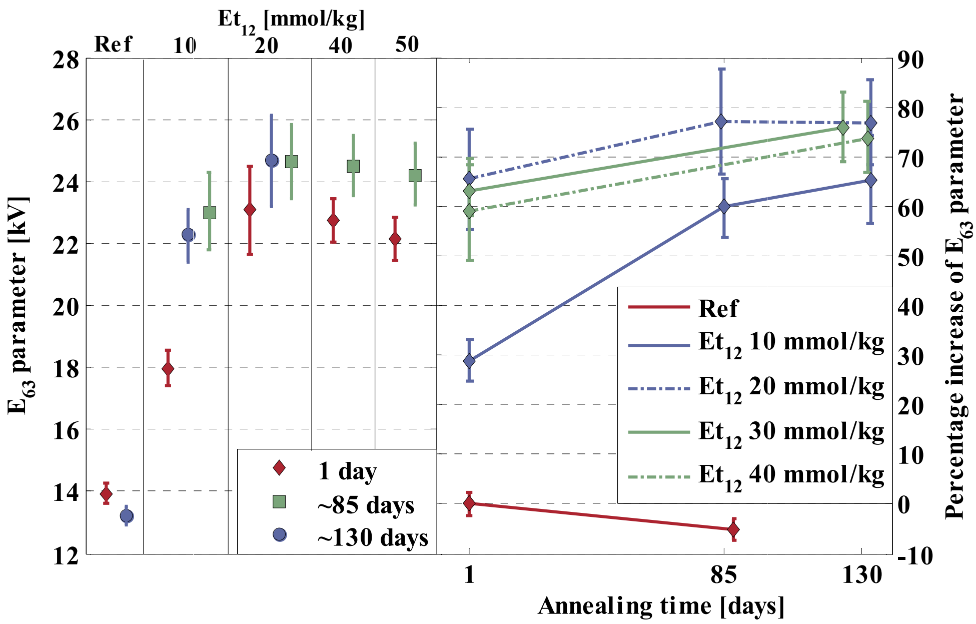

Figure 5.7 *Effect of annealing for 85 and 130 days on Weibull distribution parameters of tree initiation voltage.*

5.2.4 Other Benzil-Type Voltage Stabilisers

To further analyse the efficiency of benzil-type stabilisers, a total of eight compounds are tested, in which the benzil core is modified with alkyl chains of different lengths. Three different families of benzil-type structures with different side chains are compared to the reference XLPE. They are of ether, ester and tertiary amine type. Figure 5.8 shows the chemical structure of the different compounds: benzil, ether-type core with alkyl chains containing 1, 12 or 30 carbon atoms (Et_1, Et_{12} and Et_{30}), ester-type core with alkyl chains containing 2 or 12 carbon atoms (Es_2 and Es_{12}) and amine-type core with alkyl chains of 1 or 8 carbon atoms (Am_1 and Am_8). 4,4'-didocyloxybenzil is thus denoted here as Et_{12}. 10 mmol/kg of the stabiliser was added to the XLPE. Alkyl chains are advantageous from a processing perspective since they reduce the melting temperature of the voltage stabiliser significantly and can also give a better miscibility with polyethylene.

The attachment of side chains to the benzil core has further the benefit of decreasing the vapour pressure compared to that of neat benzil, which starts to sublimate at 133 °C, i.e. below the temperature used during cross-linking. It was also consequently discovered that pure benzil suffered from almost complete sublimation during preparation of the test objects, and this should be considered when evaluating the electrical treeing test results. Fourier transform infrared spectroscopy (FTIR) analysis confirmed however that the other stabilisers: Et_1, Et_{12}, Et_{30}, Es_2, Es_{12}, Am_1 and Am_8 remained in the polyethylene material after its cross linking without any noticeable loss.

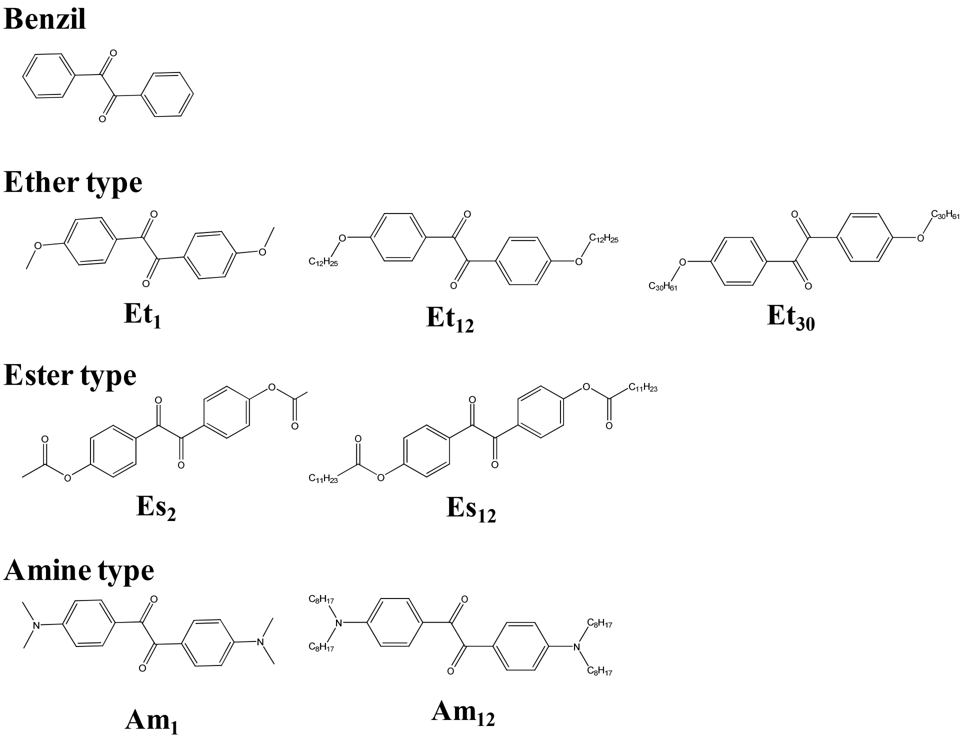

Figure 5.8 *Chemical structures of the tested benzil-type stabilisers.*

Figure 5.9 shows Weibull distributions of the tree initiation voltage of XLPE materials containing the benzil-type voltage stabilisers as well as the reference XLPE material. As can be noted the initiation voltage is increased for all stabilisers and shorter alkyl chains improved the resistance to treeing more significantly. The ester, Es_1 and amine, Am_1 have increased the E_{63} value most, by around 75 %. The threshold level is somewhat more uncertain due to a rather low number of data in some of the test series. The E_{63} and threshold levels and their respective increase in percent in relation to the reference XLPE are collectively plotted in Figure 5.10.

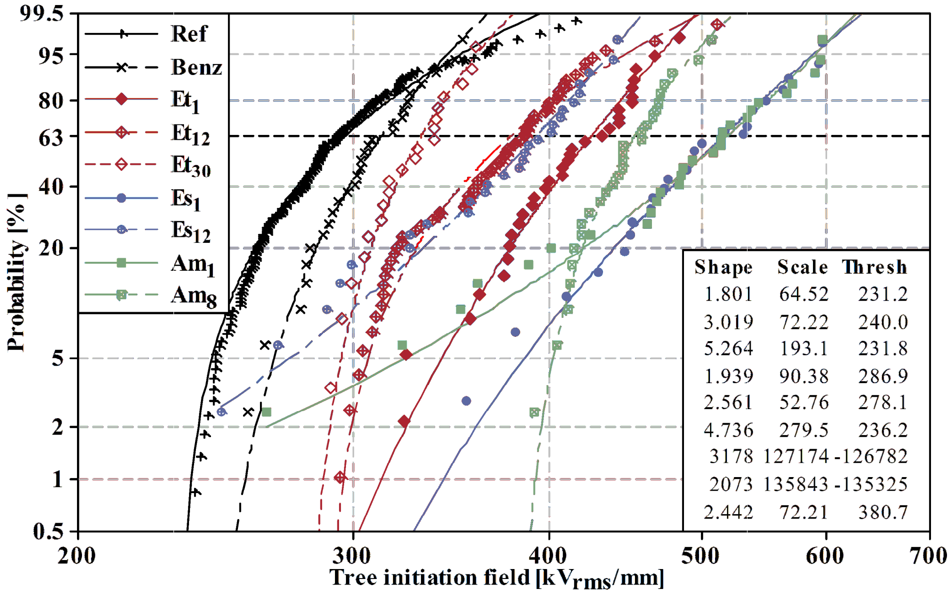

Figure 5.9 *Weibull distributions of tree initiation field for benzil-type stabilised XLPE.*

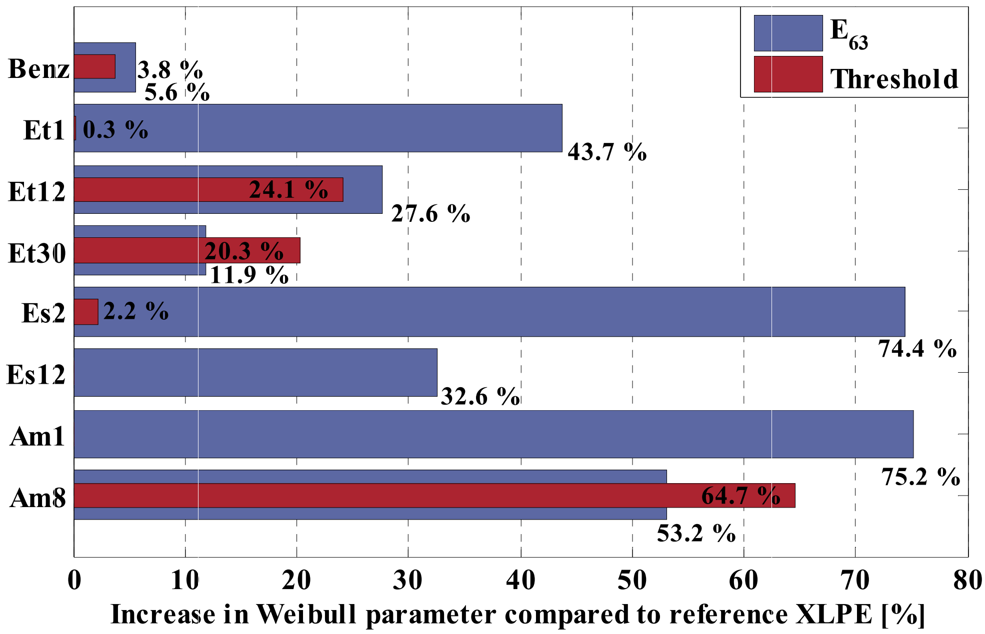

Figure 5.10 *Improvements (in %) of the threshold and E_{63} parameter of tree initiation field Weibull distributions for benzil-type stabilised materials with respect to reference material.*

To ensure that the addition of stabiliser has not affected the microstructure of the XLPE, all batches have been tested using differential scanning calorimetry (DSC) and small angle x-ray scattering (SAXS). Using DSC measurements it is found that the addition of voltage stabilisers slightly decreased the crystallinity of XLPE from about 56 % to around 50 %. Use of the Gibbs-Thomson equation [88] indicates that this results in a change of the peak lamellar thickness from 7.8 nm to 7.3-7.5 nm for the voltage-stabilised XLPE. Based on the SAXS analyses, the lamellar thickness decreases slightly, from 7.7 nm to a level between 6.4-7.5 nm. According to [89, 90] a change of lamellar thickness by ~1.3 nm should results in a change of tree initiation voltage by about 10 %. As the results from the presented treeing tests are clearly above 10 %, it is postulated that the microstructure variation due to addition of benzil-type stabilisers is unlikely the main cause of the increased dielectric strength. It is rather believed that other mechanisms cause this effect, as further discussed and highlighted in the next section.

5.3 Influence of Ionisation Potential and Electron Affinity on the Stabilising Efficiency

It is a well-established knowledge within high voltage engineering that breakdown strength of gaseous and liquid dielectrics depends strongly on electron affinity of these media [91]. The ability to form negative ions by capturing free electrons is in these cases competing with the molecule ionisation process.

In order to check if a similar process could be responsible for the observed stabilising efficiency of the tested molecules, their ionisation potentials (IP) and electron affinities (EA) were considered, using data from Publications XI-IX. In addition, data on treeing efficiency for stabilisers found in literature [52, 55, 57, 92-95] were also included in the analyses. The calculations have been performed by using Gaussian 09, DFT B3LYP/6-311+G(d,p) software. Table 5.1 presents IP and EA values for the stabilisers tested within the framework of this thesis, all values corresponding to the literature data can be found in Publication IX. Chemical structures and full names of the abbreviated ones in the table are provided in Appendix 2. The numbers in column (No) refers to list of all the compounds, as presented in Publication IX. Fullerene and PCBM are listed with experimental data on ionisation potential and electron affinity [96-99].

Table 5.1 *Adiabatic ionisation potentials and electron affinities for stabilisers presented in Figures 5.11 and 5.12. For further details regarding the calculations for the different compounds, refer to Publication IX.*

No	Stabiliser type	Adiabatic ionisation potential (IP) [eV]	Adiabatic electron affinity (EA) [eV]
1	Et_1	7.714	1.397
2	Es_2	8.018	1.753
3	Am_1	6.819	1.128
4	MeOTX	7.336	0.956
5	HOTX	7.490	0.999
6	ITX	7.563	0.950
8	OTXMa	7.210	1.328
9	OTXAc	7.420	1.312
10	Triazine 1	7.182	-0.688
11	Triazine 2	6.487	-0.210
12	MPT	6.664	-0.368
13	DTDCPB	6.419	3.435
14	DOABP	7.050	0.523
15	Anthracene	7.108	0.717
55	C_{60}	7.6	2.67
56	PCBM	7.17	2.63

The obtained values are then correlated to the stabilising efficiency, Φ, found from the electrical treeing tests, as defined in Equation 5.1.

$$\Phi = \left(\frac{E_{63} - E_{63,XLPE}}{E_{63,XLPE}} \right) \cdot \frac{1}{c} \tag{5.1}$$

E_{63} and $E_{63,XLPE}$ denotes the 63 % probability percentiles from the Weibull fits of electrical tree initiation of stabilised and reference XLPE, respectively, and c is the molal concentration of the stabiliser.

In Figure 5.11 the stabilising efficiency, Φ is plotted as a function of the ionisation potential for all the stabilisers tested in this thesis (indicated by diamonds), as listed in Table 5.1. Stabilisers 1 through 15 (marked with filled diamonds) where tested at a concentration of 10 mmol/kg. The data points for C_{60} and PCBM (marked as unfilled diamonds), were obtained at lower stabiliser concentrations. The data for the stabilisers with stabilising efficiency retrieved from literature are also included in the figure (unfilled other markers together with reference in the label). It should be considered that these are tested with varying test methods. No clear correlation between the stabilising efficiency and the ionisation potential could be found in this plot, even though existence of such a correlation was claimed in [52].

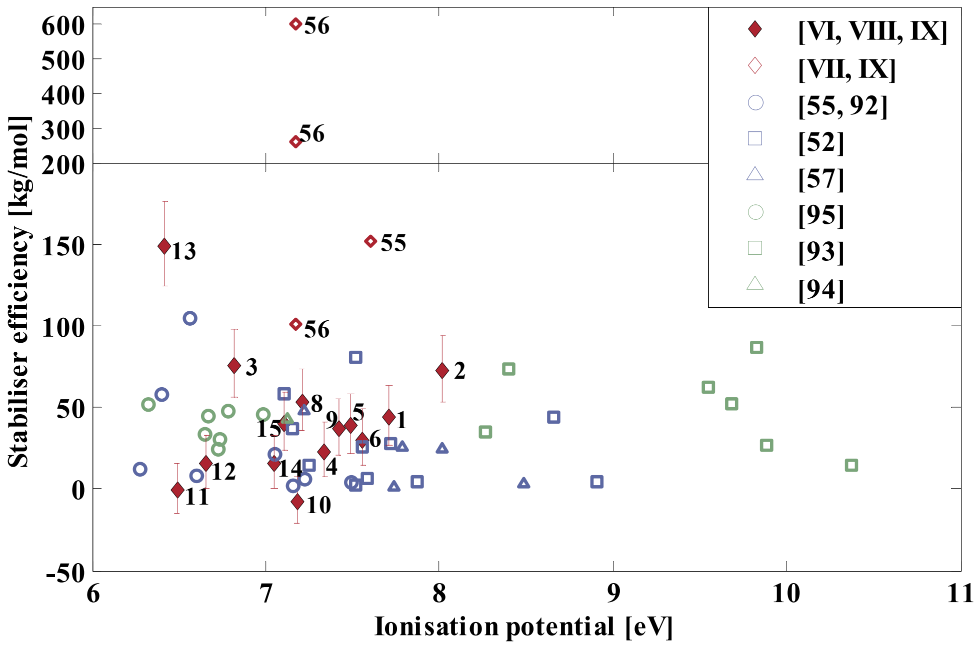

Figure 5.11 *Stabilising efficiency, Φ, for various stabilising compounds plotted as a function of their ionisation potential. The numbered points refer to the compounds tested in this thesis, as listed in Table 5.1. The literature references to the remaining points are provided in the legend.*

When on the other hand the electron affinity of the tested stabilising molecules is considered instead, as seen in Figure 5.12, a significant correlation is found, as illustrated by a second polynomial fit of the data points represented by the filled diamonds, i.e. stabilisers tested under equal conditions. The most significant outliers identified by unfilled diamonds, showing a stabilising efficiency much higher than predicted, represent the low concentration effects of the fullerenes, PCBM and C_{60}. As indicated earlier, it is difficult to judge the other observed outliers, as these data come from various publications.

The existing correlation between stabilising efficiency and electron affinity suggests operation of an electron scavenging mechanism and the effective voltage stabilisers have typically their adiabatic electron affinities in a range of ~0.5-3.5 eV which in this case is the energy gained by the system when a stabilising molecule binds a free electron. Similar trends have been found in breakdown tests of polyethylene films, as reported by Yamano [100] and Kisin et al. [51].

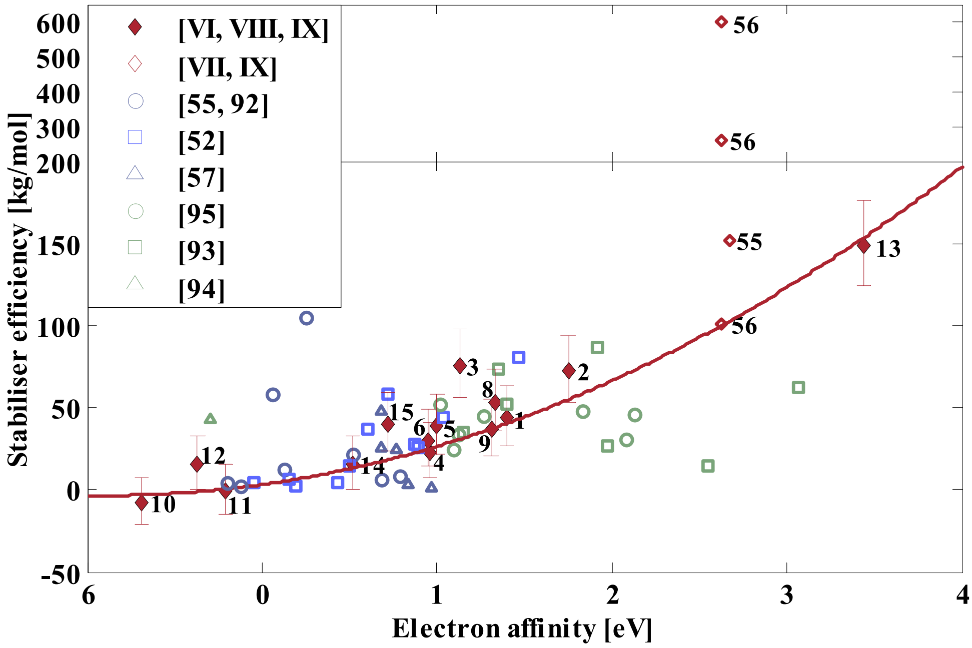

Figure 5.12 *Stabilising efficiency, Φ, of various stabilising compounds as a function of their electron affinity. The numbered points refer to the compounds tested in this thesis, as listed in Table 5.1. The literature references to the remaining points are provided in the legend.*

Chapter 6

Conclusions

A wire type object for testing of electrical treeing resistance in polymer insulation has been developed. It was found to be advantageous in several aspects as compared to the traditional needle type objects, especially for material characterisation and comparisons of newly developed materials. By removing the semi-conducting tab, the benefits of this type of test object has become further enhanced and the main remaining disadvantage is now the tendency to kink formation. This behaviour is however not considered to be serious, as no evidence has been found that trees formed along the wire electrode would influence each other. Furthermore, a new way of analysing the appearance of multiple trees in each test object is proposed, which has given rise to a more beneficial use of the multitude of data received from the treeing tests with a slightly altered approach for the statistical analysis. The presented attempt utilizes the first four trees in each tested object for further statistical analyses.

Also an interesting aspect with the new method is that a relatively large volume of the material is stressed, presumably also in its weakest points, as in contrast to the needle objects, the tree growth is not forced to one specific location. The performed SEM investigations could not indicate any variations in the material morphology close to the wire electrode. It is therefore believed that use of wire-electrode objects provides an opportunity to better explore the influence of material structure and constituency on electrical tree inception.

At the first stage, optical measurements have been applied to describe the initiation and growth of electrical trees in relation to the applied AC voltage; if however the test objects are non-transparent this will introduce considerable difficulties. Thus to further improve the possibility to characterize different insulation materials, electrical detection of PD events in the tree channels during initiation and growth has been implemented and resulted in elaboration of a promising methodology. A number of observations are presented, defining the most important parameters for determining the initiation of a tree. These include the summed PD amplitude and the number of PDs detected, whereas the maximum and the average PD amplitude may additionally contribute to the analysis. The number of PDs per cycle and the summed PD amplitude per cycle show strong correlations to optical observations of tree growth. Thus both the optical observations as well as the electrical measurements seem suitable for characterising materials' resistance towards electrical treeing and monitoring of the gradual treeing progress, e.g. at different ramp rates or containing various additives. In conclusion the electrical measurements allowed for distinguishing between differences in tree initiation voltage.

Several promising stabilisers, within several groups, including benzil-, thiaxanthone- fullerene- and melamine-types, have been tested and characterised. Most of them exhibit promising behaviour, by increasing the resistance towards electrical treeing of cross-linked polyethylene in the range between around twenty up to well above a hundred percent. The efficiency of these stabilisers with respect to tree initiation voltage was found to depend strongly on electron affinity of the molecules rather than on their ionisation potential, which opens for new possibilities when designing new and efficient additives, with the aim of improving insulation of high voltage power cables.

Chapter 7

Future Work

Some possible continuation tracks can be foreseen for future research in the field: one deals with the development of the electrical detection methodology, to further improve the accuracy in the measurement system and also how to correlate these measurement to the physical processes of the treeing in a more prominent manner, a second track is to consider where along the wire the trees initiate and to study these spots, for expanding the knowledge on tree inception. To improve the understanding further, various material characterisation techniques could be applied. Expanding the electrical treeing tests to be made at operating cable temperature would further provide more knowledge on the performance of additives and the insulation.

In regarding to the PD analyses, it would be beneficial to perform additional tests with constant voltage amplitudes. Thus avoiding the influence of voltage ramping. In addition, tests utilising different voltages, e. g. square, PWM and DC voltages, can possibly bring new light to material behaviour in situations when transients or disturbances appear and how they affect the lifetime of the insulation. Further it can be an advantage to support the PD analyses by measuring the increase in capacitance or loss current inflicted by the gradual growth of electrical trees. This will require an efficient shielding of the test object against parasitic influences and external disturbances but is believed to provide additional interesting results.

References

[1] "Roadmap to the Supergrid Technologies", *Friends of the Supergrid*, update report, 2013.

[2] M. Jarvid, "Voltage Stabilizers: From Design to Synthesis, Processing and Electrical Characterization", Thesis for the degree of Doctor of Philosophy, ISBN 978-91-7597-059-2, *Chalmers University of Technology*, Gothenburg, Sweden, 2014.

[3] L. A. Dissado and J. C. Fothergill, "Electrical Degradation and Breakdown in Polymers", ISBN 0 86341 196 7, *Peter Peregrinus Ltd*, London, United Kingdom, 1992.

[4] J.-F. Wang, X.-Q. Zheng, J. Wu, Y.-X. Li and Z.-J. Zhang, "Study on the Transformation of Electrical Tree from Water Tree Degradation in XLPE", *2012 IEEE 10th International Conference on the Properties and Applications of Dielectric Materials (ICPADM)*, 2012.

[5] D. W. Kitchin and O. S. Pratt, "Treeing Effects in Polyethylene", *Electrical Engineering*, vol. 77, iss. 3, pp. 218-223, 1958.

[6] J. Holto and E. Ildstad, "Electrical Treeing in Extruded Polypropylene High Voltage Cable Insulation*", 2010 International Conference on High Voltage Engineering and Application (ICHVE)*, pp. 373-376, 2010.

[7] S. Bahadoorsingh and S. M. Rowland, "Investigating the Influence of the Lubricant Coating on Hypodermic Needles on Electrical Tree Characteristics in Epoxy Resin", *IEEE Transactions on Dielectrics and Electrical Insulation*, vol. 17, no. 3, pp. 701-708, 2010.

[8] B. X. Du, Z. L. Ma and Y. Gao, "Phenomena and Mechanism of Electrical Tree in Silicone Rubber", *Proceedings of the 9th International Conference on Properties and Applications of Dielectric Materials (ICPADM)*, pp. 37-40, 2009.

[9] Y. Cui, G. Wu, C. Wu and Y. Luo, "Possible Mechanism of Electrical Treeing and Breakdown for Polyimide Nanocomposite Film Used in Inverter-Fed Motor", *2010 Annual Report Conference on Electrical Insulation and Dielectric Phenomena (CEIDP)*, 2010.

[10] I. Kitani and K. Arii, "DC Tree Associated with Space Charge in PMMA", *IEEE Transactions on Electrical Insulation*, vol. EI-22, no. 3, pp. 303-307, 1987.

[11] J. C. Fothergill, L. A. Dissado and P. J. J. Sweeney, "A Discharge-Avalanche Theory for the Propagation of Electrical Trees. A Physical Basis for their Voltage Dependence", IEEE Transactions on Dielectrics and Electrical Insulation, vol. 1, no. 3, pp. 474-486, 1994.

[12] C. Laurent and G. Teyssedre, "Hot Electron and Partial-Discharge Induced Ageing of Polymers", *Nuclear Instruments and Methods in Physics Research B: Beam Interactions with Materials and Atoms*, vol. 208, pp. 442-447, 2003.

[13] T. Mito, Y. Muramoto and N. Shimizu, "Electroluminescence Properties and Degradation of XLPE" *2007 Annual Report Conference on Electrical Insulation and Dielectric Phenomena (CEIDP)*, pp. 171-174, 2007.

[14] G. Teyssedre and C. Laurent, "Evidence of Hot Electron-Induced Chemical Degradation in Electroluminescence Spectra of Polyethylene", *Journal of Applied Physics*, vol. 103, pp. 046107-046107-2, 2008.

[15] T. Tanaka, "Charge Transfer and Tree Initiation in Polyethylene Subjected to ac Voltage Stress", *IEEE Transactions on Electrical Insulation*, vol. 27, no. 3, pp. 424-431, 1992.

[16] M. Mammeri, C. Laurent and J. Salon, "Influence of Space Charge Buildup on the Transition to Electrical Treeing in PE under ac Voltage", *IEEE Transactions on Dielectrics and Electrical Insulation*, vol. 2, no. 1, pp. 27-35, 1995.

[17] L. A. Dissado, "Understanding Electrical Trees in Solids: From Experiment to Theory", *IEEE Transactions on Dielectrics and Electrical Insulation*, vol. 9, no. 4, pp. 483-497, 2002.

[18] N. Rouha and A. Beroual, "Physico-Chemical Diagnosis of EPDM Electrical Aging by Tree Phenomenon", *IEEE Transactions on Dielectrics and Electrical Insulation*, vol. 20, no. 5, pp. 1577-1583, 2013.

[19] S. S. Bamji, A. T. Bulinski, Y. Chen and R. J. Densley, "Threshold Voltage for Electrical Tree Inception in Underground HV Transmission Cables", *IEEE Transactions on Electrical Insulation*, vol. 27, no. 2, pp. 402-404, 1992.

[20] X. Chen, Y. Xu, X. Cao, S. J. Dodd, and L. A. Dissado, "Effect of Tree Channel Conductivity on Electrical Tree Shape and Breakdown in XLPE Cable Insulation Samples", *IEEE Transactions on Dielectrics and Electrical Insulation*, vol. 18, no. 3, pp. 847-860, 2011.

[21] J. Holto and E. Ildstad, "Electrical Tree Growth in Extruded s-Polypropylene", *2010 10th IEEE International Conference on Solid Dielectrics (ICSD)*, 2010.

[22] J. J. Yang and S. Brilasekaran, “Characteristic Features of Electrical Treeing in XLPE and PE”, IPEC 2005. *The 7th International in Power Engineering Conference*, 2005.

[23] L. A. Dissado, S. J. Dodd, J. V. Champion, P. I. Williams and J. M. Alison, “Propagation of Electrical Tree Structures in Solid Polymeric Insulation”, , *IEEE Transactions on Dielectrics and Electrical Insulation*, vol. 4, no. 3, pp. 259-279, 1997.

[24] X. Zheng and G. Chen, “Propagation Mechanism of Electrical Tree in XLPE Cable Insulation by investigating a Double Electrical Tree Structure”, *IEEE Transactions on Dielectrics and Electrical Insulation*, vol. 15, no. 3, pp. 800-807, 2008.

[25] R. Sarathi, A. Nandini and T. Tanaka, “Understanding Electrical Treeing Phenomena in XLPE Cable Insulation under Harmonic AC Voltages Adopting UHF Technique”, *IEEE Transactions on Dielectrics and Electrical Insulation*, vol. 19, no. 3, pp. 903-909, 2012.

[26] B. X. Du, T. Han, Y. Gao, Z. L. Ma and X. H. Zhu, “Dependence of Electrical Treeing Behavior on Cross-Linking Temperature of XLPE”, *2010 Annual Report Conference on Electrical Insulation and Dielectric Phenomena (CEIDP)*, 2010.

[27] “ASTM D3756 – 97 Standard Test Method for Evaluation of Resistance to Electrical Breakdown by Treeing in Solid Dielectric Materials Using Diverging Fields (Reapproved 2010)”, *ASTM International*, 2010.

[28] D. W. Auckland, J. M. Cooper and B. R. Varlow, “Factors Affecting Electrical Tree Testing”, *IEE Proceedings A: Science, Measurement and Technology*, vol. 139, iss. 1, pp. 9-13, 1992.

[29] A. B. Johansson, A.-M. B. Sandberg, B. Sonerud, J. Blennow and S. Gubanski, “Wire-Plane Electrode System for Electrical Tree Initiation Exposed to AC and DC Voltage Stress, *Proceedings of the 17th International Symposium on High Voltage Engineering (ISH)*, 2011.

[30] Y. Sekii, H. Kawanami, M. Saito, K. Sugi and I. Komatsu, “DC Tree and Grounded DC Tree in XLPE”, *2005 Annual Report Conference on Electrical Insulation and Dielectric Phenomena (CEIDP)*, pp. 523-526, 2005.

[31] G. Katsuta, T. Itaya, T. Nakatsuka, H. Miyata, T. Takahashi and T. Niwa, “DC and Impulse treeing characteristics in Insulating Material for HVDC Cable”, *Proceedings of the 5th International Conference on Properties and Applications of Dielectric Materials (ICPADM)*, pp. 422-425, 1997.

[32] L. Wang, X. Chen, L. Hu, S. M. Gubanski and J. Blennow, “Electrical Tree Formation as a Measure of Degradation Resistance in Polymeric Materials for HVDC Applications”, *2013 Annual Report Conference on Electrical Insulation and Dielectric Phenomena (CEIDP)*, pp. 510-513, 2013.

[33] Y. Liu and X. Cao, “Electrical Tree Initiation in XLPE Cable Insulation by Application of DC and Impulse Voltage”, *IEEE Transactions on Dielectrics and Electrical Insulation*, vol. 20, no. 5, pp. 1691-1698, 2013.

[34] H. Kawamura and M. Nawata, "dc Electrical Treeing Phenomena and Space Charge", *IEEE Transactions on Dielectrics and Electrical Insulation*, vol. 5, no. 5, pp. 741-747, 1998.

[35] M. Selsjord and E. Ildstad, "Electrical Treeing Caused by Rapid DC-Voltage Grounding of XLPE Cable Insulation", *Conference Record of the 2006 IEEE International Symposium on Electrical Insulation*, pp. 502-505, 2006.

[36] Y. Sekii, "Initiation and Growth of Electrical Trees in LDPE generated by Impulse Voltage", *1996 IEEE Annual Report - Conference on Electrical Insulation and Dielectric Phenomena*, pp. 775-778, 1996.

[37] K. Kudo, "Impulse Treeing Breakdown in Polyethylene Under Non-Uniform and Quasi-Uniform Fields", *1989 Annual Report Conference on Electrical Insulation and Dielectric Phenomena (CEIDP)*, pp. 259-264, 1989.

[38] G. Salge, "Influence of Impulse Overvoltages and Intermitting Stationary Voltages on the Electrical Treeing Process in Polyethylene", *11th International Symposium on High Voltage Engineering (ISH)*, vol.4 , pp. 261-264, 1999.

[39] H. Wang, J. He, X. Zhang, Z. Li, L. Li and G. Guan, "Electrical Tree Inception Characteristics of XLPE Insulation Under Power-Frequency Voltage and Superimposed Impulse Voltage", *11th International Symposium on High Voltage Engineering (ISH)*, vol.4 , pp. 320-323, 1999.

[40] S. Bahadoorsingh and S. M. Rowland, "Investigating the Impact of Harmonics on the Breakdown of Epoxy Resin through Electrical Tree Growth", *IEEE Transactions on Dielectrics and Electrical Insulation*, vol. 17, no. 5, pp. 1576-1584, 2010.

[41] G. Berg, H. H. Sæternes, J. Aakervik and S. Hvidsten, "The Effect of Hydrostatic Pressure on Electrical Treeing in Silicone Cable Joints", *Conference Record of the 2012 IEEE International Symposium on Electrical Insulation (ISEI)*, pp. 609-612, 2012.

[42] D. W. Auckland, A. Taha, and B. R. Varlow, "Correlation of Mechanical Properties with Electrical Treeing Behaviour at Elevated Temperatures", *1993 Annual Report Conference on Electrical Insulation and Dielectric Phenomena (CEIDP)*, pp. 636-641, 1993.

[43] W. Wu and F. Hao, "Electrical Treeing and Stress Cracking in Polyethylene at Cryogenic Temperature", *Proceedings of the 3rd International Conference on Properties and Applications of Dielectric Materials (ICPADM)*, pp. 322-326, 1991.

[44] A. Harlin, M. Shuvalov, V. Ovsienko and J. Juhanoja, "Insulation Morphology Effects on the Electrical Treeing Resistance", *IEEE Transactions on Dielectrics and Electrical Insulation*, vol. 9, no. 3, pp. 401-405, 2002.

[45] S. J. Dodd, J. V. Champion, Y. Zhao, A. S. Vaughan, S. J. Sutton and S. G. Swingler, "Influence of Morphology on Electrical Treeing in Polyethylene Blends", *IEE Proceedings - Science, Measurement and Technology*, vol. 150, no. 2, pp. 58-64, 2003.

[46] Y. Xu, P. Luo, M. Xu and T. Sun, "Investigation on Insulation Material Morphological Structure of 110 and 220 kV XLPE Retired Cables for

Reusing", *IEEE Transactions on Dielectrics and Electrical Insulation*, vol. 21, no. 4, pp. 1687-1696, 2014.

[47] J. V. Champion, S. J. Dodd, A. S. Vaughan, Y. Zhao and S. J. Sutton, "The Effect of Voltage, Temperature and Morphology on Electrical Treeing in Polyethylene Blends", *2000 8th International Conference on Dielectric Materials, Measurements and Applications*, pp. 35-40, 2000.

[48] E. David, J.-L. Parpal and J. P. Crine, "Influence of Internal Mechanical Stress and Strain on Electrical Performance of Polyethylene: Electrical Treeing Resistance", *IEEE Transaction on Dielectrics and Electrical Insulation*, vol. 3, no. 2, pp. 248-257, 1996.

[49] P. Blümler, N. Paus and G. Salge, "Nuclear Magnetic Resonance Imaging of Morphological Changes during Electrical Treeing in Polyethylene due to Partial Discharges", *Proceedings of the 1998 IEEE 6th International Conference on Conduction and Breakdown in Solid Dielectrics*, pp. 168-172, 1998.

[50] F. Wuerstlin and F. Feichtmayr, "Electrical Insulating Compositions Based on Olefin Polymers", *United States Patents 3,674,695*, 1972.

[51] S. Kisin, J. den Doelder, R. F. Eaton and P. J. Caronia, "Quantum Mechanical Criteria for Choosing Appropriate Voltage Stabilization Additives for Polyethylene", *Polymer Degradation and Stability*, vol. 94, pp. 171-175, 2009.

[52] A. C. Ashcraft, R. M. Eichhorn and R. G. Shaw, "Laboratory Studies of Treeing in Solid Dielectrics and Voltage Stabilization of Polyethylene*", IEEE International Symposium on Electrical Insulation (ISEI)*, pp. 213-218, 1976.

[53] E. Peschke and R. von Olshausen, "Cable Systems for High and Extra-High Voltage: Development, Manufacture, Testing, Installation and Operation of Cables and their Accessories", ISBN 978-3895781186, *Publicis MCD verlag*, 2000.

[54] F. Feichtmayr and F. Wuerstlin, "Voltage Stabilization of Low Density Polyethylene", *Kunststoffe*, vol. 60, pp. 381-385, 1970.

[55] V. Englund, R. Huuva, S. M. Gubanski and T. Hjertberg, "Synthesis and Efficiency of Voltage Stabilizers for XLPE Cable Insulation", *IEEE Transactions on Dielectrics and Electrical Insulation*, vol. 16, no. 5, pp. 1455-1461, 2009.

[56] S. S. Bamji, A. T. Bulinski and J. Densley, "Electrical Tree Suppression in High-Voltage Polymeric Insulation", *United States Patent 4,870,121*, 1989.

[57] L. Martinotto, F. Peruzzotti and M. Del Brenna, "Cable, in Particular for Transport or Distribution of Electrical Energy and Insulating Composition", *United States Patent US 6,696,154 B2*, 2004.

[58] S. Alapati and M. J. Thomas, "Electrical Treeing and the Associated PD Characteristics in LDPE Nanocomposites", *IEEE Transactions on Dielectrics and Electrical Insulation*, vol. 19, no. 2, pp. 697-704, 2012.

[59] F. Guastavino, A. Dardano, G. C. Montanari, L. Testa, and F. Bellucci, "Electrical Treeing in EVA-Boehmite and EVA-Montmorillonite

Nanocomposites", *2009 IEEE Electrical Insulation Conference (EIC)*, pp. 382-386, 2009.

[60] X. Huang, F. Liu and P. Jiang, "Effect of Nanoparticle Surface Treatment on Morphology, Electrical and Water Treeing Behavior of LLDPE Composites", *IEEE Transactions on Dielectrics and Electrical Insulation*, vol. 17, no. 6, pp. 1697-1704, 2010.

[61] M. H. Ahmad, H. Ahmad, N. Bashir, A. A. A. Jamil, M. A. M. Piah, Z. A. Malek and S. J. Dodd, "Electrical Treeing in Silicone Rubber/Organo-Montmorillonite", *2012 Annual Report Conference on Electrical Insulation and Dielectric Phenomena (CEIDP)*, pp. 898-901, 2012.

[62] Y. Yamano and M. Iizuka, "Improvement of Electrical Tree Resistance of LDPE by Mixed Addition of Nanoparticles and Phthalocyanine", *IEEE Transactions on Dielectrics and Electrical Insulation*, vol. 18, no. 1, pp. 329-337, 2011.

[63] E. J. McMahon, "A Tutorial on Treeing", *IEEE Transactions on Electrical Insulation*, vol. EI-13, no.4, pp. 277-288, 1978.

[64] N. Yoshimura, S. Fujita and F. Noto, "Comparison of Single and Double Needle Tests for Evaluation of Resistance to Treeing Breakdown", *IEEE Transactions on Electrical Insulation*, vol. EI-18, no. 1, pp. 42-47, 1983.

[65] J. H. Mason, "Breakdown of Solid Dielectrics in Divergent Fields", *Proceedings of the IEE - Part C: Monographs*, vol. 102, pp. 254-263, 1955.

[66] G. Chen and C. H. Tham, "Electrical Treeing Characteristics in XLPE Power Cable Insulation in Frequency Range between 20 and 500 Hz", *IEEE Transactions on Dielectrics and Electrical Insulation*, vol. 16, no. 1, pp. 179-188, 2009.

[67] M. Olyphant, "Breakdown by Treeing in Epoxy Resins", *IEEE Transactions on Power Apparatus and Systems*, vol. 82, pp. 1106-1112, 1963.

[68] R. Huuva, V. Englund, S. M. Gubanski and T. Hjertberg, "A Versatile Method to Study Electrical Treeing in Polymeric Materials", *IEEE Transactions on Dielectrics and Electrical Insulation*, vol. 16, no. 1, pp. 171-178, 2009.

[69] A. K. Vijh and J.-P. Crine, "Influence of Metallic Electrodes on Electrical Tree Initiation in Polyethylene", *Journal of Applied Physics*, vol. 65, pp. 398-399, 1989.

[70] S. S. Bamji, A. T. Bulinski, R. J. Densley and M. Matsuki, "Degradation Mechanism at XLPE/Semicon Interface Subjected to High Electrical Stress", *IEEE Transactions on Electrical Insulation*, vol. 26, no. 2, pp. 278-284, 1991.

[71] A. Hadid, C. Laurent, M. Mammeri, R. Clavreul, F. Duchateau and J. Berdala, "An Investigation into Electrical Ageing of Insulating Polymers by Detection of Charge Injection under Alternative Divergent Field", *Journal de Physique III*, pp. 35-53, 1994.

[72] E. M. Jarvid, A. B. Johansson, J. H. M. Blennow, M. R. Andersson, and S. M. Gubanski, "Evaluation of the Performance of Several Object Types for Electrical Treeing Experiments", *IEEE Transactions on Dielectrics and Electrical Insulation*, vol. 20, no. 5, pp. 1712-1719, 2013.

[73] R. Schurch, S. M. Rowland, R. S. Bradley and P. J. Withers, "A Novel Approach for Imaging of Electrical Trees", *2012 Annual Report Conference on Electrical Insulation and Dielectric Phenomena (CEIDP)*, pp. 593-596, 2012.

[74] R. Bozzo, G. Coletti and F. Guastavino, "Studies About the Electrical Treeing Growth Based on the Evolution of the PD Patterns", *Conference Record of the 1998 IEEE International Symposium on Electrical Insulation*, vol.2, pp. 415-419, 1998.

[75] S. J. Dodd, N. M. Chalashkanov and J. C. Fothergill, "Partial Discharge Patterns in Conducting and Non-Conducting Electrical Trees", *2010 10th IEEE International Conference on Solid Dielectrics (ICSD)*, 2010.

[76] B. Sonerud, T. Bengtsson, J. Blennow, S. M. Gubanski and S. Nilsson, "Capacitance Measurements and Tree Length Estimation during Electrical Treeing in Sub-picofarad Samples", *IEEE Transactions on Dielectrics and Electrical Insulation*, vol. 16, no. 6, pp. 1707-1709, 2009.

[77] W. Weibull, "A Statistical Theory of the Strength of Materials", Ingeniörsvetenskapsakademiens Handlingar nr 151, *Generalstabens Litografiska Anstalts Förlag*, Stockholm, Sweden, 1939.

[78] R. M. Hill and L. A. Dissado, "Theoretical Basis for the Statistics of Dielectric Breakdown", *Journal of Physics C: Solid State Physics*, vol. 16, pp. 2145-2156, 1983.

[79] G. C. Montanari, G. Mazzanti, M. Cacciari and J. C. Fothergill, "In Search of Convenient Techniques for Reducing Bias in the Estimation of Weibull Parameters for Uncensored Tests", *IEEE Transactions on Dielectrics and Electrical Insulation*, vol. 4, no.3, pp. 306-313, 1997.

[80] J. Griač, V. Adamec and J. H. Calderwood, "On the Comparability of Single and Double Needle Tests for Treeing Resistance", *IEEE Transactions on Electrical Insulation*, vol. EI-17, no. 4, pp. 356-358, 1982.

[81] T. Hibma and H. R. Zeller, "Direct Measurement of Space-Charge Injection from a Needle Electrode into Dielectrics", *Journal of Applied Physics*, vol. 59, pp. 1614-1620, 1986.

[82] A. B. C. Bowers, "The Maximum Electric Field Strength for Several Simple Electrode Configurations", *Phillips Technical Review*, vol. 6, 1941.

[83] T. Andrews, R. N. Hampton, A. Smedberg, D. Wald, V. Waschk and W. Weissenberg, "The Role of Degassing in XLPE Power Cable Manufacture", *IEEE Electrical Insulation Magazine*, vol. 22, no. 6, pp. 5-16, 2006.

[84] O. Hällqvist, "Electrical Treeing in XLPE", Bachelor Thesis, Department of Chemical and Biological Engineering, *Chalmers University of Technology*, Gothenburg, Sweden, 2011.

[85] E. Lindell, "Partial Discharges at Repetitive Rapidly Changing Voltages" Thesis for the degree of Doctor of Philosophy, ISBN 978-91-7385-312-5, *Chalmers University of Technology*, Gothenburg, Sweden, 2009.

[86] T. Hammarström, "Detection of Partial Discharges in Cavities at Fast Rising Voltages", Thesis for the degree of Licentiate of Engineering, ISSN 1652-8891, *Chalmers University of Technology*, Gothenburg, Sweden, 2011.

[87] B. Sonerud, "Characterization of Electrical Insulation Exposed to Arbitrary Voltage Waveforms", Thesis for the degree of Doctor of Philosophy, ISBN 978-91-7385-373-6, *Chalmers University of Technology*, Gothenburg, Sweden, 2010.

[88] U. W. Gedde, "Polymer Physics", ISBN 0 412 59020 4, *Chapman and Hall*, London, United Kingdom, 1995.

[89] Y. Zhou, X. Wang, P. Yan, X. Liang, Z. Guan, and N. Yoshimura, "Annealing Effect on the Morphology of Polyethylene Materials and the Tree Initiation Voltage", *2001 Annual Report Conference on Electrical Insulation and Dielectric Phenomena (CEIDP)*, pp. 241-244, 2001.

[90] T. Takahashi, H. Ohtsuka, H. Takehana and T. Niwa, "Study on Improvements to the Dielectric Breakdown Strength of Extruded Dielectric Cables", *IEEE Transactions on Power Apparatus and Systems*, vol. PAS-104, no. 8, pp. 1945-1950, 1985.

[91] E. Kuffel, W. S. Zaengl and J. Kuffel, "High Voltage Engineering: Fundamentals", ISBN 978-0-7506-3634-6, *Elsevier Ltd*, Oxford, United Kigdom, 2000.

[92] V. Englund, R. Huuva, S. M. Gubanski and T. Hjertberg, "High Efficiency Voltage Stabilizers for XLPE Cable Insulation", *Polymer Degradation and Stability*, vol. 94, pp. 823-833, 2009.

[93] L. J. Heidt, "Voltage Stabilized Polyolefin Dielectric", *Canadian Patent CA832524 A*, 1970.

[94] H. Kato and N. Maekawa, "Polyolefin Composition for Electrical Insulation", *United States Patent 3,956,420*, 1976.

[95] H. J. Davis, "Electrical Insulating Composition Based on Polyolefin Containing Dye Additives as Voltage Stabilizers", *United States Patent 4,216,101*, 1980.

[96] R. K. Yoo, B. Ruscic and J. Berkowitz, "Vacuum Ultraviolet Photoionization Mass Spectrometric Study of C_{60}", *The Journal of Chemical Physics*, vol. 96, pp. 911-918, 1992.

[97] C. Brink, L. H. Andersen, P. Hvelplund, D. Mathur and J. D. Voldstad, "Laser Photodetachment of C_{60}^- and C_{70}^- Ions Cooled in a Storage Ring", *Chemical Physics Letters*, vol. 233, pp. 52-56, 1995.

[98] K. Akaike, K. Kanai, H. Yoshida, J. Tsutsumi, T. Nishi, N. Sato, Y. Ouchi and K. Seki, "Ultraviolet Photoelectron Spectroscopy and Inverse Photoemission Spectroscopy of [6,6]-Phenyl-C_{61}-Butyric Acid Methyl Ester

in Gas and Solid Phases", *Journal of Applied. Physics*, vol. 104, pp.. 023710-1-023710-5, 2008.

[99] B. W. Larson, J. B. Whitaker, X.-B. Wang, A. A. Popov, G. Rumbles, N. Kopidakis, S. H. Strauss and O. V. Boltalina, "Electron Affinity of Phenyl–C_{61}–Butyric Acid Methyl Ester (PCBM)", *The Journal of Physical Chemistry C*, vol. 117, pp. 14958-14964, 2013.

[100] Y. Yamano, "Roles of Polycyclic Compounds in Increasing Breakdown Strength of LDPE Film", *IEEE Transactions on Dielectrics and Electrical Insulation*, vol. 13, no. 4, pp. 773-781, 2006.

Appendices

Appendix A

List of studies made within this twin PhD work with the following data provided: Abbreviation of stabiliser (full name and chemical structure is provided in Appendix B), concentration of stabiliser, voltage ramp rate used for electrical testing, type of object, annealing time, (time between manufacturing of objects and electrical testing), number of yielded data point from electrical tests, threshold parameter from fit to the three-parametric Weibull distribution, E_{63} parameter from fit to the three-parametric Weibull distribution, improvement in E_{63} parameter as compared to the reference material from the same study and in which publications the data has been published. Listed in chronological order of testing.

Stabiliser	Concentration [mmol/kg]	Voltage ramp rate [V_{rms}/s]	Object type	Annealing time [days]	Number of data	Treshold [kV_{rms}/mm]	E_{63} [kV_{rms}/mm]	E_{63} improvement [%]	Publication
Study 1: Initial stabiliser test									
–	–	500	A	–	18	128	566	–	
Et_{12}	17.3	500	A	–	8	415	713	26.9	
Et_{11}	18.3	500	A	–	9	384	661	16.8	
Am_8	14.5	500	A	–	5	–	680	20.1	
Study 2: Test object comparison									
–	–	500	A	<30	16	393	462	–	IV
–	–	500	$B_{10\mu m}$	<30	64	391	519	–	IV
–	–	500	$B_{20\mu m}$	<30	56	311	368	–	IV
–	–	500	C	<30	10	1118	1476	–	IV
–	–	500	D	<30	15	1185	1517	–	IV
Study 3: Voltage ramp rate and stabilisers									
–	–	500	$B_{10\mu m}$	–	31	408	455	–	
–	–	500	$B_{20\mu m}$	–	0	–	–	–	
–	–	250	$B_{10\mu m}$	–	37	–	420	–	
–	–	250	$B_{20\mu m}$	–	15	320	365	–	
Et_{12}	17.3	500	$B_{10\mu m}$	–	29	462	560	23.1	
Et_{12}	17.3	250	$B_{10\mu m}$	–	25	320	523	24.5	
2ambenz	84.6	250	$B_{10\mu m}$	–	21	344	800	90.5	
Study 4: Annealing, comparing Study 1									
Et_{12}	17.3	500	A	~450	20	360	455	-19.6	
Et_{11}	18.3	500	A	~450	25	321	459	-18.9	
Am_8	14.5	500	A	~450	16	244	577	1.9	

Stabiliser	Concentration [mmol/kg]	Voltage ramp rate [V_{rms}/s]	Object type	Annealing time [days]	Number of data	Treshold [kV_{rms}/mm]	E_{63} [kV_{rms}/mm]	E_{63} improvement [%]	Publication
Study 5: Ramprates, stabilsers and PD									
–	–	500	$B_{10\mu m}$	<40	40	364	445	–	III
–	–	160	$B_{10\mu m}$	<40	48	316	370	–	III
–	–	80	$B_{10\mu m}$	<40	54	304	361	–	
–	–	40	$B_{10\mu m}$	~120	24	279	344	–	III
–	–	20	$B_{10\mu m}$	<40	32	231	277	–	III
Et_{12}	10	500	$B_{10\mu m}$	<40	39	458	574	29.0	III
Et_{12}	10	160	$B_{10\mu m}$	<40	38	404	542	46.5	III
Et_{12}	10	80	$B_{10\mu m}$	<40	57	343	513	42.1	
Et_{12}	10	40	$B_{10\mu m}$	~120	40	304	448	30.2	III
Et_{12}	10	20	$B_{10\mu m}$	<40	25	332	456	64.6	III
Et_{12}	20	80	$B_{10\mu m}$	<40	72	368	582	61.2	
Am_8	20	80	$B_{10\mu m}$	<40	54	348	525	45.4	
Tri1	20	80	$B_{10\mu m}$	~120	57	119	369	2.2	
Triami	20	80	$B_{10\mu m}$	~120	52	302	370	2.5	
Study 6: Different preparation methods									
–	–	20	$B_{10\mu m}$	<80	40	251	322	–	
Et_{12}	10	20	$B_{10\mu m}$	<80	24	343	476	47.8	
$Et_{12\,noheat}$	10	20	$B_{10\mu m}$	<80	31	–	454	41.0	
$Et_{12\,60°}$	10	20	$B_{10\mu m}$	<80	35	–	399	23.9	
$Et_{12\,10\,ml}$	10	20	$B_{10\mu m}$	<80	29	174	454	41.0	
Et_{12}	5	20	$B_{10\mu m}$	<80	41	200	404	25.5	
Am_8	10	20	$B_{10\mu m}$	<80	32	159	329	2.2	
Am_8	5	20	$B_{10\mu m}$	<80	20	316	344	6.8	
DPPD	20	20	$B_{10\mu m}$	<80	40	270	411	27.6	
Study 7: Radiation cross linking									
– LDPE	–	20	$B_{10\mu m}$	1	28	250	414	–	XI & XII
– XLPE	–	20	$B_{10\mu m}$	1	32	–	486	–	XI & XII
$Et_{12,LDPE}$	10	20	$B_{10\mu m}$	1	28	328	487	17.6	XI & XII
$Et_{12,XLPE}$	10	20	$B_{10\mu m}$	1	28	48	447	-8.0	XI & XII

Study 6 contains data from Et_{12} prepared in different ways. noheat has not undergone a final heat treatment similar to that described in Chapter 5.1, 60° has been degassed at this temperature (as opposed to 90 °C used for the rest of the batches in this study, 10 ml has been dissolved in 10 ml DCM for soaking the polyethylene (as opposed to 300 ml DCM).

Stabiliser	Concentration [mmol/kg]	Voltage ramp rate [V_{rms}/s]	Object type	Annealing time [days]	Number of data	Treshold [kV_{rms}/mm]	E_{63} [kV_{rms}/mm]	E_{63} improvement [%]	Publication
Study 8a: Stabilisers, concentration and annealing									
– SR1	–	20	$B_{10\mu m}$	1	60	249	299	–	VI - IX
– SR2	–	20	$B_{10\mu m}$	1	12	269	331	–	
– SR3	–	20	$B_{10\mu m}$	1	24	218	291	–	
– SR3	–	20	$B_{10\mu m}$	88	24	133	277	-7.4	
– SR4	–	20	$B_{10\mu m}$	1	13	242	264	–	
– RNS	–	20	$B_{10\mu m}$	1	8	259	295	–	
$-_{nondeg}$	–	20	$B_{10\mu m}$	1	16	137	682	128	
Benz	10	20	$B_{10\mu m}$	1	28	240	312	4.3	VI & IX
$Benz_{diff}$	10	20	$B_{10\mu m}$	1	4	307	334	11.7	
Et_1	10	20	$B_{10\mu m}$	1	32	232	425	42.1	VI & IX
Et_1	10	20	$B_{10\mu m}$	127	24	339	392	31.1	
Et_{12}	10	20	$B_{10\mu m}$	1	67	287	377	26.1	VI
Et_{12}	10	20	$B_{10\mu m}$	85	24	251	468	56.5	
Et_{12}	10	20	$B_{10\mu m}$	133	24	216	483	61.5	
Et_{12}	20	20	$B_{10\mu m}$	1	23	229	484	61.9	VI
Et_{12}	20	20	$B_{10\mu m}$	84	21	–	518	73.2	
Et_{12}	20	20	$B_{10\mu m}$	133	20	340	517	72.3	
Et_{12}	30	20	$B_{10\mu m}$	1	28	–	478	59.9	VI
Et_{12}	30	20	$B_{10\mu m}$	124	24	255	514	71.9	
Et_{12}	40	20	$B_{10\mu m}$	1	24	164	465	55.5	VI
Et_{12}	40	20	$B_{10\mu m}$	132	27	445	508	69.9	
Et_{30}	10	20	$B_{10\mu m}$	1	20	278	331	10.7	VI
Es_2	10	20	$B_{10\mu m}$	1	24	236	516	72.6	VI & IX
Es_2	10	20	$B_{10\mu m}$	153	36	404	614	105	
Es_{12}	10	20	$B_{10\mu m}$	1	28	–	392	31.1	VI
Am_1	10	20	$B_{10\mu m}$	1	28	–	518	73.2	VI & IX
Am_8	10	20	$B_{10\mu m}$	1	28	381	453	51.5	VI

$-_{nondeg}$ is reference XLPE tested without degassing (containing methane, acetophenone and cumylalcohol), SR1 through SR4 and RNS are different batches of reference XLPE. In $Benz_{diff}$ the stabiliser has been added through diffusion after cross linking.

Stabiliser	Concentration [mmol/kg]	Voltage ramp rate [V_{rms}/s]	Object type	Annealing time [days]	Number of data	Treshold [kV_{rms}/mm]	E_{63} [kV_{rms}/mm]	E_{63} improvement [%]	Publication
Study 8a: Stabilisers, concentration and annealing (continuing)									
ITX	10	20	$B_{10\mu m}$	1	28	296	385	28.8	VIII & IX
ITX	40	20	$B_{10\mu m}$	1	32	218	423	41.5	VIII & IX
ATX	10	20	$B_{10\mu m}$	1	28	233	334	11.7	VIII
OTXMa	10	20	$B_{10\mu m}$	1	28	112	441	47.5	VIII & IX
MeOTX	10	20	$B_{10\mu m}$	1	28	39	362	21.1	VIII & IX
OTXAc	10	20	$B_{10\mu m}$	1	28	314	404	35.1	VIII & IX
HOTX	10	20	$B_{10\mu m}$	1	24	283	410	37.1	VIII & IX
Es12TX	10	20	$B_{10\mu m}$	1	28	244	288	-3.7	VIII
Triazine 1	10	20	$B_{10\mu m}$	1	28	254	273	-8.7	VIII & IX
Triazine 2	10	20	$B_{10\mu m}$	1	16	–	293	-2.0	VIII & IX
C_{60}	1	20	$B_{10\mu m}$	1	28	258	340	13.7	VII & IX
PCBM	1	20	$B_{10\mu m}$	1	20	280	372	24.4	VII & IX
DPPD	10	20	$B_{10\mu m}$	1	28	242	322	7.7	
June1	10	20	$B_{10\mu m}$	1	20	256	334	11.7	
22Th	10	20	$B_{10\mu m}$	1	28	257	318	6.4	
Study 8b: Constant AC voltage									
–	–	–	$B_{10\mu m}$	1	23	205 [s]	880 [s]	–	
–	–	–	$B_{10\mu m}$	1	24	9 [s]	163 [s]	–	
Et_{12}	10	–	$B_{10\mu m}$	1	0	–	–	–	
Et_{12}	10	–	$B_{10\mu m}$	1	9	100 [s]	461 [s]	184	
Study 9: Further stabilisers									
$–_{perox}$	–	20	$B_{10\mu m}$	1	20	–	517	–	
$PCBM_{perox}$	1	20	$B_{10\mu m}$	1	20	465	573	10.8	
$PCBM_{diff}$	1	20	$B_{10\mu m}$	1	16	304	391	30.8	IX
$Anth_{diff}$	10	20	$B_{10\mu m}$	1	24	336	414	38.5	IX
Anth	10	20	$B_{10\mu m}$	1	16	256	289	-3.5	
DTDCPB	10	20	$B_{10\mu m}$	1	20	239	683	128	IX

$–_{perox}$ is non cross-linked reference XLPE, which is used as reference for $PCBM_{perox}$. Batches of diffusion loaded stabilisers were also made for anthracene and PCBM.

Appendix B

List of experimentally tested voltage stabilisers within this twin PhD project. Abbreviation used within this thesis, followed by full name for some stabilisers and their chemical structure.

Abbr.	Molecular structure and name
Benzil-type	
Benz	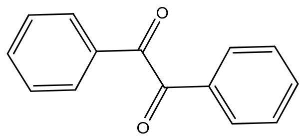 Benzil
Et_1	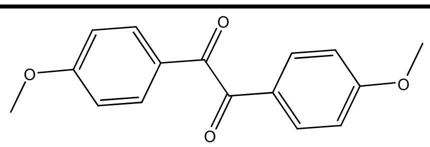 4,4'-dimethoxybenzil
Et_{12}	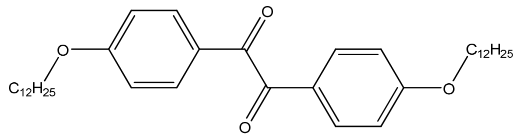 4,4'-didodecyloxybenzil
Et_{30}	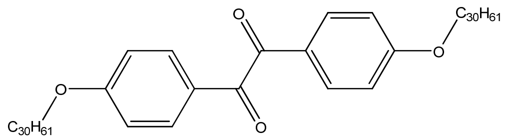
Es_2	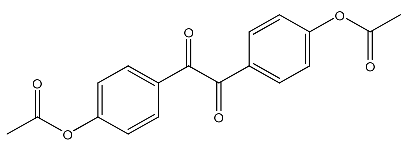
Es_{12}	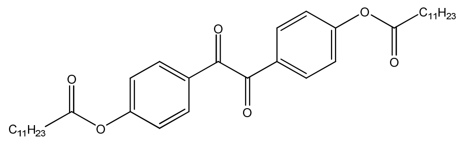
Am_1	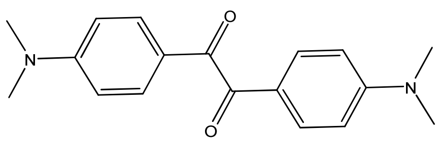
Am_8	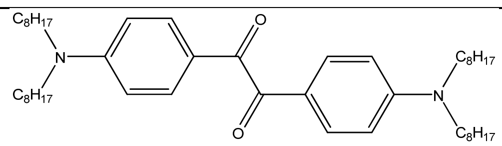 N,N,N',N'-tetraoctyl-4,4'-diaminobenzil
Et_{11}	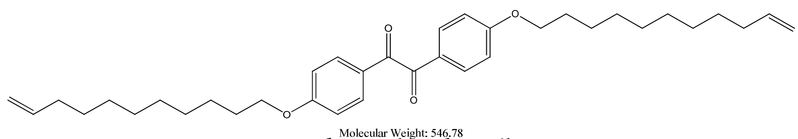 undecenyloxybenzil

Thiaxanthones	
HOTX	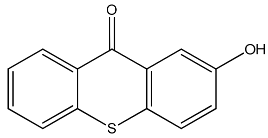
MeOTX	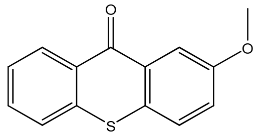
ITX	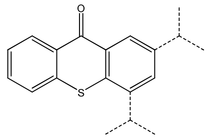
OTXMa	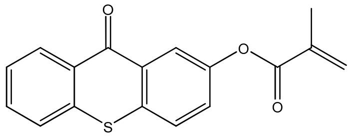
OTXAc	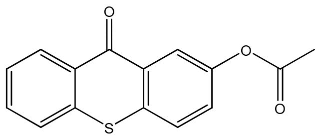
TXEs12	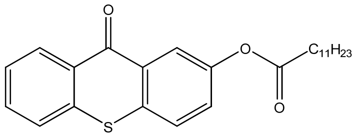
ATX	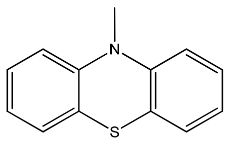
Fullerenes	
C_{60}	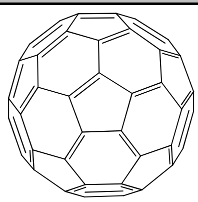 Buckminster fullerene
PCBM	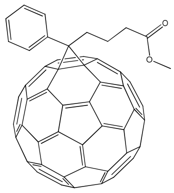 Phenyl–C61–Butyric Acid Methyl Ester

Melamines	
Triazine 1	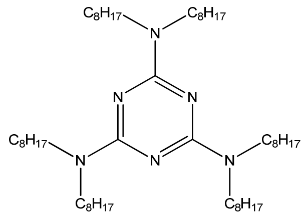
Triazine 2	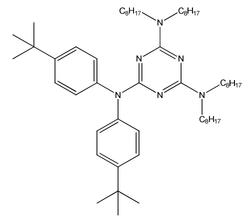
Other	
June1	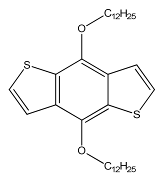
Triami	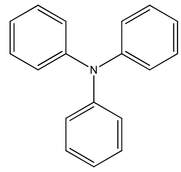 Triphenylamine
Tri1	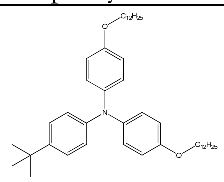 Triphen 1
22Th	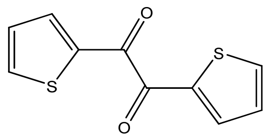 2,2'-thenil
2ambenz	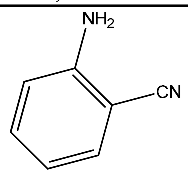 2-aminobenzonitrile

Other (continuing)	
DPPD	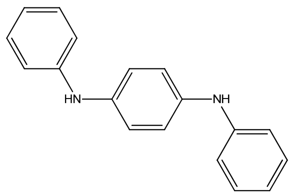
Anth	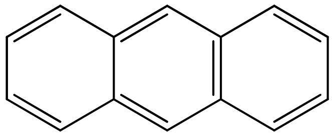 Anthracene
DTDCPB